Theses and Dissertations

2012

Linear Regression Based Damage Detection Algorithm Using Data from a Densely Clustered Sensing System

Yuchen Pan
Lehigh University

Follow this and additional works at: http://preserve.lehigh.edu/etd

Linear Regression Based Damage Detection Algorithm Using

Data from a Densely Clustered Sensing System

By

Yuchen Pan

A Thesis

Presented to the Graduate and Research Committee

of Lehigh University

in Candidacy for the Degree of

Master of Science

in

Structural Engineering

Lehigh University

January, 2013

Yuchen Pan

This thesis is accepted and approved in partial fulfillment for the requirements of the Master of Science in Structural Engineering.

_____

Date

_____

Dr. Shamim N. Pakzad

Thesis Advisor

_____

Dr. Sibel Pamukcu

Department of Civil and Environmental Engineering

Acknowledgement

I would like to express the deepest appreciation to my thesis advisor, Professor Shamim N. Pakzad, for his guidance on the researches I did during my master program. Without him, there is no chance I could finish such a meaningful research.

I would also like to thank for the support provided by computer technician, Peter Bryan and lab stuffs, Darrick Fritchman, Carl Bowman and Adam Kline, for their help to prepare and conduct the structural tests.

The helps from my fellow graduate students, Siavash Dorvash, who gave me a lot of useful advice during my research, Mallory Nigro, who did the model updating with me, Elizabeth Labuz, who did the prior researches on this topic and passed them to me, and Minwoo, who developed the SMIT program and generously shared it to me, are greatly appreciated. This appreciation also extends to the all the other members in the same research group with me for their technical and nontechnical helps.

At the end, I want to thank my parents, Jianrong Pan and Ruiqiu Yu, who provided all the financial supports and supported my two-and-a-half-year master's study with their love.

Table of Content

List of Tables

List of Figures

Abstract

For the purpose of identify the early appearance of damage on under-service structures, cost-effective and precise ways of damage detecting are needed. In this thesis, a structural behavior based damage detection method is introduced. This method utilizes dynamic responses collected by a densely clustered sensor network on the structure and processes them with linear regression based algorithms. The regression coefficients in the linear regression function are used to calculate damage indicators in the algorithm. The coefficient of determination and the variable inflation factor are introduced to verify the reliability of each damage indicator to be used to identify damages. Also control indicators are calculated to reveal the level of noise in the tests and set up a base line for useful damage indicators.

Test specimen used in the research is a scaled two-bay steel frame at Lehigh University's ATLSS Center. A finite element model of the frame is also developed based on this frame. Tests are conducted on both the finite element model and the specimen. Results are analyzed and compared to check the performance of the algorithm. In the tests, the frame is subjected to a single horizontal input which is brought by an actuator. A sensor network with 21 accelerometers is implemented on the frame to collect acceleration responses that are perpendicular to the surface of the frame from 21 locations on the frame.

The effectiveness of three different linear regression based algorithm is discussed in this thesis. The single-variable linear regression based algorithm is first evaluated using both simulation data and test data. Then an advanced algorithm, the two-variable linear regression based algorithm, is introduced and assessed. The same data is again

used and damage prediction results from this algorithm are compared with ones from the single-variable linear regression based algorithm. At last, based on the performance of the previous to algorithms, an iterative linear regression based algorithm is introduced and its performance on analyzing data from random input tests is presented showing the effectiveness of this method.

Chapter 1 Introduction

1.1   Overview

Structures such as high-rise buildings, bridges, off-shore platforms and aerospace stations are exposed to various static and dynamic loadings. They get damaged during their daily service or during some natural disasters like earthquakes and hurricanes. When a structure suffers from serious damages, both the proper functioning of the structure and the safety of people and properties inside the structure will be jeopardized. Also the cost to repair a seriously damaged structure is large, not to mention tearing down an irreparable structure and building a new one. Therefore damage detection in the early appearance of structural damages can be important and useful. Information given by NDE (Non-destructive Damage Evaluation) can be used to 1) immediately determine the integrity and workability of the structure after natural disasters and 2) provide evidence for maintaining and repairing structures under service.

However, structural damage detection is not a simple task. There are five stages in damage detection:

1) Identify the existence of damage in the system;

2) Find the location of damage;

3) Determine the type of damage;

4) Find out the extent of the damage;

5) Do prognosis on the remaining useful time. (Rytter 1993)

The understanding about the damaged structure increases as the five questions are answered in the order represented.

There are some traditional NDE methods in industrial use, which include thermography, ultrasonic waves, liquid penetrant, visual inspection, eddy current and etc. one thing in common for these traditional NDE methods is that they need to get close enough to the damaged area, in order to detect. That means a rough estimation of damaged area and the access to the area are needed. Due to the complexity of damage scenarios, those two requirements mentioned before cannot always be satisfied.

Another kind of damage detection methods that use structural dynamic properties to identify the damage has been developed in the past decades. These methods draw dynamic features of a possibly damaged system from test data and compare them to the values from the undamaged system to identify damages. Several commonly chosen dynamic properties are Resonant frequency (Salawu. 1997a; Lew and Juang 2002; Ruotolo and Surace 1997), frequency response function (Mottershead et al. 1999a; Trendafilava 2003), mode shapes (Kim et al. 1997), mode shape curvatures (Pandey 1991), modal strain energy (Shi, Law and Zhang 1998), dynamic flexibility (Pandey 1994), damping (Kawiecki 2001), ritz vectors (Sohn and Law 2001; Burton, Farrar, and Doebling 1998), ARMA family models (Sohn and Farrar 2001; Bodeux and Golinval 2000), time-frequency analysis (Bonato et al. 1999; Staszewski et al. 1999) and finite model updating (Jaish and Ren 2007; Beardsley, Fritzen, Jennewein and Kiefer 1998).

Since a large amount of dynamic features are used as damage indicators in the damage detection methods, discussions have been made to determine which one is the most useful in damage detection. One important criterion is that if the chosen structural feature is sensitive to certain types of damages. Global dynamic features such as mode shape and modal frequencies give out a global state of the system, but they're not

sensitive to local or slight damage. That means that only the first stage of damage identification, identifying the existence of damage in the system, can be achieved by using these damage indicators.

Another criterion is that whether prior knowledge about the structural property is needed. For various reasons, prior knowledge about a structure, for example, mass, stiffness and damping ratio, is not accessible. But these values are important to some damage detecting algorithms, such as dynamic flexibility based methods and finite element model updating methods. Although approximations can be made as alternatives of the exact values, they'll still have unpredictable effect on the outcome of analysis.

To content the two criteria mentioned above, an algorithm using on densely clustered sensor network was introduced (Labuz 2010). Influence coefficients obtained by applying linear regression onto the dynamic response of the structure are used as damage indicator in that paper. In this research, further researches including simulated and experimental test results are conducted to explore the use of such damage detection algorithm. Both an advanced single-variable linear regression based algorithm and multi-variable linear regression based algorithms will be discussed. And a more direct and vivid way of presenting the damage location are developed.

1.2   Research objective

This research aims at verifying the workability of a new local damage detection method, i.e. the linear-regression based damage detection method, that uses the relationship between two nodes as an indicator to identify the existence, or even more, the location of

damages on a structure. Also the application of such method onto field structure testing will be discussed. Objectives presented in the paper are organized in details as:

1) To update the single-variable-linear-regression based method with new damage indicator.

2) To develop a two-variable-linear-regression based damage detection method and update this method according to detecting result.

3) To develop a N-variable-linear-regression based damage detection.

4) To develop a more detailed SAP2000 model and compare the simulated results with test results.

1.3　Scope of research

To get the objectives listed in section 1.2, following jobs are accomplished. a theoretical foundation for linear-regression based damage detection method is formed by relating the linear behavior of a dynamic system to the linear regression procedure. A finite element model based on the test frame is built to simulate tests. A two-bay girder frame is developed and instrumented with a dense network sensor system. Accelerations from 21 nodes are recorded during the tests. MATLAB codes are written to process test data and simulation data with proposed damage detection methods. Both mathematical and graphical results are produced and saved.

1.4　Organization of this thesis

This thesis will be organized in the listed order.

Chapter 1 introduces the study providing a general overview, research objectives, and organization of the thesis.

Chapter 2 presents the theoretical foundation of linear regression based damage detection method, both structurally and mathematically and introduces the test specimen. Also the updating procedure of a SAP2000 simulating model is introduced in this chapter.

Chapter 3 presents the basic ideas about single-variable method and results from simulated SAP2000 model and test specimen. The requirements for applying single-variable method are discussed.

Chapter 4 presents the basic ideas about two-variable method and results from both SAP2000 model and test specimen by applying two-variable method. Comparison is made between application of single-variable method and two-variable method. The validation of two-variable method is discussed.

Chapter 5 presents results of applying linear regression with multiple variables to random input test data. Application requirement is discussed.

Chapter 6 presents a summary of the thesis work, conclusions, and possible future work.

Chapter 2   Development of Linear Regression Based Local Damage Detection Algorithm

2.1   Introduction

This chapter first illustrate the theoretical foundation for the linear regression based local damage detection algorithms, both single-variable and multi-variable linear regression methods. Then the set-up of the test specimen and equipment are introduced. At last, an updated finite element model is developed for the purpose of performing simulation tests.

A basic idea about the algorithms developed in this research is that changes in structural property will alter the linear relationship between dynamic responses of a node pair. Coefficients or coefficient vectors from the linear regression function will be used to calculate factors to indicate the occurring of damage. As mentioned in the Chapter 1, there are 4 levels in damage detection. Detecting the occurring of the damage is the 1st level, which can be achieved by just observing the changes in coefficients/coefficient vectors. To obtain the 2nd level damage detection, i.e. identifying the location of damage, changes of the calculated factors from different node pairs are compared. Some particular patterns of such changes are identified to show the brief location of damage.

2.2   Structural Theory

In order to justify the application of linear regression to outputs of a structure, two assumptions are introduced to the system. One is the assumption of linear damage which assures the linear behavior of structure before and after the damage. The other one is that

the structural system has classical damping. The two assumptions rule out situations that are too complicated to discuss in the amount of work for a master's thesis, such as nonlinear behavior of the system.

2.2.1 Linear Damage

One of the basic assumptions made in this paper is that the damage occurs in the system is always a linear damage. A linear damage is defined as 'the case when the initial linear-elastic structure remains linear-elastic after damage' which is introduced by Doebling et al. 1998. Since all damages discussed in this paper are relatively small in order to simulate the early appearance of structural damage, the linear behavior of structure is assumed to remain after the damage. However in the real world, damages such as cracks will cause non-linear behavior of the structure when they open during the tension phase and close during the compression phase.

2.2.2 Classical damping

Classic damping is a restriction of applying modal superposition, which will be introduced in the later sections. Due to the lack of measurement, the exact damping matrix of the structure can not be determined. Since the specimen used in the test is a simplified and scaled-down steel frame with no bracing or any other kind of man-made damping mechanism and only data from adjacent nodes will be compared, it is proper to assume that the system has classical damping.

2.3 Dynamic Response of a Linear System

If external dynamic forces are given, the dynamic response of a multi-degree-freedom (MDF) system shown in Figure 2.1 can be determined by solving

$$\ddot{q}_n(t) 2\xi_n \omega_n \dot{q}_n(t) + \omega_n^2 q_n(t) = \frac{P_n(t)}{M_n} \tag{2.1}$$

for the modal coordinate $q_n(t)$. Once the modal coordinates $q_n(t)$ have been determined, in the modal displacements $\mathbf{u}$(t) is

$$\boldsymbol{u}_n(t) = \boldsymbol{\phi}_n q_n(t) \tag{2.2}$$

and combining these modal contributions gives the total displacements:

$$\boldsymbol{u}(t) = \sum_{n=1}^{N} \boldsymbol{u}_n(t) = \sum_{n=1}^{N} \boldsymbol{\phi}_n q_n(t) \tag{2.3}$$

The displacement for a specific node j is

$$u_j(t) = \sum_{n=1}^{N} \phi_{jn} q_n(t), j = 1 \dots m \tag{2.4}$$

Since the test data is recorded in discrete time series, displacement at a time point for node j can be expressed as:

$$u_j(n) = \phi_{j1} q_1(n) + \cdots + \phi_{jn} q_n(n), j = 1 \dots m \tag{2.5}$$

For the same reason

$$\ddot{u}_j(n) = \phi_{j1} \ddot{q}_1(n) + \cdots + \phi_{jn} \ddot{q}_n(n), j = 1 \dots m \tag{2.6}$$

(Chopra 2001)

2.4 Vector Space

In Linear Algebra (May 1970), the principle of Corollary is expressed as

Suppose $W_1 = L\{\overline{X}_1, \overline{X}_2, \dots, \overline{X}_n\}$ and $W_2 = L\{\overline{Y}_1, \overline{Y}_2, \dots, \overline{Y}_m\}$. Then $W_1 = W_2$ if and only if all of the vectors $\overline{X}_1, \overline{X}_2, \dots, \overline{X}_n$ are in W_2, and all of the vectors $\overline{Y}_1, \overline{Y}_2, \dots, \overline{Y}_m$ are in W_1.

For convenience, *m* will always be assumed larger than *n*, which means the number of nodes will always be larger than the number of modes that are taken into account. Take out *n* nodal acceleration responses together with *n* modal coordinates to form

$$\begin{pmatrix} \ddot{u}_1(n) \\ \vdots \\ \ddot{u}_n(n) \end{pmatrix} = \begin{pmatrix} \phi_{11} & \cdots & \phi_{1n} \\ \vdots & \ddots & \vdots \\ \phi_{n1} & \cdots & \phi_{nn} \end{pmatrix} \cdot \begin{pmatrix} \ddot{q}_1(n) \\ \vdots \\ \ddot{q}_n(n) \end{pmatrix} \tag{2.7}$$

or simplified as

$$\ddot{u}(n)_{n\times 1} = \boldsymbol{\Phi}_{n\times n} \cdot \ddot{q}(n)_{n\times 1} \tag{2.8}$$

From Eqs. 2.7, one can tell that $\ddot{u}_1(n)$, $\ddot{u}_2(n)$,..., $\ddot{u}_n(n)$ are clearly linear combinations of $\ddot{q}_1(n), \ddot{q}_2(n), ..., \ddot{q}_n(n)$, i.e. they are in $L\{\ddot{q}_1(n), \ddot{q}_2(n), ..., \ddot{q}_n(n)\}$. To prove that $\ddot{q}_1(n), \ddot{q}_2(n), ..., \ddot{q}_n(n)$ are in $L\{\ddot{u}_1(n), \ddot{u}_2(n),..., \ddot{u}_n(n)\}$, Eqs. 2.7 need to be solved for $\left(\ddot{q}_1(n) ... \ddot{q}_n(n)\right)^T$ and should have one and only one solution. Therefore

$$r\left(\boldsymbol{\Phi}\big|\ddot{u}(n)\right) = r(\boldsymbol{\Phi}) = n \tag{2.9}$$

becomes the only requirement. Due to the orthogonality of mode shapes, Eq. 2.9 is naturally satisfied. So $\ddot{q}_1(n), \ddot{q}_2(n), ..., \ddot{q}_n(n)$ are also linear combinations of $\ddot{u}_1(n)$, $\ddot{u}_2(n)$,..., $\ddot{u}_n(n)$, i.e. they are in $L\{\ddot{u}_1(n), \ddot{u}_2(n),..., \ddot{u}_n(n)\}$.

Hereby, the principle of Corollary has been proved valid between $\ddot{u}_1(n)$, $\ddot{u}_2(n)$,..., $\ddot{u}_n(n)$ and $\ddot{q}_1(n), \ddot{q}_2(n), ..., \ddot{q}_n(n)$. Known from Eq.2.6, all nodal acceleration responses, $\ddot{u}_1(n)$, $\ddot{u}_2(n)$,..., $\ddot{u}_m(n)$, are in $L\{\ddot{q}_1(n), \ddot{q}_2(n), ..., \ddot{q}_n(n)\}$. According to the principle of Corollary, they should also be in $L\{\ddot{u}_1(n), \ddot{u}_2(n),..., \ddot{u}_n(n)\}$ which leads to the conclusion that each nodal acceleration response can be expressed as a combination

of other *n* nodal acceleration responses, where *n* is the number of modal coordinates included.

$$\ddot{u}_j(n) = \phi_{j1}\ddot{u}_1(n) + \cdots + \phi_{jn}\ddot{u}_n(n), j = 1 \ldots m \tag{2.10}$$

2.5 Linear Regression

According to what has been discussed in section 2.4, linear relationship can be expected between dynamic responses from nodes on the structure. In the thesis, accelerations will be discussed particularly. In order to find such linear relationship, linear regression will be applied to data from both specimen tests and finite element simulating tests.

In statistics, linear regression is an approach to model the relationship between a dependent variable Y and one or more independent variables denoted as X. The case with one independent variable is called simple regression and the case with more than one independent variables is called the multi-variable regression. An example of single regression is given in Figure 2.1. Noticing the existence of statistical error, a general linear regression model will be presented as:

$$Y = \alpha + \sum \beta_i \cdot X_i + \varepsilon \tag{2.11}$$

where,

    Y = dependent variable;

    X_i = independent variables;

    α = Y-intercept;

    β_i = regression coefficients;

    ε = error in prediction.

Error in this research will include noise during the test and the effect of neglected dynamic responses from high modes.

Comparing Eq. 2.10 with Eq. 2.11, one can see that they have the same form. It proves that linear regression can be applied to analyze the linear relationship between structural dynamic responses. Detailed application will be introduced in the following chapters.

2.6   Experimental Model

Test specimen used in the research is a scaled two-bay steel girder frame (Figure 2.3), which is a simplified model of a normally used column-beam frame system. As shown in Figure 2.4, this kind of column-beam system can be observed almost in every structure system. Usually they are more complicated structure systems with more stories and spans systems into a one-story two-span, simple but representative example. It contains two side columns and a middle column which take both the two general positions of columns into consideration. Its self-weight works as vertical dead load and there is an actuator simulating the horizontal dynamic load.

2.6.1 Geometrical Description

Description of the dimension of the frame is given in Figure 2.5a. The frame is 2'-8" high. The left span is 7'-6" wide and the right one is 12'-6" wide. There are nine interchangeable sections on the frame, shown in Figure 2.5b with nominations to the damage location. Each of them has two kinds of frame sections to switch between undamaged state and damage state. Section properties are shown in Table 2.1. As can be seen from the table, the only difference between the undamaged and damaged section is

that the damaged section has thinner walls which causes 20% reduction on section stiffness. A picture of the interchangeable section is shown in Figure 2.6. One thing worth to be mention is that, in order to make the section able to be removed or fixed onto the frame, 0.85 inch thick plates with 6 drill holes are welded on both end of the interchangeable hollow section as well as on the ends of the permanently undamaged portions of the structure. The end plate connections seem to increase the structural stiffness around bolting area, but they have little effect on the overall stiffness of the structure which can be demonstrated by the equation below:

$$\frac{1}{k_o} = \frac{1}{k_p} + \frac{1}{k_s} \tag{2.12}$$

where

k_o = The overall stiffness of the structure

k_p = Stiffness around end plates area

k_s = Stiffness of other structure members, beams or columns.

When k_p becomes much larger than k_s, the overall stiffness k_o will only depends on the value of k_s.

The structure is placed on an I-shaped steel section which is clamped onto the ground. During the dynamic test, slight vibration is observed on the steel base which could be reaction to the structural vibration or the ambient vibration from the lab. From the comparison made in Figure 2.7, one can see that the magnitude of the vibration on the steel base is much smaller than that of the frame and that means these kind of noise won't have much influence on the test data.

2.6.2 Test Equipment

To fulfill the test, several pieces of equipment were used. They were generally performing in three 'groups', a loading group, a sensing group and a data acquisition and pre-processing group.

2.6.2.1 Actuator and Load Cell

MODAL 50A actuator shown in Figure 2.10 carried out by MB Dynamic was used to produce the dynamic load in the experiments. The peak force it can give is 25 lbs without a cooling system and doubled peak force, 50lbs, with cooling. Table 2.2 presents more specifications for the MODAL 50A. The applied excitation type and amplitude was controlled by a MATLAB program called SigLab and a signal controller call SL500VCF Power Amplifier shown in Figure 2.11 (Spectral Dynamics, Inc. 2001; MB Dynamics 2001). The SigLab controller provides a digital control on the excitation. For example, when a resonant sinusoidal input is subjected onto the frame, even if the peak force is small, the dynamic response could be large and beyond the linear region. That's the reason a peak voltage control shall be set in the SigLab. The SL500VCF Power Amplifier has analog jog which can also give an output voltage level to control the amplitude of loading analogically. It is an instant and secondary control on the input during the test when a quick and precise input control is needed.

2.6.2.2 Sensing system

The sensing system instrumented on the frame was a sensor network contains 21 wired accelerometers. The 21 accelerometers were generally divided into three groups locating around joint areas at 8-inch intervals, six on the left joint nominated with 'L' and numbers, nine on the center joint nominated with 'C' and numbers and six on the right

joint nominated with 'R' and numbers. Accelerometers arrangement is shown in Figure 2.12.

Accelerometers used in the tests were model number 2210-002 produced by Silicon Design. Inc. (2010) shown in Figure 2.13. The 2210-002 accelerometer combines an integrated model 1210L accelerometer with high drive. The anodized aluminum case is epoxy sealed and is bolted via two #4 screws. The 2210-002 model has a full scale acceleration of ±2g. In this research the peak acceleration was seen around ±1g. Other properties of the 2210-002 model are shown in Table 2.3

2.6.2.3 Data acquisition system

The CR9000 data acquisition system shown in Figure 2.14 combined with the PC9000 support software by Campbell Scientific, Inc. (2005; 2009) was used to collect test data. CR9000 system has a peak sampling rate of 100 kHz. The sampling rate in the experiments was 500 Hz which means 0.002s interval in observed in test data.

There were 10 sets of data for each damage scenario, 5 for the undamaged case and 5 for the damaged case. Each set of data contains 21 columns of data from the 21 sensors and each column has 10 thousand data points inside. The total amount of data processed in the research is 1.45 GB.

2.6.3 Dynamic Property

The tests conducted were all dynamic tests. So it is important to know some of the dynamic properties, for example, natural frequencies of the frame. An ambient-input test was conducted before doing the forced-frequency tests. Data from 21 nodes on the frame was recorded by 21 accelerometers and a MATLAB program called SMITM (Figure 2.8)

developed by Chang et al. (2010) and his group was used to get modal parameters of the system.

Running the program using the ERA-Next-AVR modular, result shown in Figure 2.9 was obtained. From the plot, one can identify three modes frequencies, one around 13.66Hz, one around 21.95Hz and another around 31.58Hz.

2.7 Simulated SAP2000 Model

A Simulated SAP2000 model was built up to verify the performance of the damage detection method and gave a prior knowledge of what results could be expected the from field tests. The SAP2000 model shown in Figure 2.15 was first built with the real geometrical dimensions of the test frame with boundary condition of three fixed ends. It was not a proper simulation of the real structure, so model updating was needed.

2.7.1 Model Updating

A basic rule of model updating is to update limited number of parameters in a structural system to match several selected model features to the real ones. Considering the countless number of features there are for a dynamic system, goal features of the structure shall be selected to simplify the updating procedure, meanwhile get a precise enough finite element model. First, the first three nature frequencies, shown in Figure 2.9, were chosen because they were the most important and basic features of the system. And the conclusion would be more convincing when results from simulation tests and lab tests with resonant input were compared if the natural frequencies converge. Then acceleration responses were also selected to justify if the model updated was a good simulation to the

real specimen in lab. There are 21 nodes in the system which means 21 acceleration responses. But it is impossible and unnecessary to use all of them and converge them to the real ones. So, to be representative, accelerations from node L4 and node R4, shown in Figure 2.16, were used in this research. The reason to choose these two nodes was that they were the closest nodes to the top floor and their responses were relatively large. Table 2.4 gives the value for the five features mentioned. Here the amplitudes of the two accelerations were from a test with a 20Hz input. With these system features, model updating can be started.

2.7.1.1 First Trial

The first attempt to update the model was updating supporting boundary conditions of the model. In the original model, all three supports were fixed ends. However, the real lab specimen was bolted onto the base which means they were not perfectly fixed ends and slight rotation was allowed. So the idea of updating the supporting condition was to replace these fixed ends with simply supported ends and moment springs, in Figure 2.17. And since the three ends were bolted in the same way, an assumption was made that the stiffness of the springs were the same.

Figure 2.18 presents the system natural frequencies for each case when the stiffness of the moment springs were changed, starting from the case with fixed ends. The red dash lines are the goal values. As one can see from the plot, the first two natural frequencies are getting close to the real ones when the stiffness goes down, but the two curves eventually go flat and are never going to reach the goal values. Figure 2.19 gives the curves for the amplitude of the two acceleration responses. Although both two curves

go across the dash lines at some points, they don't happen at the same point. Actually when one curve is crossing its goal line, the other one is always far away from its goal line.

To sum up, neither one of the selected features could converge at the same. The first trial to update the finite element model wasn't successful.

2.7.1.2 Second Trial

Since simply updating the supporting conditions couldn't accomplish the goal of getting a good simulation of the real lab specimen, more properties of the finite element shall be considered in the updating. Knowing that there are nine interchangeable sections bolted on the specimen, it was natural to think that those connections on the ends of the sections, which were assumed to be rigid connections, should also be updated. The idea was the same as updating the supports. Rigid connections were replaced with hinges with moment springs, shown in Figure 2.20. There were totally 21 moment springs in this case. Based on their location, those springs were divided into four groups, six on the left beam, six on the right beam, six on the three columns and three on the supports. To simplify the updating, moment springs in the same group would be assigned with same stiffness. But even after this simplification, there were four parameters to update and five features to match. So the relationship between the parameters and features, i.e. which feature is most sensitive to which parameter, needs to be discovered.

Figure 2.21 shows the first three mode shapes. It is clear that the first mode is mainly about the vibration of the right beam, the second mode is about the horizontal vibration of the column and the third mode is about the vibration of the left beam. So

relationships between members on the structure and structural modes were built and presented in Table 2.5.

Based on the parameter-feature sensitivity relationship, a series of updating trials were performed to first let the first three mode frequencies converge. Parameter combinations and the corresponding natural frequencies are given in Figure 2.22. Compare trial 1 and trial 3, the only change in parameters was the spring stiffness on the right beam. A relatively large change was seen in the first natural frequency, decreased by 0.84Hz. Compare trial 4 and trial 5, the spring stiffness on the left beam was reduced from 40 to 20; correspondingly, the third natural frequency was significantly decreased from 35.32Hz to 30.9Hz. From trial 5 to trial 9, the stiffness of springs on the supports was increased to make the second mode frequency converge while keeping the other two stay the same. From trial 10 to trial 12, springs on the columns were altered, but all three frequencies didn't change much. The final combination of the four parameters are 20/25/80/120 kip·ft/rad for springs on the left beam, right beam, columns and supports, respectively. Figure 2.23 to Figure 2.26 summarize the pattern got from these trial updates. For each plot, one of the four parameters is changing while the other three remain. And the results verify that springs on the left beam control the 3rd mode frequency, springs on the right beam control the 1st mode frequency, springs on the columns control nothing and springs on the supports control the 2nd mode frequency.

The parameters were then applied for simulation tests to get accelerations on node L4 and node R4. The amplitudes of the two acceleration responses were 0.966g and 0.86g for L4 and R4, respectively. Table 2.6 summarizes the percentage differences between the simulated features and the actual features. As shown in the table, the

percentage differences for natural frequencies were acceptable, however, the error for accelerations were too large to be accurate. They were far from matching the results from the real test. So, further updates were still needed.

Figure 2.27 shows the impact of changing the stiffness of the column springs on the acceleration responses from node L4 and node R4. One can see that while the springs on the column don't have much effect on the natural frequencies, they do alter the accelerations from node L4 and node R4. From the plot, it's clear that the best simulation of accelerations are found when the stiffness of the springs is around 60 kip·ft/rad. Simulated features were again found and the percentage error was calculated and summarized in Table 2.7. This time errors for all five goal features were acceptable. The errors for acceleration were still larger than those for natural frequencies, but they were significantly reduced compared the unrevised ones in Table 2.6. Although further updating could revise the results more, the accuracy of the finite element model was enough for this research. The model updating stopped at this step and the combination 20/25/60/120 kip•ft/rad for spring stiffness was applied.

Table 2.1 Dimensions of the Interchangeable Section

Section Dimensions	Undamaged Section	Damaged Section
Outer Dimension of the Hollow Cross Section	2" X 2"	2" X 2"
Wall Thickness	0.085"	0.0065"
Length	8"	8"
End Plate Dimension	4" X 4"	4" X 4"
End Plate Thickness	0.085"	0.085"

Table 2.2 Specifications of MODAL 50A Actuator

STROKE		1" peak-peak(continuous duty) 1.1" between stops
FORCE OUTPUT	Convection Cooling:	25 pounds (peak)
	Shop Air by User:	50 pounds (peak)
	Portable Cooling:	50 pounds (peak) - optional
STINGER ATTACHMENTS		Chuck and collets handle stinger sizes from .020" to .125" (0.5 – 3.2mm)
SHAKER ATTACHMENTS (for mounting)		Floor: adjustable trunnion base & screw feet. Suspended: multiple turnbuckles
TEST SPECIMEN STATIC PRE-LOAD		Capable of tensioning stinger in excess of 50 pounds
WEIGHT		Shaker with trunnion base: 55 pounds
BOUNCE MODE OF 'LARGE INERTIAL CONFIGURATION' ON ARMATURE SUSPENSION		Approx. 1 Hz
DIMENSIONS		11 ½" H (to top of collet chuck with feet retracted) 7 ½" x 9 ¼" footprint
DRIVE CABLE LENGTH		30' standard (100' cable available as option)

Table 2.3 Specifications of Silicon Designs 2210-002 Accelerometers

Model Number	2210-002
Input Range	±2 g
Frequency Response	0 – 300 Hz
Sensitivity	2000 mV/g
Output Noise	13 $\mu g/(\sqrt{Hz})$
Max. Mechanical Shock	2000 g

Table 2.4 System Features Used for Model Updating

1st Natural Frequency	2nd Natural Frequency	3rd Natural Frequency	Amplitude of Acceleration L4	Amplitude of Acceleration R4
13.66 Hz	21.95 Hz	31.58 Hz	1.18 g	1.18 g

Table 2.5 Parameter-Feature Sensitivity Relationship

Parameter	Most Related Feature
Springs on the left beam	3rd Mode Frequency
Springs on the right beam	1st Mode Frequency
Springs on the column	2nd Mode Frequency and Accelerations
Springs on the supports	2nd Mode Frequency and Accelerations

Table 2.6 Percentage Error between Simulated Features and Actual Features

Parameter	First Mode Frequency (Hz)	Second Mode Frequency (Hz)	Third Mode Frequency (Hz)	Acceleration From L4 (g)	Acceleration From R4 (g)
Actual Girder Features	13.66	21.945	31.581	1.18	1.18
Simulation Features	13.68	21.812	31.906	0.86	0.966
Percent Error (%)	**0.307%**	**0.606%**	**1.029%**	**27.11%**	**18.14%**

Table 2.7 Percentage Error between Revised Simulated Features and Actual Features

Parameter	First Mode Frequency (Hz)	Second Mode Frequency (Hz)	Third Mode Frequency (Hz)	Acceleration From L4 (g)	Acceleration From R4 (g)
Actual Girder Features	13.66	21.945	31.581	1.18	1.18
Revised Simulation Features	13.568	21.512	31.545	1.11	1.22
Percent Error (%)	**0.67%**	**1.97%**	**0.11%**	**5.84%**	**3.80%**
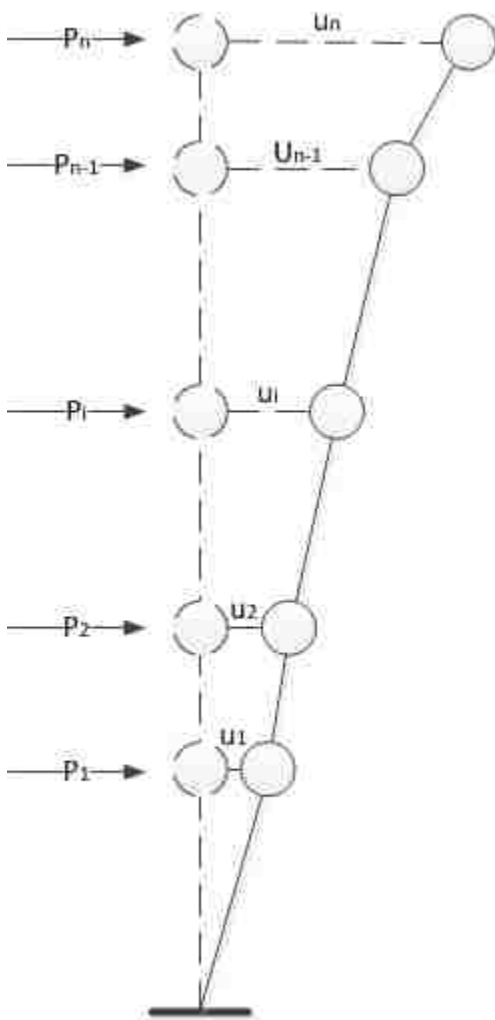
Figure 2.1 Multi-Degree Freedom System

Single Regression

X value	Y value
1.8	32
1	24
1.7	27
2.8	47
2.2	35
0.8	17
3.6	52
1.1	20
2	38
2.6	45

◆ Scatter Diagram
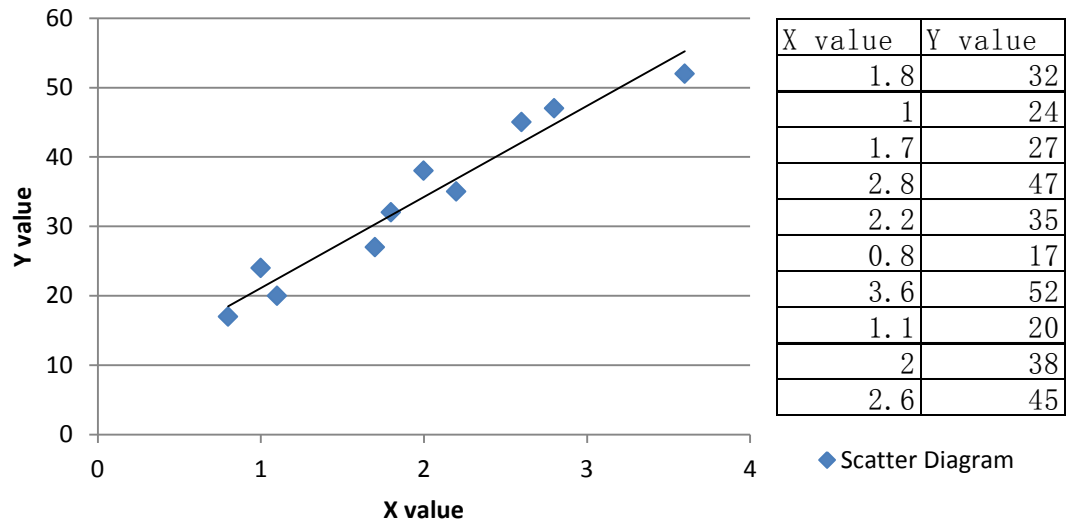
Figure 2.2 An example of single regression

Figure 2.3 Test Specimen

Figure 2.4a Application of Column-Beam Frame on a Bridge

Figure 2.4b Application of Column-Beam Frame on a Steel Frame House
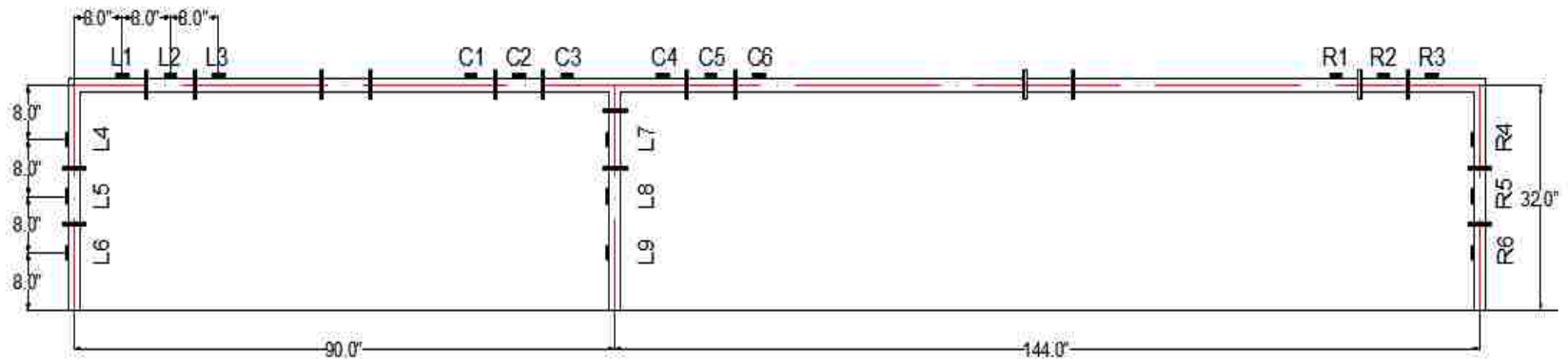
Figure 2.5 Plan of the Lab Specimen
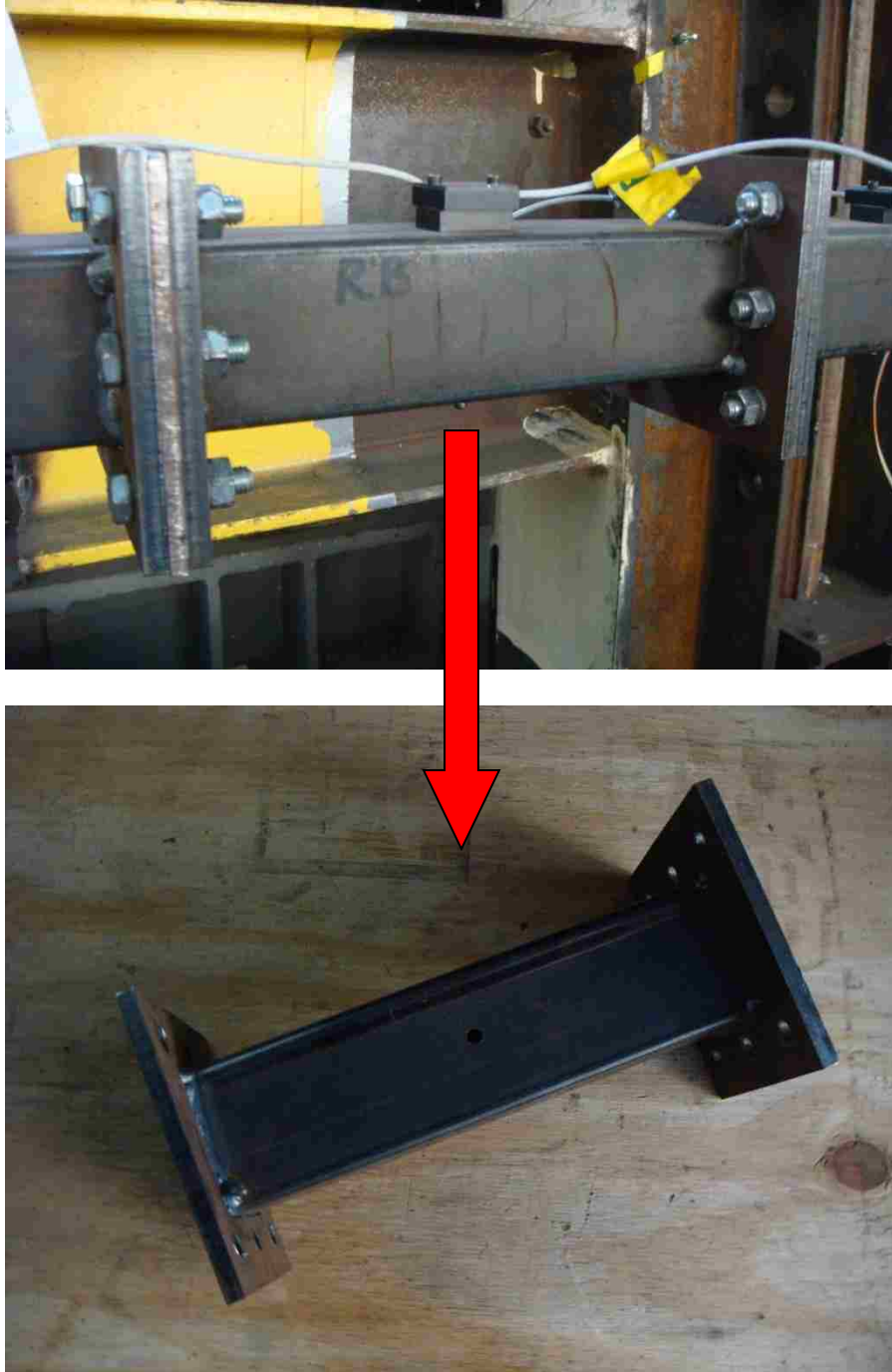
Figure 2.6 Interchangeable Section on and off the Structure
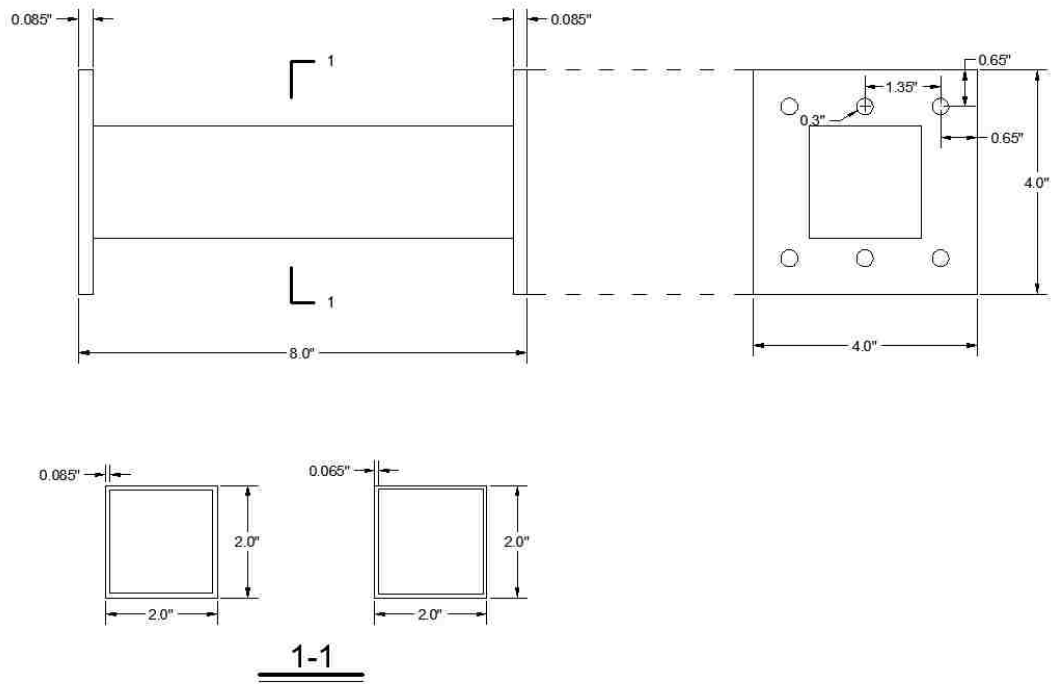
Figure 2.7 Dimensional Details of the Interchangeable Section
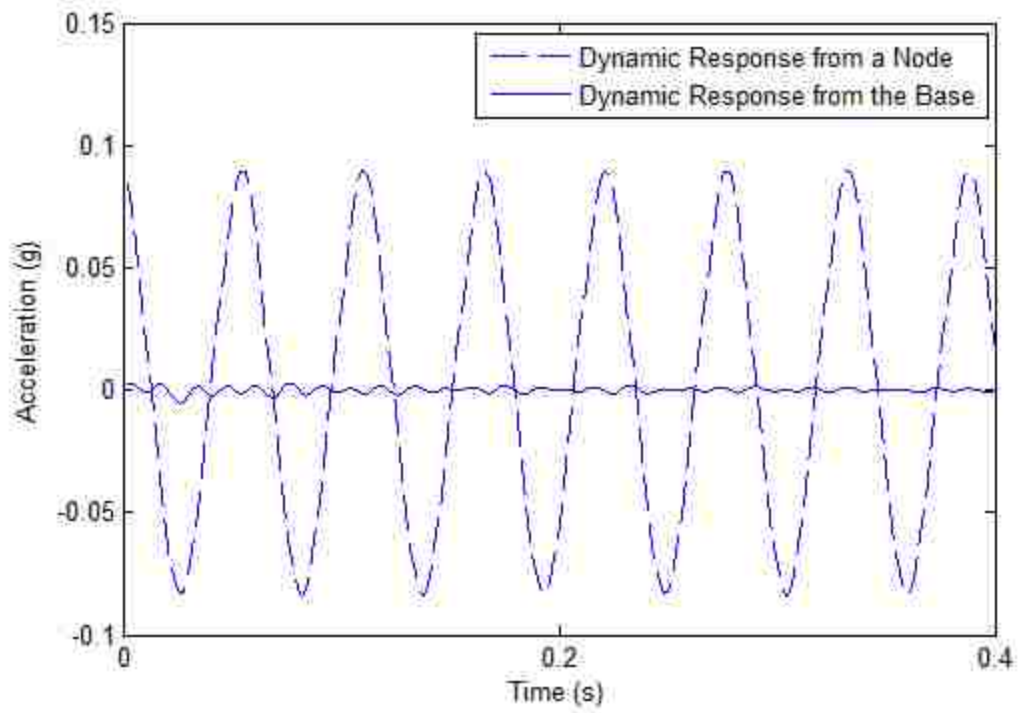
Figure 2.8 Node Response vs. Base Reaction
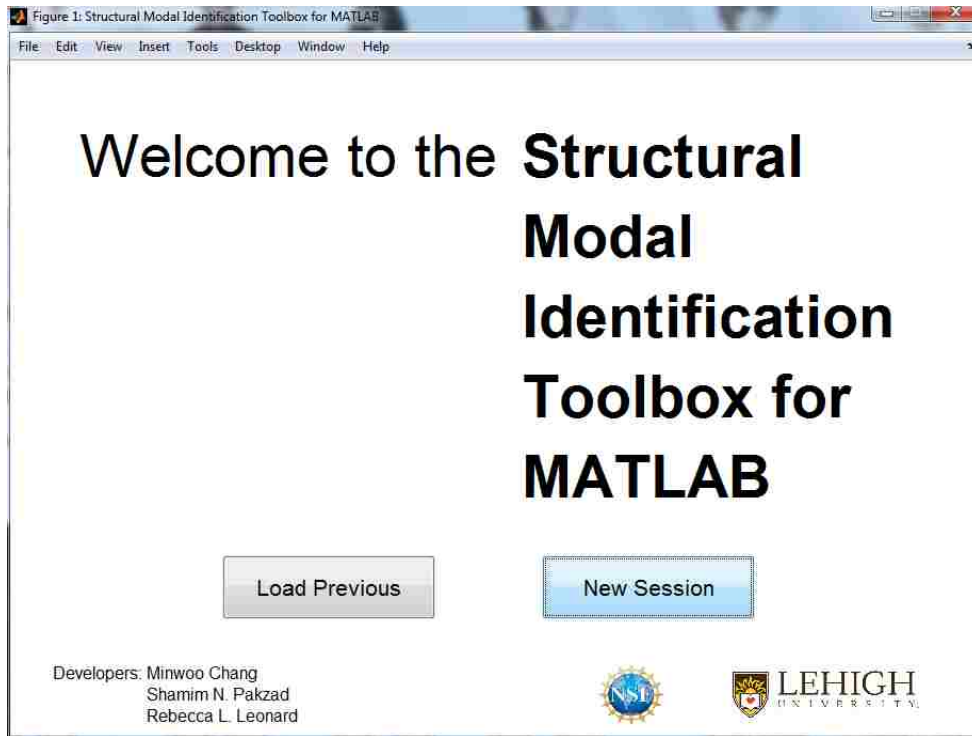
Figure 2.9 Welcome Interface of the SMITM Program
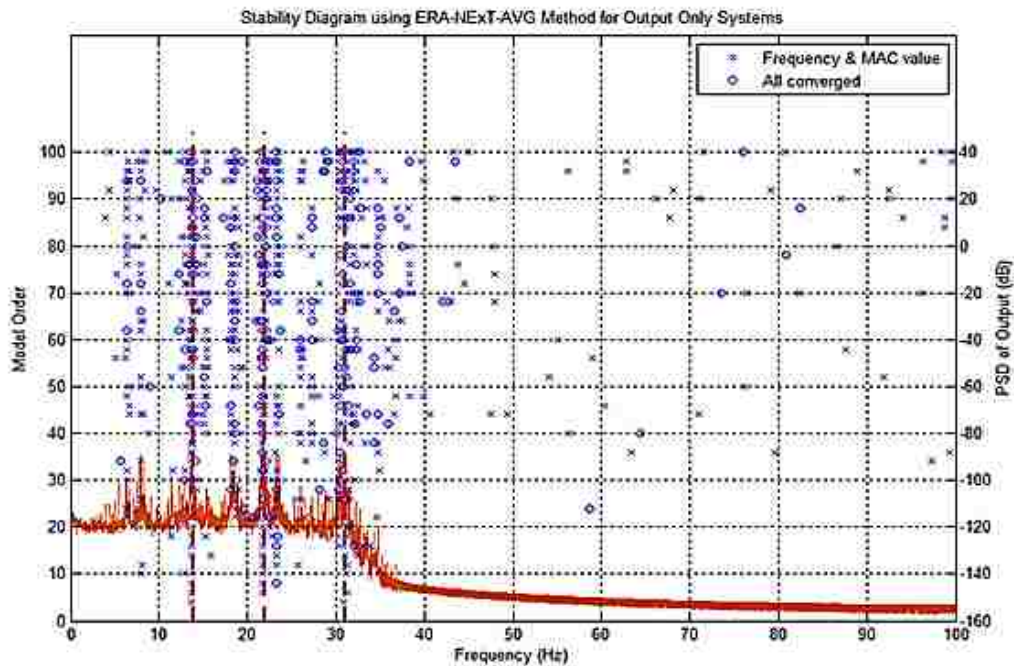
Figure 2.10 Natural Frequencies

Figure 2.11 MODAL 50A Actuator

SigLab Controller

SL 500VCF Power Amplifier
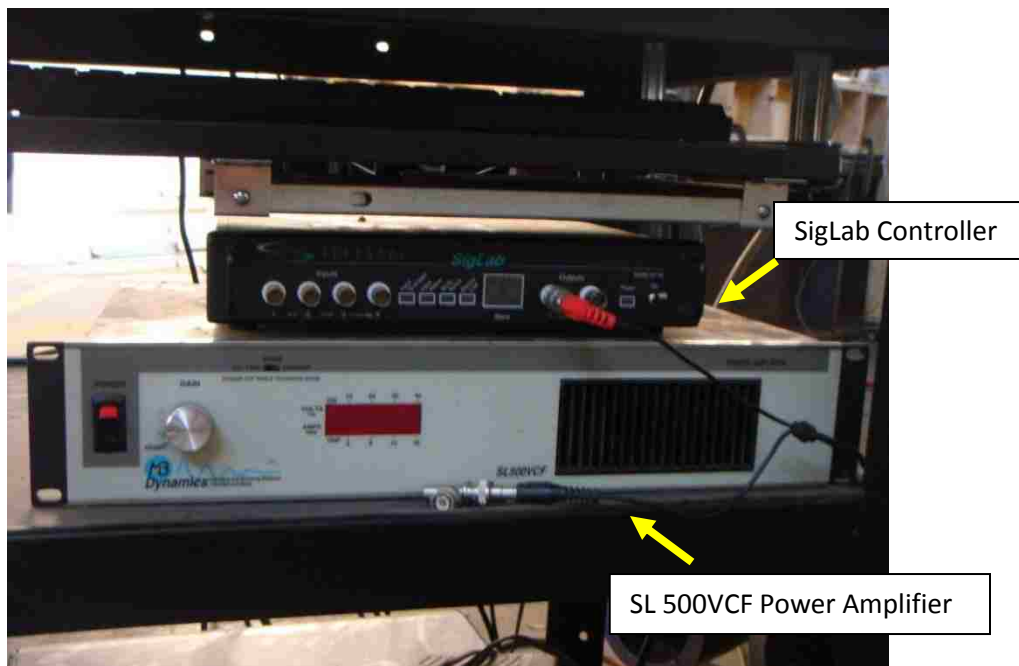
Figure 2.12 The SigLab Controller and the SL 500VCF Power Amplifier
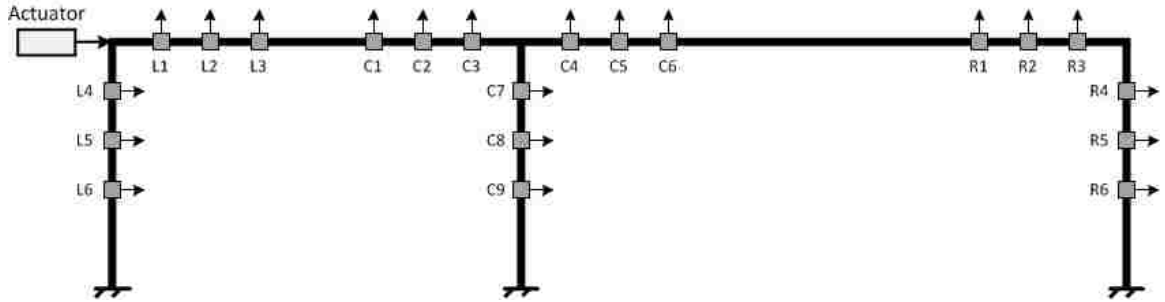
Figure 2.13 Sensor Arrangement
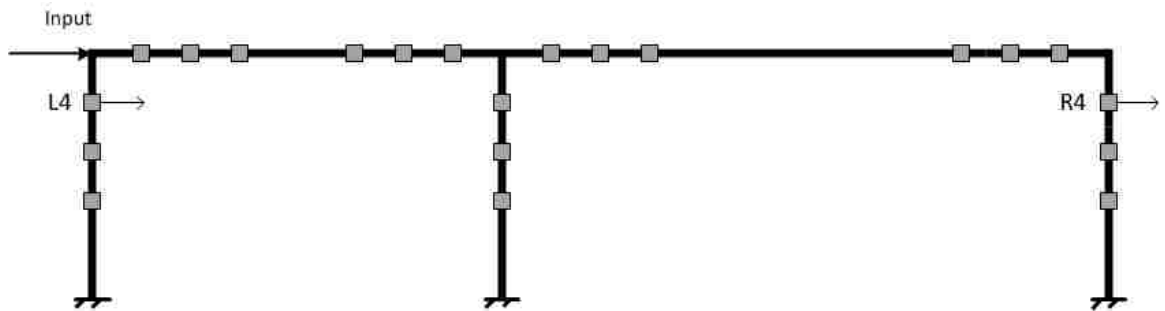
Figure 2.14 Accelerations from L4 and R4
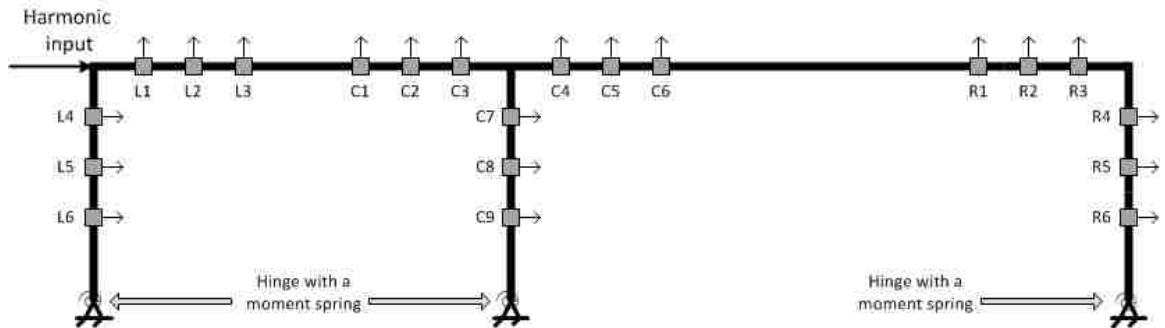
Figure 2.15 First Attempt to Update the Finite Element Model
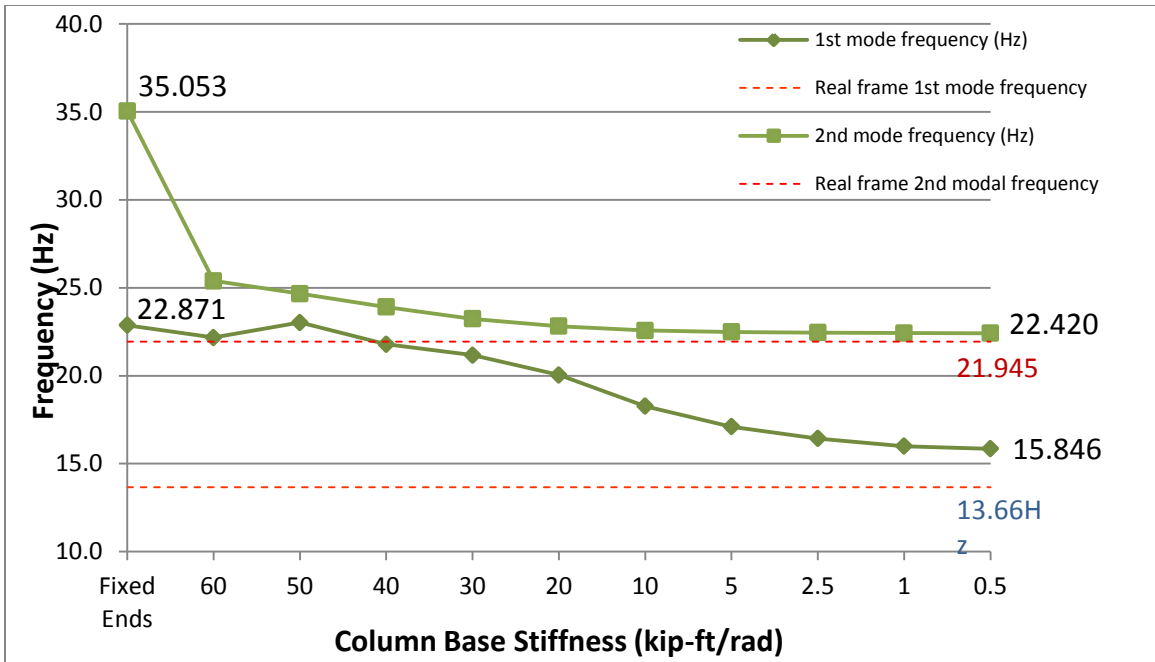
Figure 2.16 Natural Frequencies on First Trial
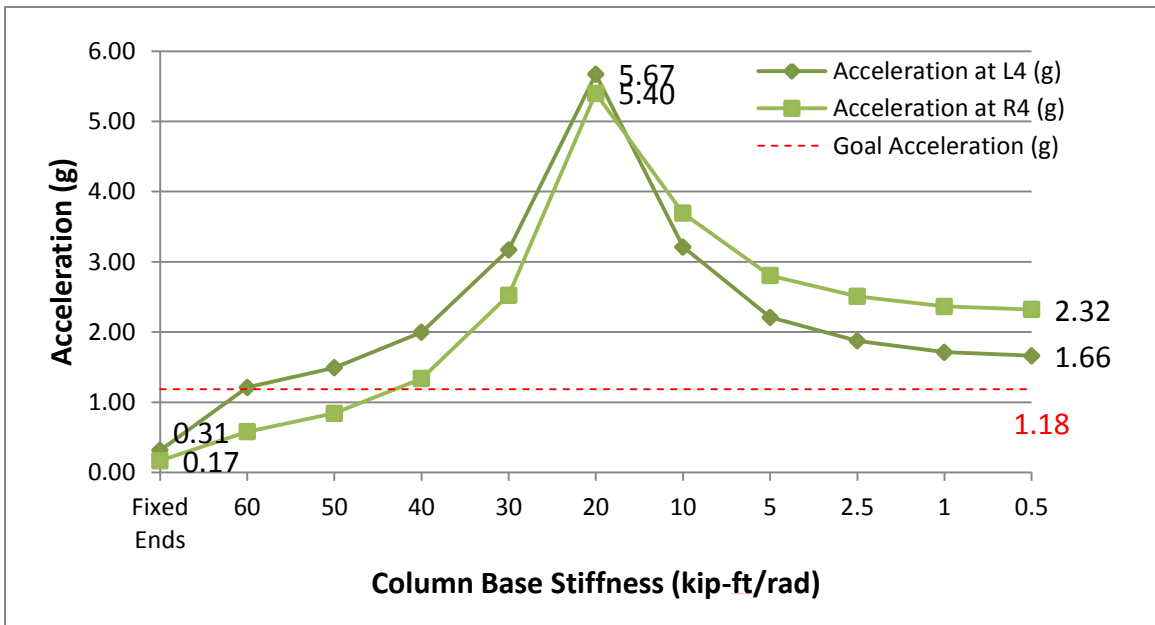
Figure 2.17 Amplitudes of Acceleration Responses on First Trial
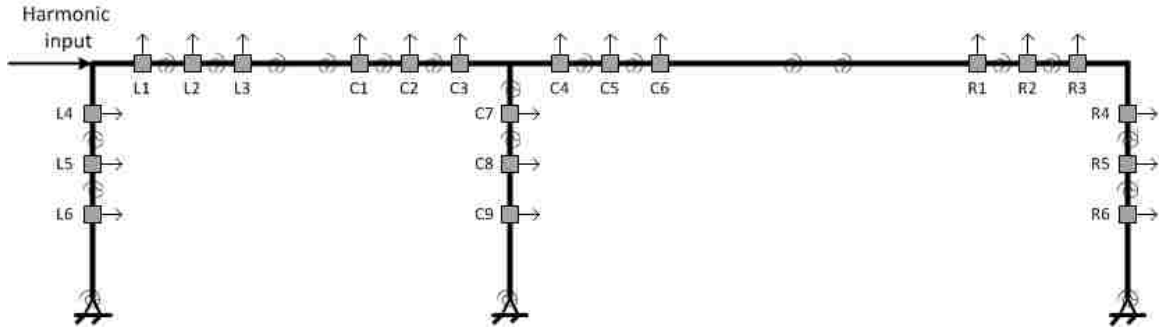
Figure 2.18 Second Attempt to Update the Finite Element Model
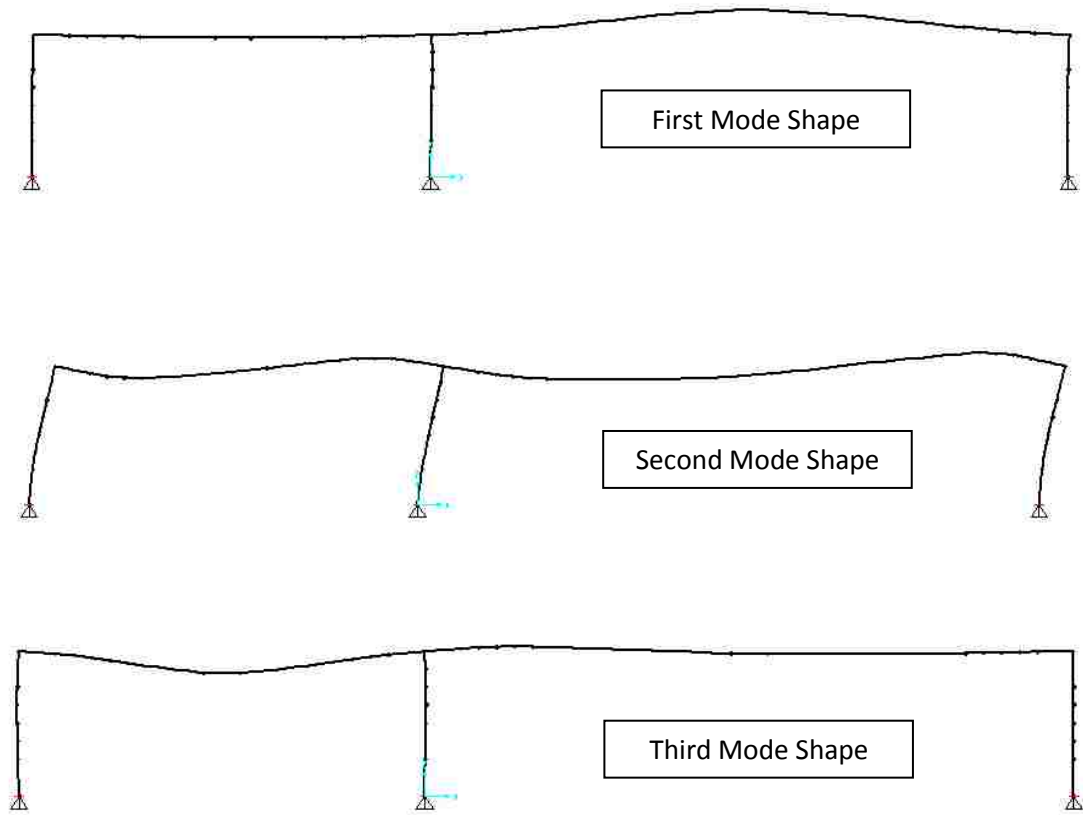
Figure 2.19 Natural Mode Shapes

Location	Trial 1	Trial 2	Trial 3	Trial 4	Trial 5	Trial 6	Trial 7	Trial 8	Trial 9	Trial 10	Trial 11	Trial 12
Fixed	40	40	40	40	40	50	90	100	120	120	120	120
Column	40	40	40	55	55	55	55	55	55	55	60	80
Left/Right Beam	40/40	80/40	40/30	40/30	20/30	20/30	20/30	20/30	20/30	20/25	20/25	20/25

	Trial 1	Trial 2	Trial 3	Trial 4	Trial 5	Trial 6	Trial 7	Trial 8	Trial 9	Trial 10	Trial 11	Trial 12
1st freq.	14.56	14.63	13.72	13.9	13.93	13.98	14.1	14.129	14.16	13.5	13.55	13.682
2nd freq.	18.97	19.64	18.64	18.8	17.9	18.77	20.8	21.185	21.73	21.52	21.603	21.84
3rd freq.	34.84	38.05	34.43	35.32	30.9	31.05	31.33	31.38	31.46	31.307	31.45	31.914
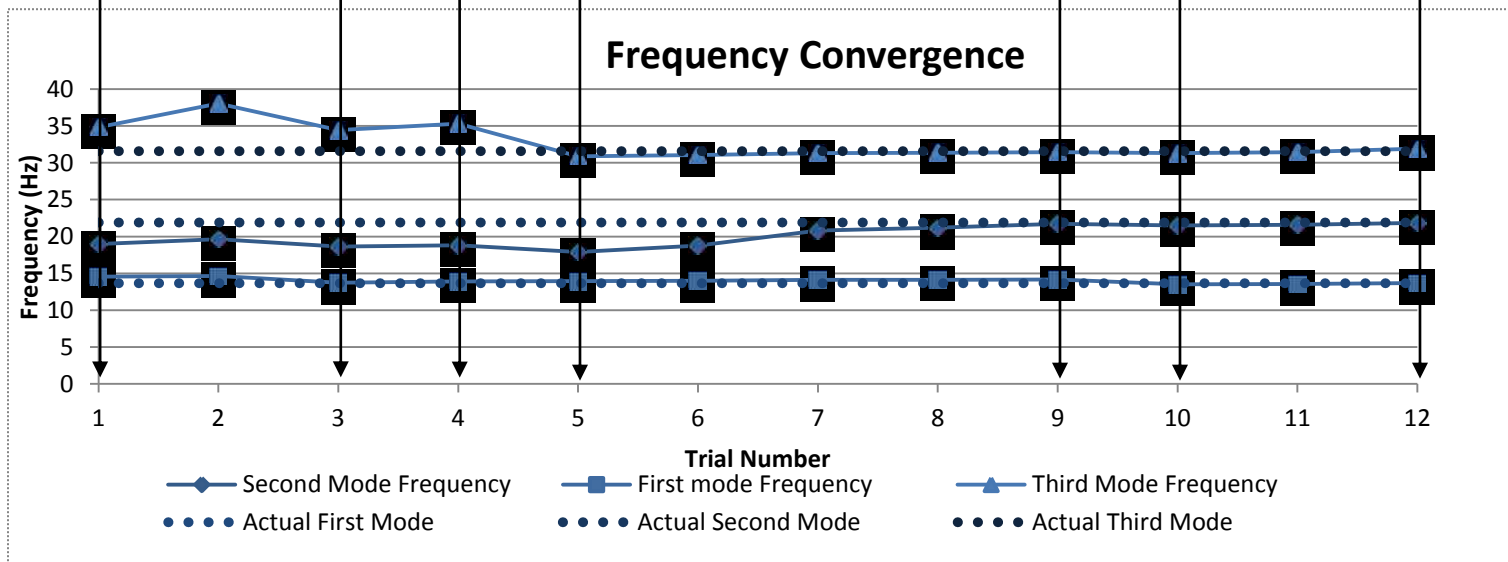
Figure 2.20 Trials of Converging to Natural Frequencies
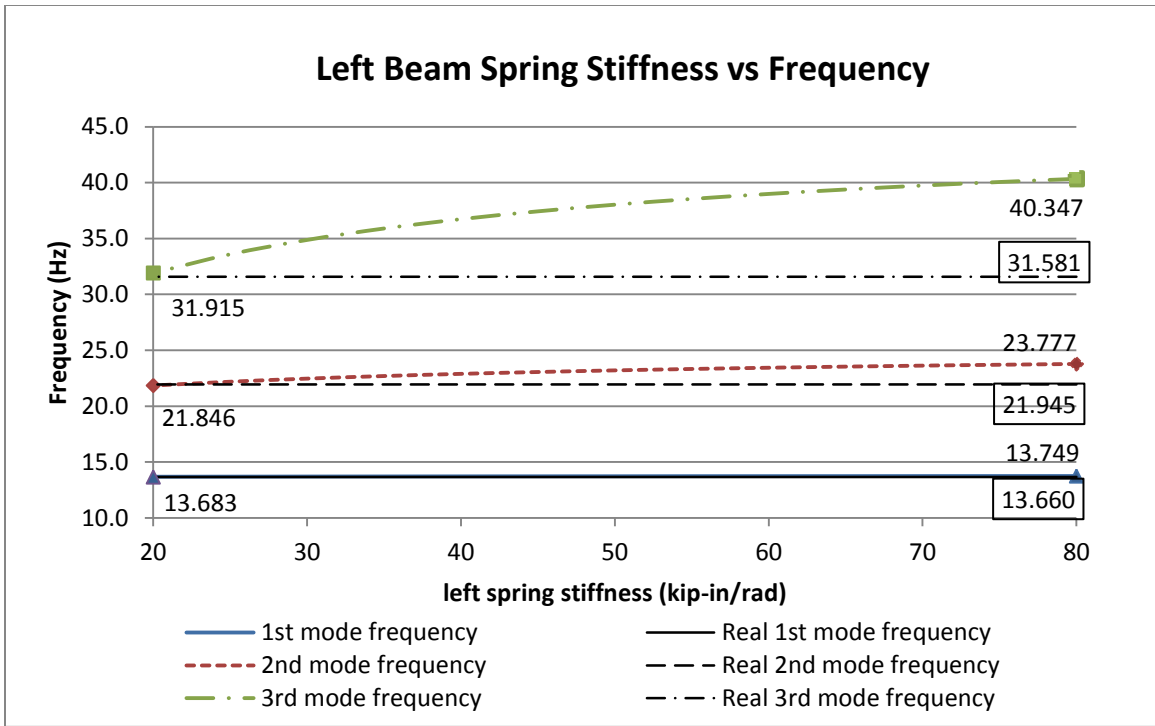
Figure 2.21 Left Beam Spring Stiffness vs. Frequencies
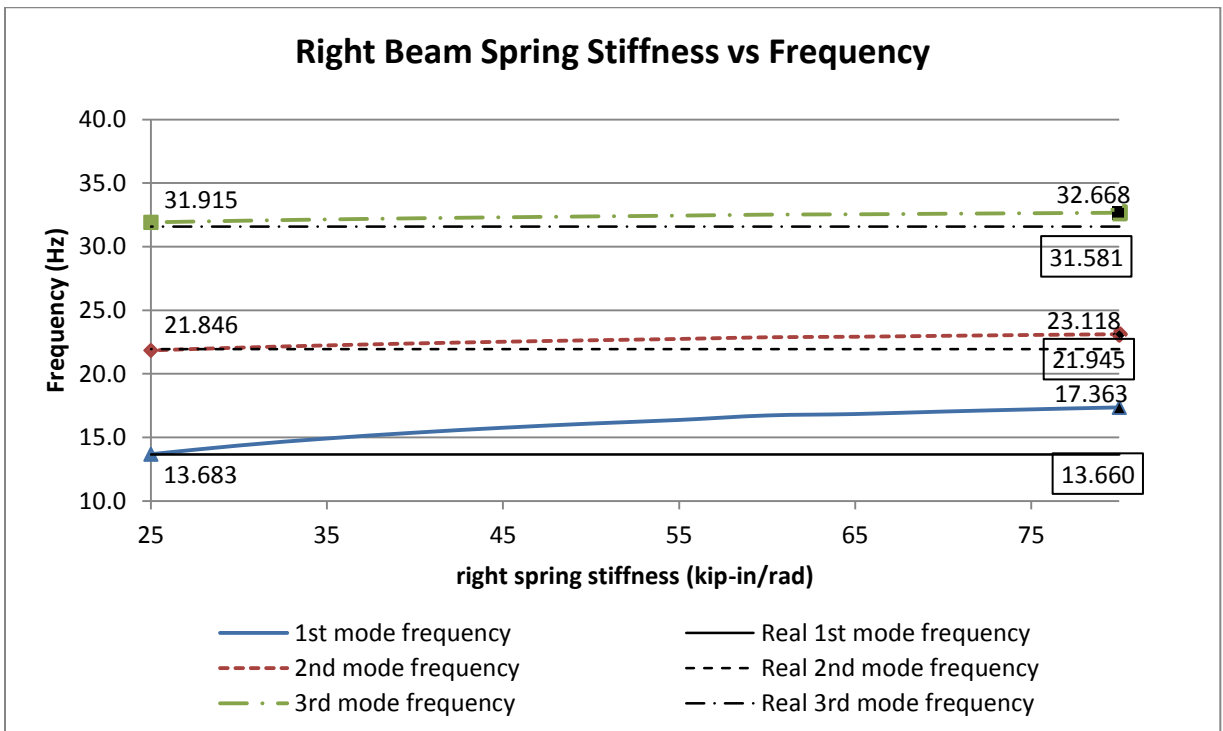
Figure 2.22 Right Beam Spring Stiffness vs. Frequencies
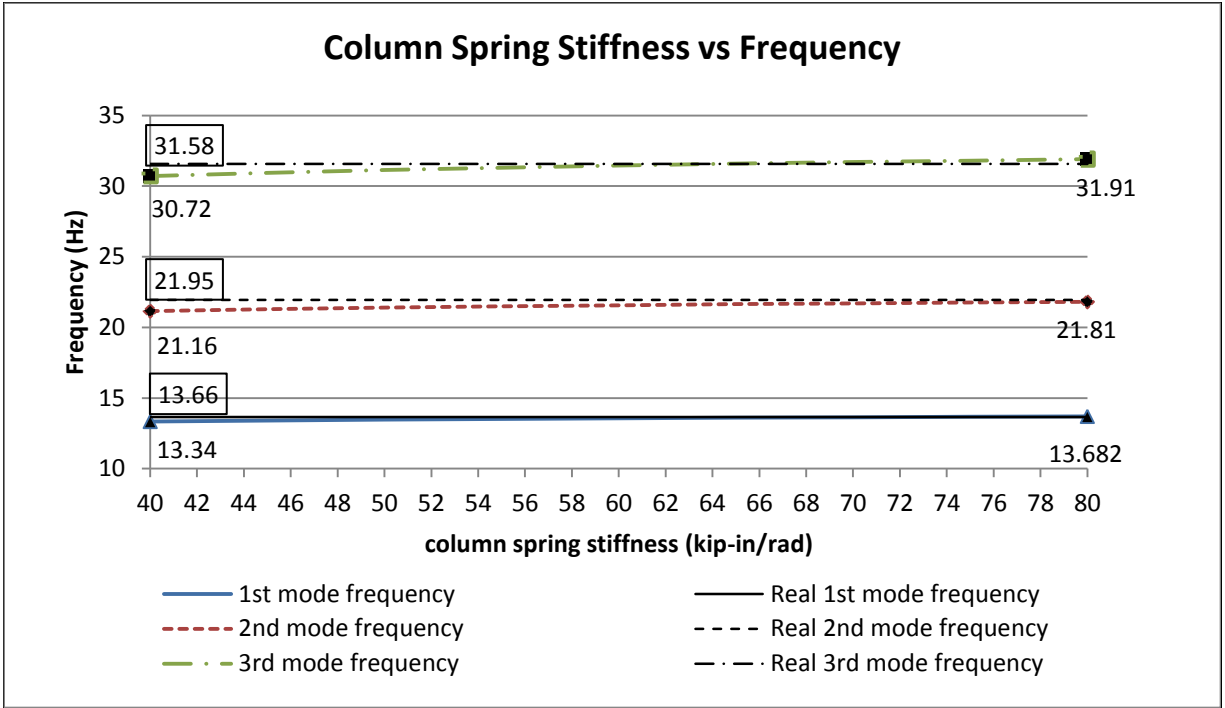
Figure 2.23 Column Spring Stiffness vs. Frequencies
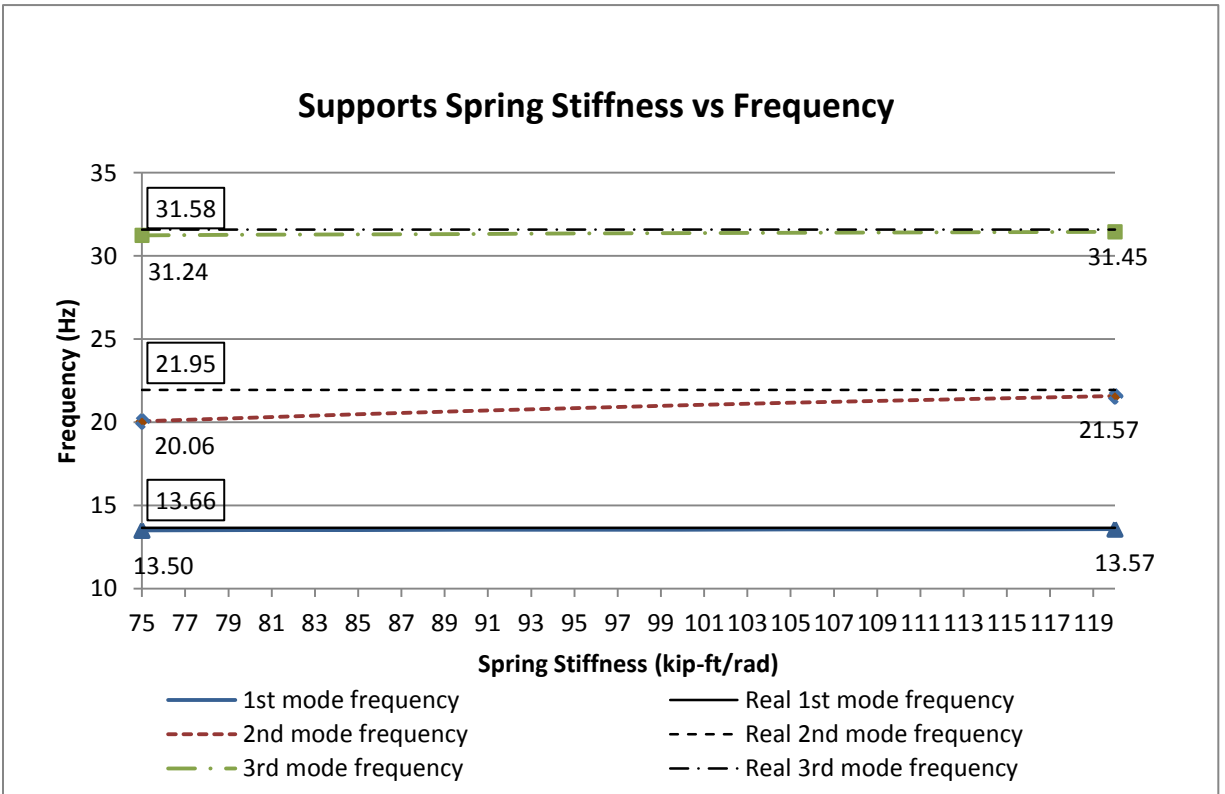
Figure 2.24 Supports Spring Stiffness vs. Frequencies
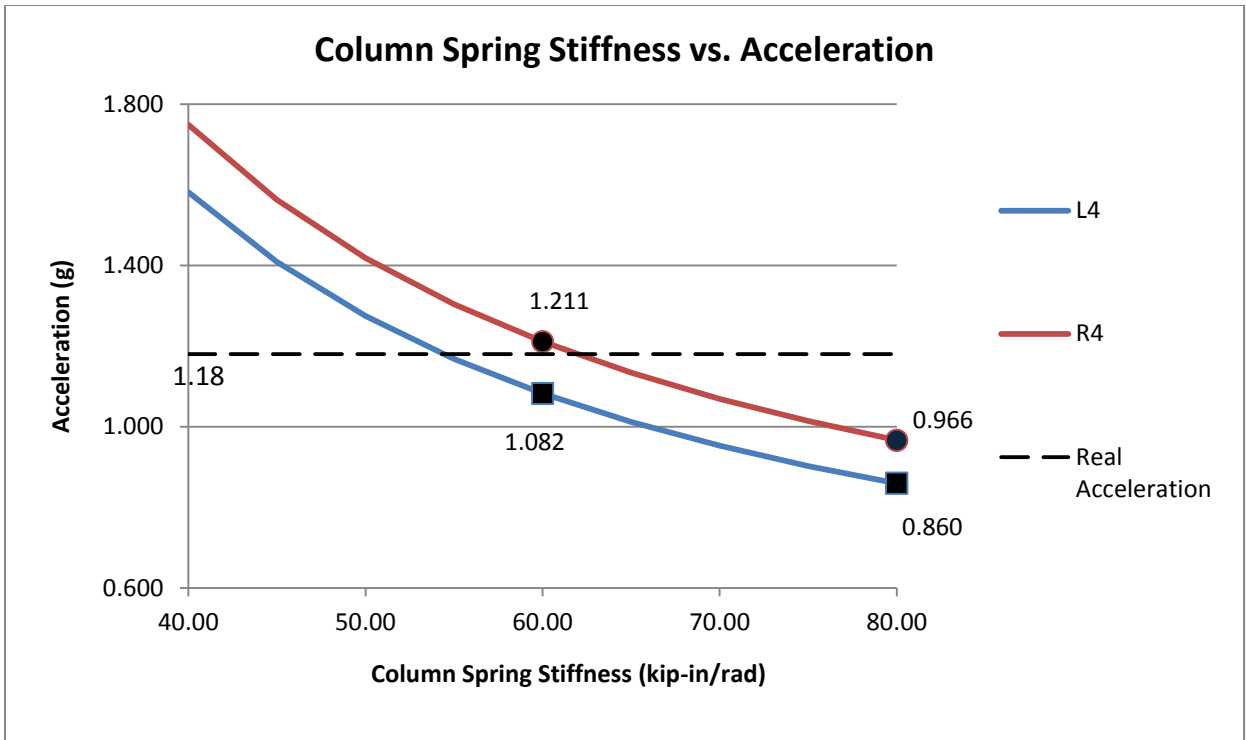
Figure 2.25 Column Spring Stiffness vs Acceleration

Chapter 3 Single-Variable Linear Regression Based Damage Detection Algorithm

3.1 Introduction

This chapter presents the application of single-variable linear regression based method to damage detection. Both simulated data and test data will be processed to verify the use of such method. Data from 21 nodes are divided into 3 groups, left (L), center (C) and right (R). All comparisons will be made inside each group to form a regional result of damage detection because local damage may affect not only the behavior on its own location but also the adjacent areas. Seven damage scenarios will be discussed in this chapter, LB, LBLC, CRB, CC, CRBCC, RB and RBRC. Also different forcing frequency cases will be applied on the structure in each damage scenarios. Details will be introduced in the following sections.

3.2 Single-variable Linear Regression and Its Solution

A single-variable linear regression describes a one-dimensional linear relationship between two variables, one dependent variable and one independent variable. It is first a statistical concept. In order to apply the single-variable linear regression to damage detection procedure, the structural foundation of the algorithm will be discussed and then the method to find a single-variable linear regression function using test data will be introduced.

3.2.1 Structural foundation

In this research, due to the limitation of experiment equipment, only one harmonic input force is subjected to the test frame. So all the modal responses can be achieved by solving the differential equations and are proportional to the input, P(t), which means,

$$\ddot{q}_i(t) = k_i \cdot P(t) \tag{3.1}$$

where k_i is a scalar and $P(t) = c \cdot \sin(\omega t)$, in which c is the peak value of the force and ω is the forced frequency.

Therefore, Equation 2.6 becomes

$$\ddot{u}_j(n) = \left(\sum \phi_{ji} \cdot k_i\right) \cdot P(n) \tag{3.2}$$

What inside the summary sign is a constant, since they all come from the properties of the structure and have nothing to do with the input. To simplify Equation 3.2, a scalar of K will be used to replace the term inside the summary sign.

$$\ddot{u}_j(n) = K_j \cdot P(n) \tag{3.3}$$

Hereby, the acceleration of one node can definitely be expressed by the acceleration of another node multiplied by a factor, shown in Equation 3.4,

$$\ddot{u}_i(n) = \frac{K_j}{K_i} \cdot \ddot{u}_j(n) = \beta_{ji} \cdot \ddot{u}_j(n) \tag{3.4}$$

Considering the fact of imperfectness of the initial condition of the experiments and noise and error that occurs in the process of recording data, an intercept term and an error term are added to the equation. So when applying single-variable linear regression, the estimated relationship between accelerations will be expressed as:

$$\widehat{\ddot{u}_i} = \beta_{ji} \cdot \ddot{u}_j + \gamma_i + \varepsilon_i , i = 1 \dots m \tag{Eq. 3.1}$$

$\ddot{u}_i$ = acceleration response from a specific node used as the independent variable

$\widehat{\ddot{u}_j}$ = estimated acceleration response of a node other than node i inside the group

β_{ij} = regression coefficient

γ_{ij} = intercept

ε_{ij} = error caused by modal truncation, initial imperfectness and noise during the test

For the convenience of referring, in this thesis, the independent node i and dependent node j together will be called a *node pair*. For example, when the independent node is L1 and the dependent node is L3, together they will be called *node pair L_{31}*.

3.2.2 Normal Equations in Matrix Form

For each node pair in one test, there were 10000 pairs of data points, $(\ddot{u}_i(n), \ddot{u}_j(n))$, to be analyzed. To estimate the best description of the linear relationship inside the node pairs, it's impossible to analyze the whole group of data point by point. With the help of modern computer, a more efficient and reliable way of estimating, matrix solution, was applied.

Any 10000 pairs of data points from a node pair produce the estimating equation

$$Y = X \cdot \widehat{\beta} \qquad \text{(Eq. 3.6)}$$

where

$$Y = \begin{bmatrix} Y_1 \\ Y_2 \\ \vdots \\ Y_n \end{bmatrix}_{n\times 1} , \qquad X = \begin{bmatrix} 1 & X_1 \\ 1 & X_2 \\ \vdots & \vdots \\ 1 & X_n \end{bmatrix}_{n\times 2} , \qquad \widehat{\beta} = \begin{bmatrix} \alpha \\ \beta \end{bmatrix}_{2\times 1}$$

Elements inside Y and X matrix are from the test data, the only unknown or to-be-estimated matrix is the $\widehat{\beta}$ matrix. To solve for the coefficient matrix $\widehat{\beta}$, transformation will be made in Eq. 3.3. An X' (the transpose of X) matrix is left-timed on both sides of Eq. 3.2 to get,

$$X' \cdot Y = (X' \cdot X) \cdot \widehat{\beta} \qquad \text{(Eq. 3.7)}$$

Since the matrix $(X' \cdot X)$ is non-singular, the inverse operation can be applied on it. A $(X' \cdot X)^{-1}$ matrix is then left-timed on both sides. Hereby

$$\widehat{\beta} = (X' \cdot X)^{-1} \cdot (X' \cdot Y) \qquad \text{(Eq. 3.8)}$$

The coefficient matrix can be achieved by solving Eq. 3.8.

3.2.3 Correlation

Although the linear relationship between dynamic responses from two nodes is found in the previous section, still the strength of such linear relationship, meaning that to what extent those two variables are alike, should be checked. The *coefficient of determination* (CoD), R^2, is introduced as an estimator of the degree of a linear relationship (Young 1979). It can be calculated as

$$R^2 = 1 - \frac{SS_{err}}{SS_{tot}} \qquad \text{(Eq. 3.9)}$$

Where,

$SS_{err} = \sum_i (y_i - f_i)^2$, the residual sum of squares;

$SS_{tot} = \sum_i (y_i - \bar{y})^2$, the total sum of squares;

y_i = data values;

f_i = modeled values;

$\bar{y} = \frac{1}{n} \sum y_i$, the average value of y.

Some examples, in Figure 3.1, are made to show the strongly linear-related variables and the weakly linear-related variables. Figure 3.1a and 3.1b show the relationships of two different strengths. When r^2 gets larger, data points on the plot intend to get closer to the estimated line which means they have a stronger linear relationship. Figure 3.2 is a ruler of categorizing the strength of linear relationship with R

from Younger (1979) in which the negative sign indicates an inverse linear relationship and positive sign indicates a direct linear relationship. According to this ruler, case in Figure 3.1.a has a moderate positive linear relationship; case in Figure 3.1.b has a moderately strong relationship.

Such determination is used in data processing to rule out those not strongly related, i.e. the value of CoD is smaller than 0.8, cases to make sure the results will be representative.

3.3 Damage Indicator

It is commonly known that the function for a straight line in a two-dimensional Cartesian coordinate system can be presented as

$$y = \beta \cdot x + e \tag{Eq. 3.10}$$

Comparing Eq. 3.5 with Eq. 3.10, one can see that they have the similar form if the error term in Eq. 3.5 becomes negligible. That means if the estimated node acceleration response is plot against the independent node acceleration response, a straight line can be expected in the plane.

As mentioned in Section 2.1, the linear relationship inside a node pair will change when damage occurs. When goes to the linear regression method, it'll be reflected on the difference in coefficient matrix before and after damage. And on the 2-D plane, one will see two straight lines, one for linear relationship before damage and one for that after damage, for one node pair. Brief demonstration is shown in Figure 3.3. The angle, α, between those two straight lines will be used as the damage indicator. Assumption is

made to be that the closer a node is to the damage location, the larger α for a node pair

that includes this node can be.

3.3.1 Solution for α

Suppose the linear function for undamaged case is

$$y = \beta \cdot x + e \qquad \text{(Eq. 3.11)}$$

and the linear function for the damaged case is

$$y' = \beta' \cdot x' + e' \qquad \text{(Eq. 3.12)}$$

There will be a vector parallel to the undamaged line, $v = (\beta, -1)$ and another vector

parallel to the damaged line, $v' = (\beta', -1)$. Now finding the angle between two straight

lines will be finding the angle between the two vectors. Eq. 3.13 will be applied.

$$\alpha = \cos^{-1} \left| \frac{v \cdot v'}{\|v\| \cdot \|v'\|} \right| = \cos^{-1} \left| \frac{\beta \cdot \beta' + 1}{\sqrt{\beta^2 + 1} \cdot \sqrt{\beta'^2 + 1}} \right| \qquad \text{(Eq. 3.13)}$$

Since only the acute angle will be looked at in the comparison, if α is larger than π/2, the

supplementary angle of it will be used.

3.3.2 Control indicator

In order to estimate the influence of noise and measurement error in the damage detection

result, a control indicator, α', is introduced.

$$\alpha' = \cos^{-1} \left| \frac{v_1' \cdot v_2'}{\|v_1'\| \cdot \|v_2'\|} \right|$$

v_1' and v_2' are both coefficient vectors from undamaged cases. Theoretically, if there is

no any kind of noise and measurement error, v_1' and v_2' should be exactly the same. So

the control indicator will be zero in this case. However, in the real tests, noise and

measurement error always exist. Sometimes they can be fairly high, enough to cover the

change caused by the damages. In this algorithm, each damage indicator will have a corresponding control indicator. If the control indicator is as equally high as the damage indicator, it means the change of structural behavior in this area is controlled by noise and measurement error, not structural damage. In another word, damage may or may not exist in the area, but the damage indicator is unable to give useful information since it is affected mostly by noise and measurement error. Examples will be shown in the following sections.

3.4 Test Results

Totally 7 damage scenarios combined with 2 kinds of harmonic inputs will be introduced in this section. The damage scenarios are shown in Figure 3.4 and damage location a labeled with blocks. They are damage scenario LB, LBLC, CC, CRB, CRBCC, RB and RBRC. Among these damage scenarios, LB, CC, CRB and RB have only one damage in each case. The LBLC, CRBCC and RBRC damage scenarios all have two damages which the structure is expected to be weaken more seriously than those who have only one damage. And the input cases are a 16Hz sinusoidal input and a 30Hz sinusoidal input. Meanwhile, control tests, tests that calculate the damage indicators between two undamaged cases, will also be conducted for each damage scenario and input combination to set up a base line for the damage indicators. Those damage indicators in control tests will be referred as control indicators in the following sections and chapters.

The levels of detection are divided into 4 categories:

Level 1: The exact or approximate damage location is identified;

Level 2: multiple possible damage locations are identified including the real damage location;

Level 3: False damage location is identified;

Level 4: No clear damage prediction can be made.

Cases that give level 2 or higher level predictions are considered successful.

3.4.1 Simulation Test Results

First simulation tests are conducted to see the performance of the single-variable linear regression algorithm. The finite element model used here is the one that is updated in section 2.7, which has the same natural frequencies and dynamic behavior of the real lab frame. Results will been shown in stem plots. The subjected input is the 16Hz sinusoidal inputs.

3.4.1.1 Damage Scenario LB

Figure 3.5 is the result of damage scenario LB with 16Hz input. One can see that damage indicators, labeled with round stems, in the L group are relatively much higher than those in the other two groups. This means a large change in structural properties is found around the left joint, which indicates damage has occurred there. A level 1 prediction is made in this case, although larger damage indicators on node L5 and L6 may suggest that the damage is more likely on the left column.

3.4.1.2 Damage Scenario LBLC

Figure 3.6 is the result of damage scenario LBLC. One can observe that damage has been predicted around the left joint which is a level 1 damage prediction. Due to the further

weakening of the left joint (an additional damage on the left column compared with damage scenario LB), damage indicators in the L group all have increased a little and so do the ones in the C group.

3.4.1.3 Damage Scenario CRB

In damage scenario CRB, shown in Figure 3.7, one can see large α values both in group C and group R. To be specific, large numbers appears at node C1 to C6 and R1 to R3. It may seems that damages locate on both the center joint and the right joint, however, according to the known damage location, large α values at node R1 to R3 are false alarms of damage. So a level 2 damage prediction is given in this case. A possible explanation for this may be that although damage is on location CRB, it may have effects on the other end of the same beam, i.e. location RB. The behavior of nodes around location RB may also be altered, thus cause the appearance of large damage indicators at node R1, R2 and R3.

3.4.1.4 Damage Scenario CC

Figure 3.9 is the result of damage scenario CC. One can observe that, in this figure, large damage indicators are on nodes from C1 to C5, which are nodes on the beam of the center joint. Since the result predicts damage on the beam of the center which is not the real damage location, a level 3 prediction is made in this case. But as an estimation of local damage on the whole structure, it provides enough information about the damage location.

3.4.1.5 Damage Scenario CRBCC

Figure 3.9 is the result of damage case CRBCC. Damage case CRBCC is basically a combination of damage case CRB and damage case CC. Damages locate both on location CC and location CRB. The general distribution of the damage indicators is much alike to the one in damage case CC, but each individual damage indicator is larger, especially for nodes in group R. It makes sense since an extra damage exists in this case compared with damage scenario CC. The total stiffness of the structure has decreased and larger changes are expected in dynamic responses from all nodes. Predictions about damage are made on location CLB, CRB and RB. So a level 2 prediction is made in this case.

3.4.1.6 Damage Scenario RB

It is not clear from Figure 3.10 that damage is at location RB or at location CRB and CLB since node C1 to C6 and R1 to R4 all have large damage indicators. Although R1 has the largest damage indicator which implies that damage is more likely at location RB, the possibility that there is damage on the beam close to the central joint can not be ignored. A level 1 prediction is made. The reason for node C1 to C6 to have large damage indicators may be the same as the one given in Section 3.4.1.3 for damage scenario CRB, damage on one end of the beam may have affected the behavior of the other end of the beam.

3.4.1.7 Damage Scenario RBRC

An extra damage on the right column is added to damage scenario RB to produce the damage scenario RBRC. The result is shown in Figure 3.11, damage is predicted on the right joint since damage indicators in group R are larger than the others and the largest α is on node R1. A level 1 prediction of damage is made in this case.

52

3.4.2 Simulation Test Result against Noise

Since noise, for example ambient vibration and error in data transferring, will show in the real tests, it is necessary to perform the damage detection algorithm against the disturb of noise. Both 5% noise and 10% noise is added to the original simulation data, Figure 3.12 gives examples of data before and after the noise is added. As can be observed from the figures, 10% noise gives a more severe disturb on the original data while the effect of 5% noise is quite slight. Test results will show in the following section.

3.4.2.1 Damage Scenario LB

Figure 3.13a and b give the result of damage scenario LB against 5% noise and 10% noise, respectively. In the 5% noise case, the control indicators are averaging at 0.052 and damage indicators in group C and group R have almost the same amount while those in group L are much larger than their corresponding control indicators. The fact that damage indicators and control indicators in C and R group are almost the same means structural responses haven't changed much from undamaged case to damaged case, i.e. damage has little effects on the structural behaviors in those two areas. And the conclusion comes to that damage occurs on the left joint. In the 10% damage case, damage indicators in C and R group have increased. However, their corresponding control indicators also have increased at the same time. The two kinds of indicators still remain at the same level. Only damage indicators in the L group are much larger than their corresponding control indicators. Level 1 predictions are made for both noise cases.

3.4.2.2 Damage Scenario LBLC

Figure 3.14a and b are the result for damage case LBLC. Same situation happens here as in the damage case LBLC. While damage indicators in group L haven't changed much, both damage indicators in group C and group R and all the control indicators have increased as the level of noise increases. Damage can be identified on the left joint in both cases, which are level 1 predictions.

3.4.2.3 Damage Scenario CRB

Figure 3.15a and b are the result of the damage scenario CRB. When 5% noise is added to the data, only node C1 to node C6 and node R1 to node R3 are clearly larger than their control indicators. One can draw the same conclusion as in Section 3.4.1.3 that damage may locates on location CRB and CLB or on location RB. However when the level of noise gets to 10%, damage indicators for node C1 to node C5 can no longer be considered useful indicators for damage detection since their corresponding control indicators are not clearly less than themselves. A level 2 prediction is made for the 5% noise case and a level 3 prediction is made for the 10% noise case.

3.4.2.4 Damage Scenario CC

Results of damage case CC with 5% noise and 10% noise are shown in Figure 3.16a and b. The damage location is identified when 5% noise is added. One can clearly see that the possible location of damage is on the beam of the central joint. Although the predicted damage location is wrong, it's close to the actual one. In Figure 3.16b, the result for 10% noise case is less clear. Although damage indicators for node C1 to node C6 are still

larger than their corresponding control indicators, the differences are not so big to make solid conclusion about the damage location. A level 3 prediction is made for the 5% noise case and a level 4 prediction is made for the 10% noise case.

3.4.2.5 Damage Scenario CRBCC

Results are shown in Figure 3.17a and b for 5% noise and 10% noise case, respectively. For the 5% noise case, excluding nodes that are not clearly large than their control indicators, one can see damage is more possibly on the beam of the central joint on the right joint, although there is also a damage on the center column. And for the 10% noise case, the same conclusion can be drawn. A level 2 prediction can be made for both cases. Since the frame is deeper weakened than case CRB and case CC, it make sense that damage locations are more clearly detected and the algorithm can resist a higher level of noise.

3.4.2.6 Damage Scenario RB

Figure 3.18a and b give the result of damage case RB with 5% and 10% noise. In the 5% noise case, shown in Figure 3.18a, it is clear that damage is around location R1, which is on the beam of the right joint. Control indicators have increased in this case but not large enough to change the identified damage location. In the 10% noise case, the difference between damage indicators for node C1 to node C6 and that for node R1 is not as much as that in the 5% noise case. So the prediction of damage location is either on the beam of the center joint or on the beam of the right joint. It is not so clear as before and also a false prediction is included. A level 1 prediction is made for the 5% noise case and a level 2 prediction is made for the 10% noise case.

3.4.2.7 Damage Scenario RBRC

In the damage scenario RBRC whose results are shown in Figure 3.19a and 3.19b, damages are clearly detected on the right joint with both 5% noise and 10% noise. One thing needs to be mentioned is that damage indicators in group L and group C are not much less than those in group R, except the damage indicator for R1. The result of having such the prediction of damage is that the corresponding control indicators in group L and group C are almost at the same level as the damage indicators. As mentioned before, the fact that a damage indicator is equally large as its corresponding control indicators indicates that the behavior of the structure at this particular location has not been altered much by the occurring of damage. So level 1 predictions can be made for both cases.

3.4.3 Lab Test Results with 16Hz Harmonic Input

After doing tests on the finite element model and getting promising damage detection results, the same damage scenarios were performed on the steel frame introduced before in the lab. Data from all seven damage scenarios, LB, LBLC, CRB, CC, CRBCC, RB and RBRC with an sinusoidal 16Hz input generated by the actuator were processed and the their results are shown in the following sections.

3.4.3.1 Damage Scenario LB

As one can see in Figure 3.20, the result for this damage case is not good. Damage indicators in group C, especially C7, C8 and C9, are larger than those in group L, which in theory should be the larger ones. A level 3 prediction is given in this damage case.

3.4.3.2 Damage Scenario LBLC

In this case, whose result is shown in Figure 3.21, damage indicators in group L are clearly larger than all the other damage indicators, which is a level 1 damage prediction.

3.4.3.3 Damage Scenario CRB

Figure 3.22 is the result for damage scenario CRB. Damage prediction points at location CRB where locates node C5 and C6, because node C5 and C6 are the two largest damage indicators. This result successfully predicts the real location of damage. A level 1 damage prediction is made in this case.

3.4.3.4 Damage Scenario CC

Figure 3.23 is the result for damage case CC. It is clear that damage should locate on the center joint since all damage indicators in group C are generally larger than the others. But it will be a problem if one needs a more accurate location of damage, because nodes on the center column, C7 to C9, and nodes on location CRB, C4 to C6, are having the close values. So a level 2 prediction is made in this case. Supplemental detection ways are needed to detect the exact location of damage.

3.4.3.5 Damage Scenario CRBCC

From the result shown in Figure 3.24, one can see damage indicators on the center are large which indicates the whole central joint is damaged, although the real damage s only exist on the central column and the right beam. A level 2 prediction is made.

3.4.3.6 Damage Scenario RB

Figure 3.25 gives the result of damage case RB. Since the largest damage indicator is seen on node R3, damage is most likely be found on the right end of right beam. But as one can see, nodes in group C also have large α values, thus the possibility of damage locating on the central joint cannot be completely ignored. A rough level 1 prediction is made in this case.

3.4.3.7 Damage Scenario RBRC

Figure 3.26 is the result of damage case RBRC. Large damage indicators are found for nodes R3, R4 and R5. It's a clear demonstration that damage locates on the right joint. And since the three nodes locate on the beam and the column respectively, there may be multiple damages on the frame, which is real situation. However the possibility that there is damage on the central column still can not be ignored. A rough level 1 prediction is made in this case.

3.4.4 Lab Test Results with 30Hz Harmonic Input

Considering the fact that when a sinusoidal input is subjected onto a system, the vibration shape will be determined and in certain shapes, some part of the system will experience very slight vibrations. It may affect the performance of the damage detection algorithm since when the forced vibration is not large enough when compared with noise, the data won't be representative. In order to see a more entire picture of the performance of this damage detection algorithm, tests with input that has a higher frequency, 30Hz, are conducted. Results are shown in the following sections.

3.4.4.1 Damage Scenario LB

Figure 3.27 gives the result of damage case LB with a 30Hz sinusoidal input. Large damage indicators are seen nodes L2 and C1. This means damages locate on the left beam, and possibly on both end of the beam. But according to the test setup, the only damage exists on left end of the left beam. The one on node C1 is a false alarm. However, compared with the result from the same case with 16Hz which only gives a level 3 detection, this result gives a level 2 detection which is a great improvement.

3.4.4.2 Damage Scenario LBLC

Figure 3.28 is the result of damage case LBLC with 30Hz input. Although a large α is seen on node C1, it is presented that damage indicators in group L all have relatively higher value than those in other groups. So damage is more likely locating on the left joint, and a level 1 damage prediction is given.

3.4.4.3 Damage Scenario CRB

From Figure 3.29 which is the result of damage case CRB with 30 Hz input, a level 1 damage prediction can be made that damage locates around node C4 which is on location CRB.

3.4.4.4 Damage Scenario CC

Result of this damage case is shown in Figure 3.30. The damage prediction is around node C4 while the real damage is on the center column. A level 3 prediction is made in this case.

3.4.4.5 Damage Scenario CRBCC

A level 2 prediction of damage is made for this damage case, shown in Figure 3.31. One thing worth to mention in this case is that the difference between the value of damage indicators on the damaged joint, the center joint and those on the undamaged joints are larger and clearer than that in the same damage case with 16Hz input. So there is no confusion about the damage locating on the central joint, although the specific damage location is unknown. A level 2 prediction is made in this case.

3.4.4.6 Damage Scenario RB

Figure 3.32 is the result for damage case RB with 30Hz input. The prediction is clear that damage exists on the right joint, to be specific, on the beam of the right joint. It is a clearer level 1 prediction of damage than the case with 16Hz input.

3.4.4.7 Damage Scenario RBRC

In this case, damage on the beam of the right joint is clearly predicted, shown in Figure 3.33. And damage indicators in group L and group C are also larger compared with the ones in the Figure 3.32, which in some aspect weakens the prediction of damage. But still it is a better prediction than that for the same case with 16Hz and it's a level 1 damage prediction.

3.5 Conclusion

After the four sets of test, finite element simulation tests, simulation tests with noise, lab tests with 16Hz input and lab tests with 30Hz test, the damage detection algorithm that applies linear regression is proved to be useful in detecting local damages in some level.

The damage detection results are organized in Table 3.1. And some other conclusions are made by analyzing the results from all the tests.

1) When comparing test results from simulation tests without noise and those from tests with noise, one can see that the value of a damage indicator that is in the damaged area, for example right joint would be the damage area in damage scenario RB and RBRC, doesn't change much when the level of noise rise. And those in the undamaged area do change according to the noise. Another thing is that when there is no noise, the damage indicator and control indicator for nodes in the undamaged area usually show big difference; however when more than a certain amount of noise is added to the data, 5% percent in this research, they will have close values, and the larger the noise is, the larger the values they will have. That means damage indicators in the undamaged area are controlled mostly by noise. When damage is added to the system, it does not change the linear relationship between structural behaviors in the area. It may also be criteria to detect damage when the noise is large.

2) It can be observed from some of the simulation tests that when damage is on one end of the beam, it will have effects on the other end of the right beam, which will make damage indicators on that area large. Examples can be seen in case CRB, in Figure 3.7. When damage is on the left end of the beam, damage indicators for nodes on the right end of the beam are also large. And there are some other cases in which situations may not be as clear as it is in case CRB, but conclusions can still be made that damage may not only

affects its adjacent area, but also areas far but on the same structural member. Further researches will also pay attention to this.

3) If the range of y axis for simulation test results and that for lab test results are compared, one can see that damage indicators in the lab tests are much larger than those in simulation tests. Take damage scenario LBLC with 16Hz input as an example. They both have a level 1 damage detection result. But for the simulation test, damage indicators in group L is around 0.2 while for the lab tests, they are around 3. There is an explanation this situation. The finite element model is too simplified that the only damage on the model is the reduction of stiffness of the damaged section. However, while doing the lab tests, all the actions on the frame, such as loosening the bolts, removing the undamaged/damaged interchangeable section, replacing it with the damaged/undamaged interchangeable section and tightening the bolts would slightly change the properties of the frame. Those changes are much bigger than simply reduction of stiffness, and so there are larger damage indicators. Further tests are needed to justify this explanation.

4) When inputs with different frequencies are subjected onto the frame, damage detection results can be different. Take one example from damage scenario LB, when a 16Hz input is subjected, only a level 3 damage detection can be achieved; but when a 30Hz is subjected, a level 2 damage detection is achieved. Another example will be damage scenario CRBCC, only this time the test with 16Hz input gives a better prediction of damage. Figure 3.34 is the vibration curvature of the frame for the 16Hz input test and the 30Hz

input test. Peak accelerations from all 21 nodes are picked out and plotted. When the input frequencies are different, different parts of the frame are excited. In the 16Hz input case, the right beams is more excited than any other parts of the frame, especially node R1,; while in the 30Hz input case, columns are the more excited the parts of the frame. Further researches are needed to determine the connection between the excited parts and the successful detection of damage on certain part of the frame.

Table 3.1 Damage Prediction Using Single-variable Linear Regression Based Algorithm Results Summary

Level of Damage Prediction		Damage Scenarios						
		LB	LBLC	CRB	CC	CRBCC	RB	RBRC
Simulation Tests		1	1	2	3	2	2	1
Simulation tests With noise	5%	1	1	2	3	2	1	1
	10%	1	1	3	4	2	2	1
Lab tests	16Hz	3	1	1	2	2	1	1
	30Hz	2	1	1	3	2	1	1
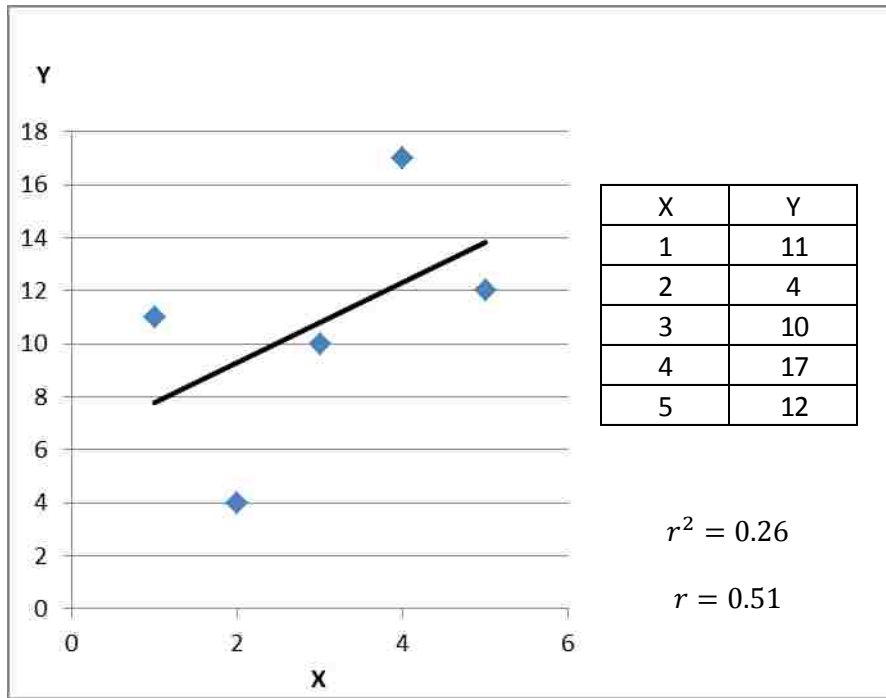
Figure 3.1.a An Example of Moderate Linear Relationship
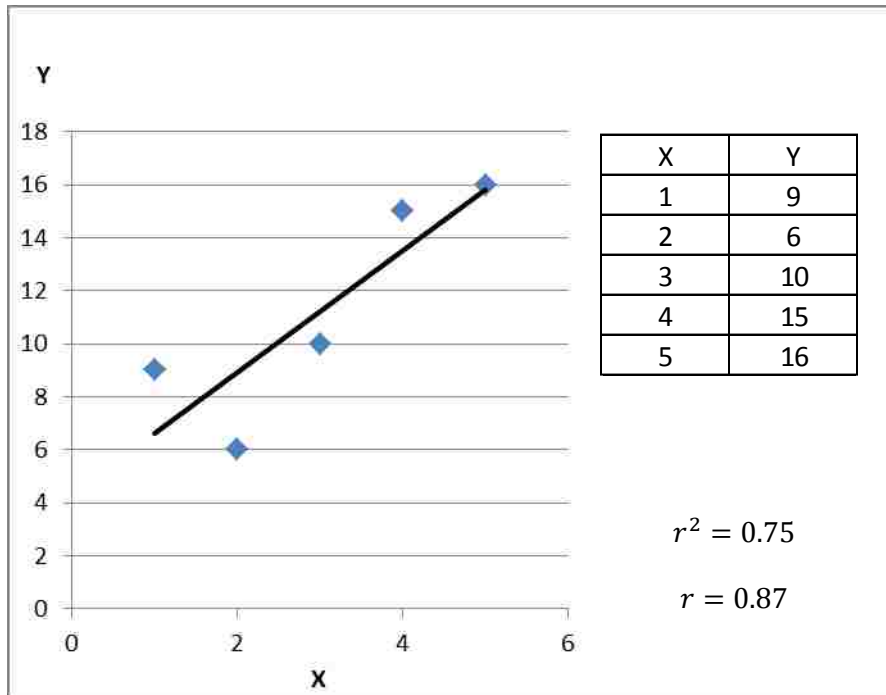
Figure 3.1.b An Example of Moderately Strong Linear Relationship
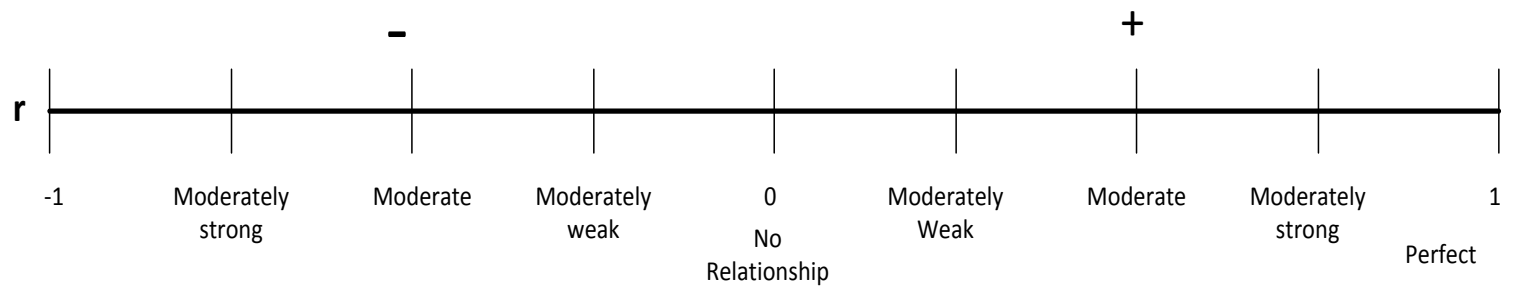
Figure 3.2 The Ruler of Corelation
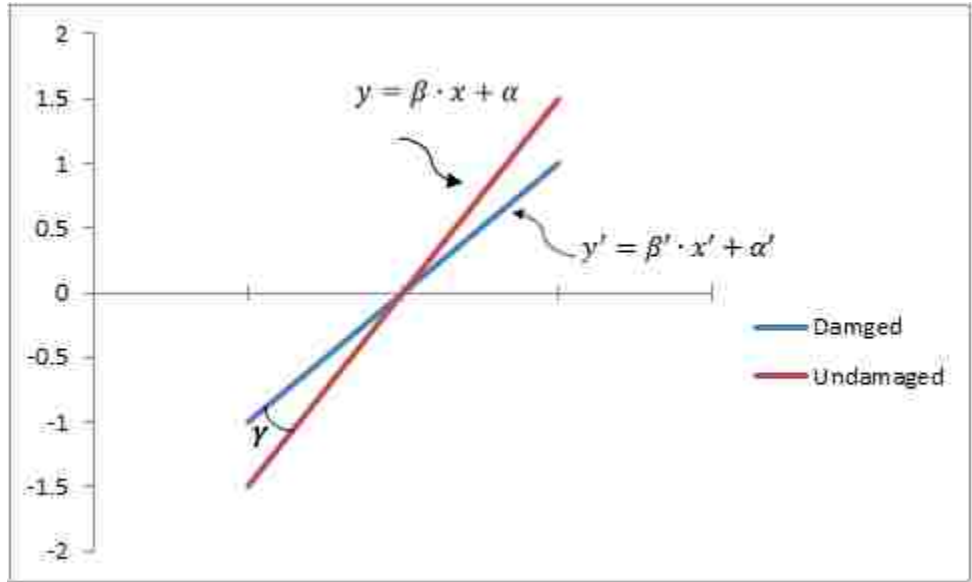
Figure 3.3 The Undamaged Case and The Damaged Case
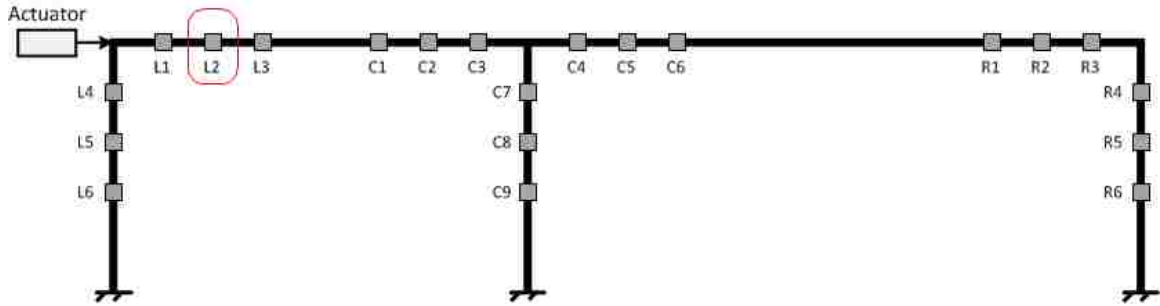
Figure 3.4a Damage Scenario LB
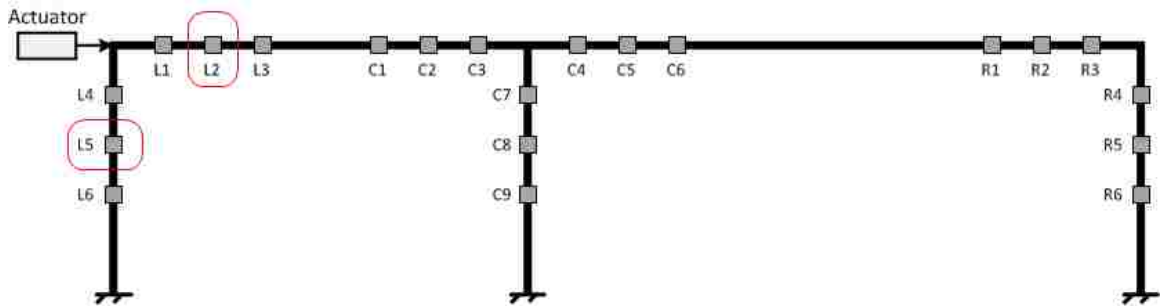
Figure 3.4b Damage Scenario LBLC
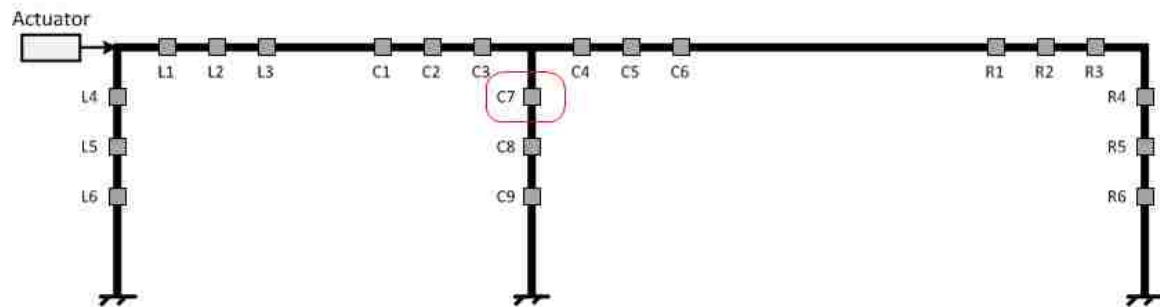
Figure 3.4c Damage Scenario CC
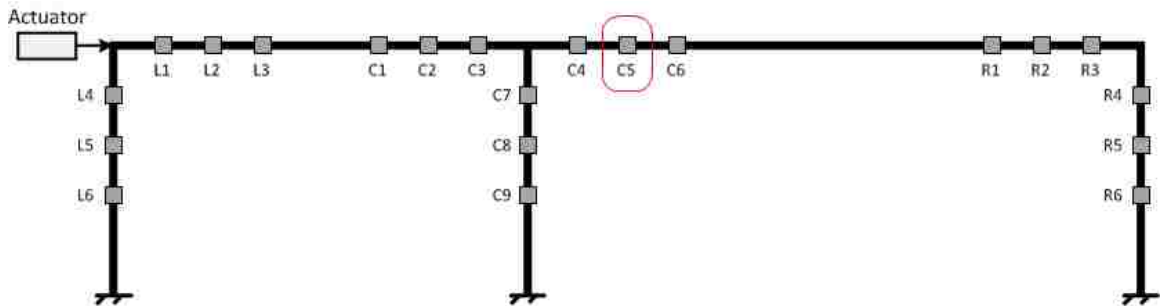
Figure 3.4d Damage Scenario CRB
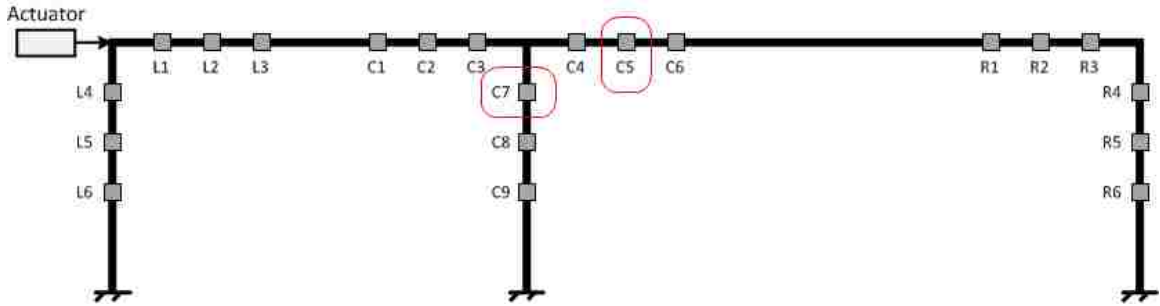
Figure 3.4e Damage Scenario CRBCC
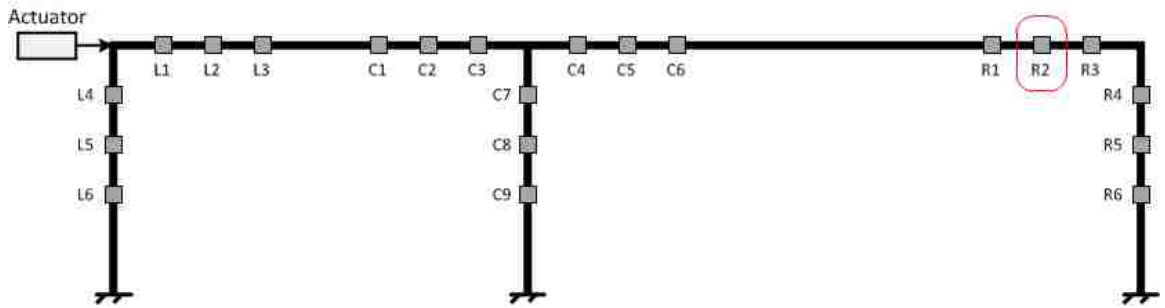
Figure 3.4f Damage Scenario RB
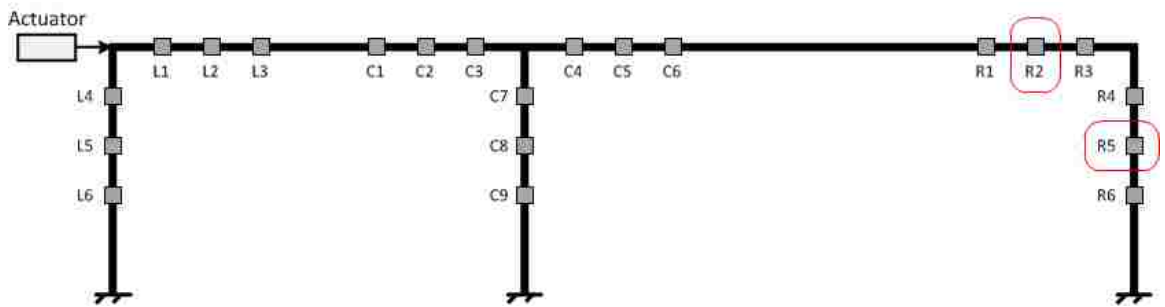
Figure 3.4g Damage Scenario RBRC
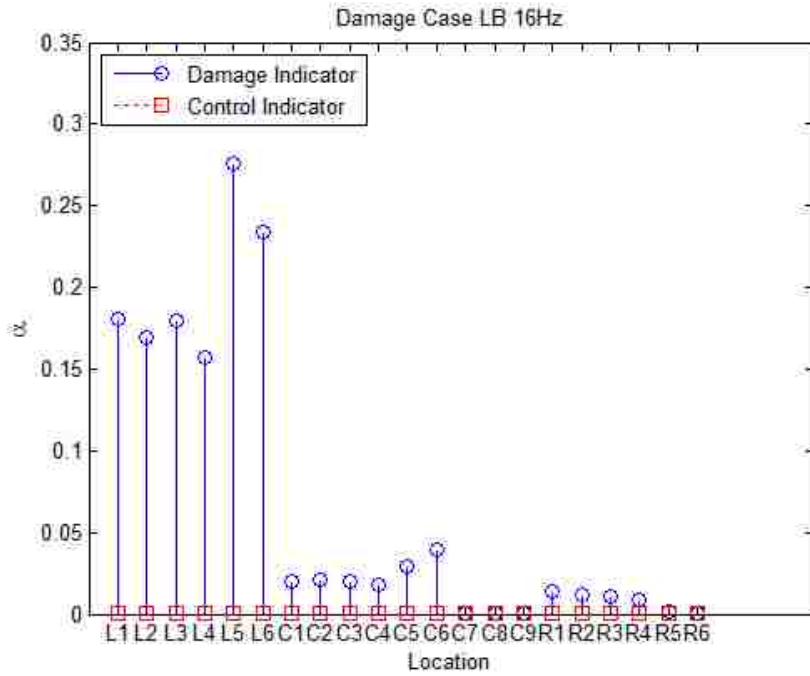
Figure 3.5 Simulation Damage Scenario LB with 16Hz Input
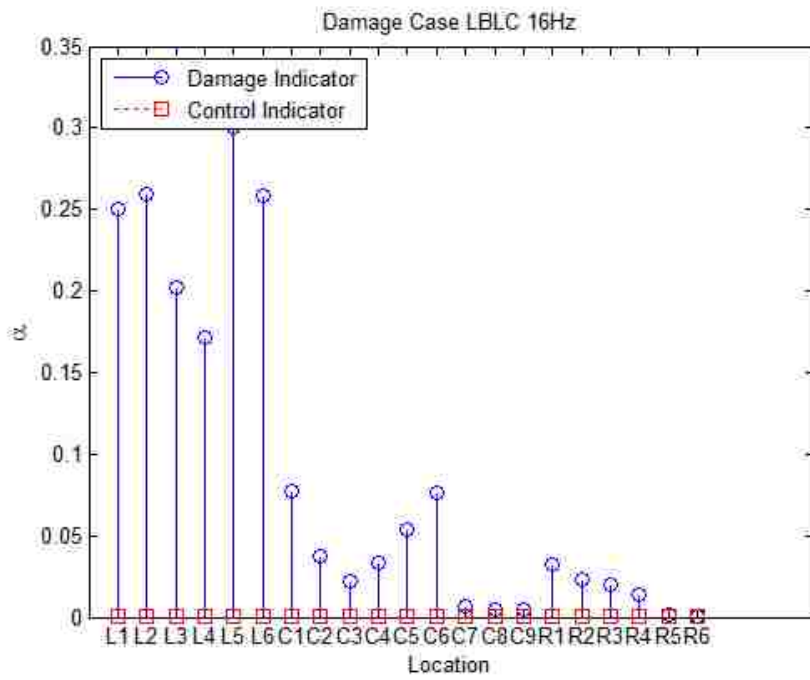
Figure 3.6 Simulation Damage Scenario LBLC with 16Hz Input
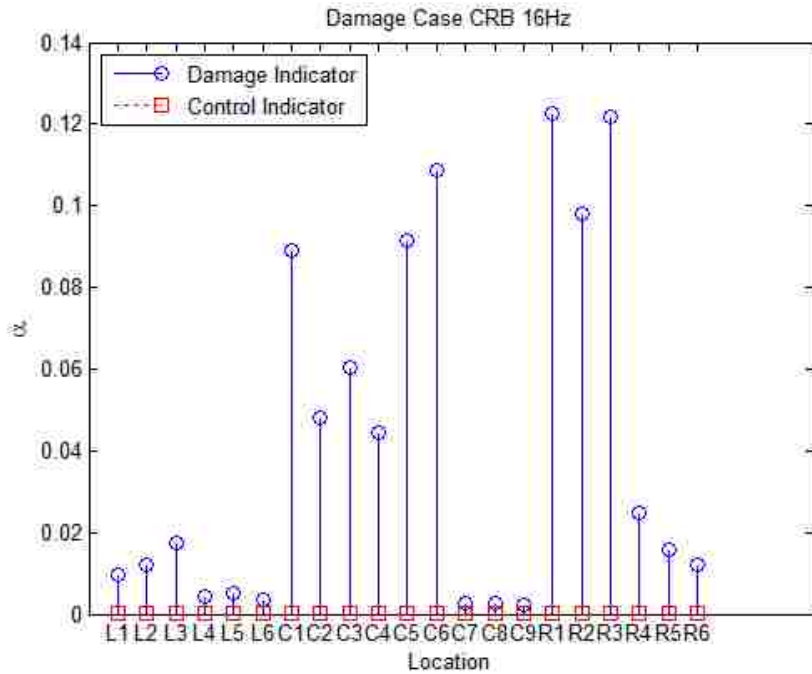
Figure 3.7 Simulation Damage Scenario CRB with 16Hz Input
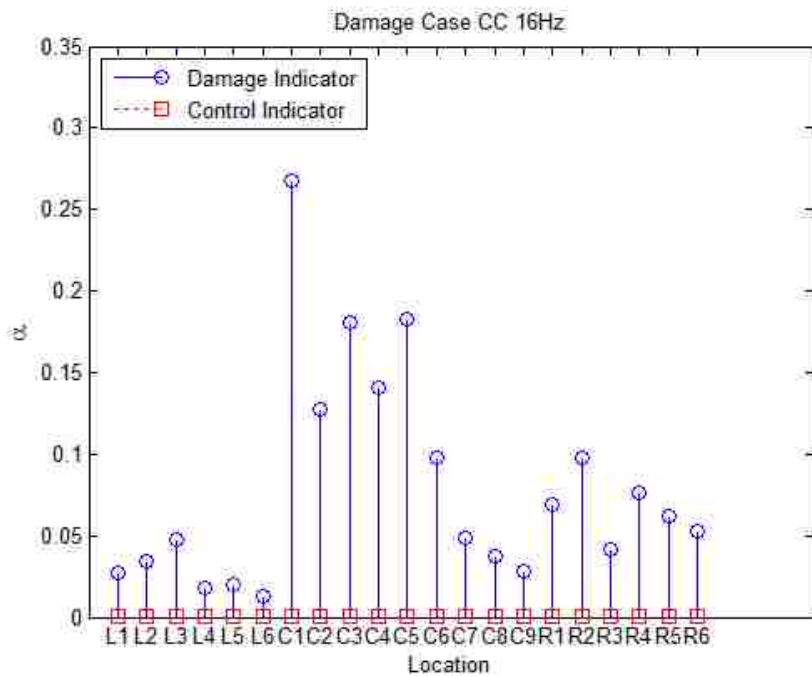
Figure 3.8 Simulation Damage Scenario CC with 16Hz Input

Figure 3.9 Simulation Damage Scenario CRBCC with 16Hz Input

Figure 3.10 Simulation Damage Scenario RB with 16Hz Input
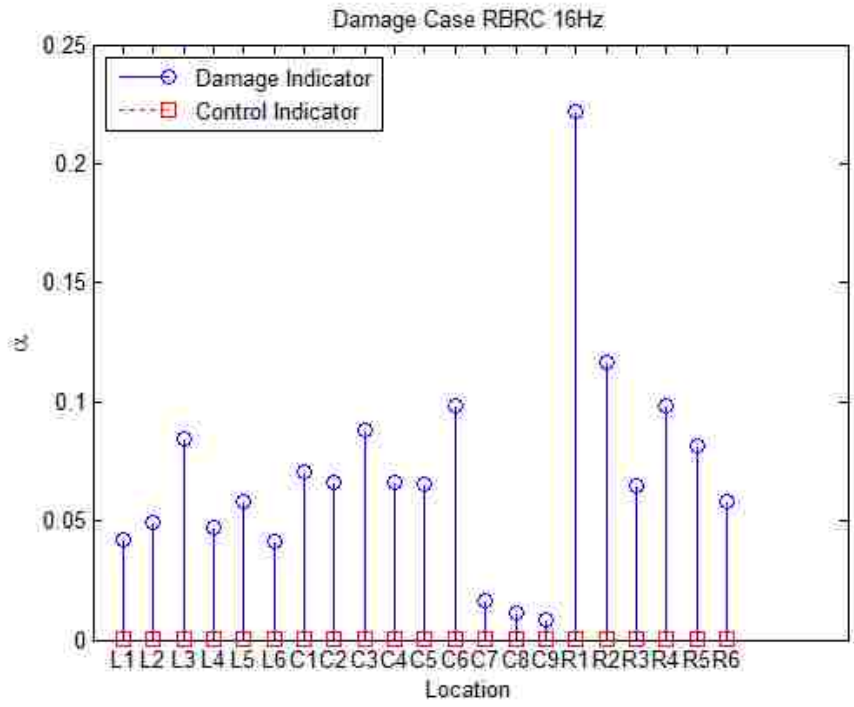
Figure 3.11 Simulation Damage Scenario RBRC with 16Hz Input
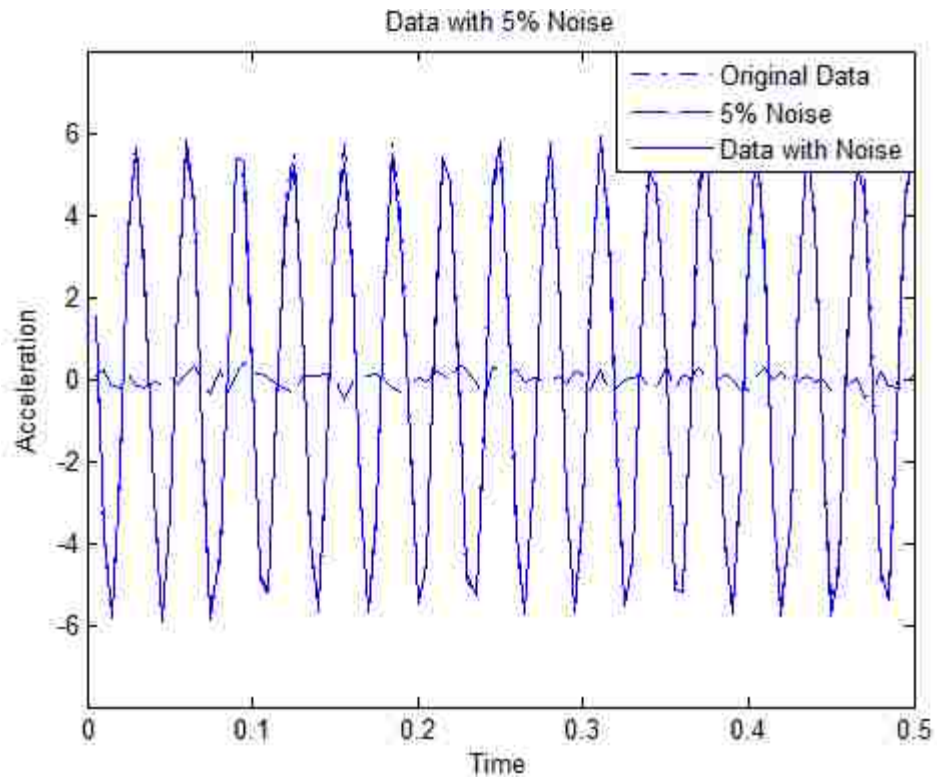
Figure 3.12a Original Data and Data with 5% Noise
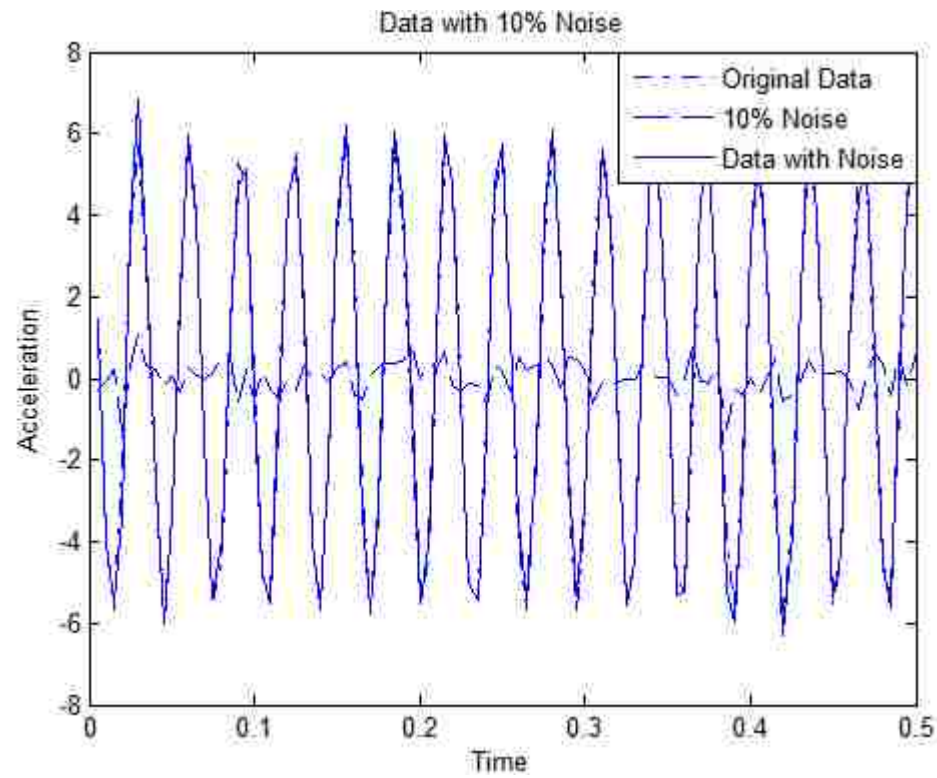
Figure 3.12b Original Data and Data with 10% Noise
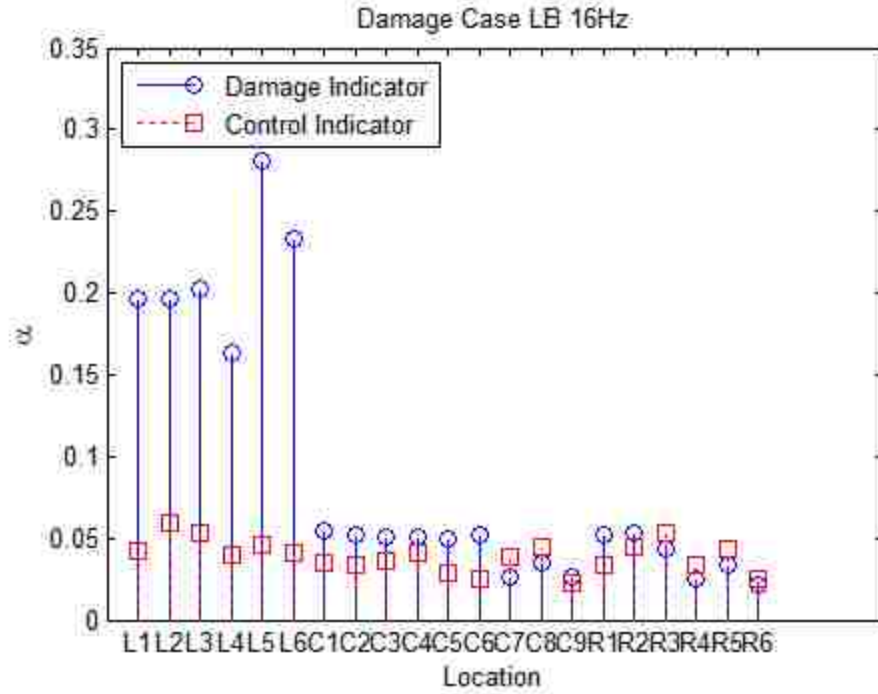
Figure 3.13a Simulation Damage Scenario LB with 5% Noise
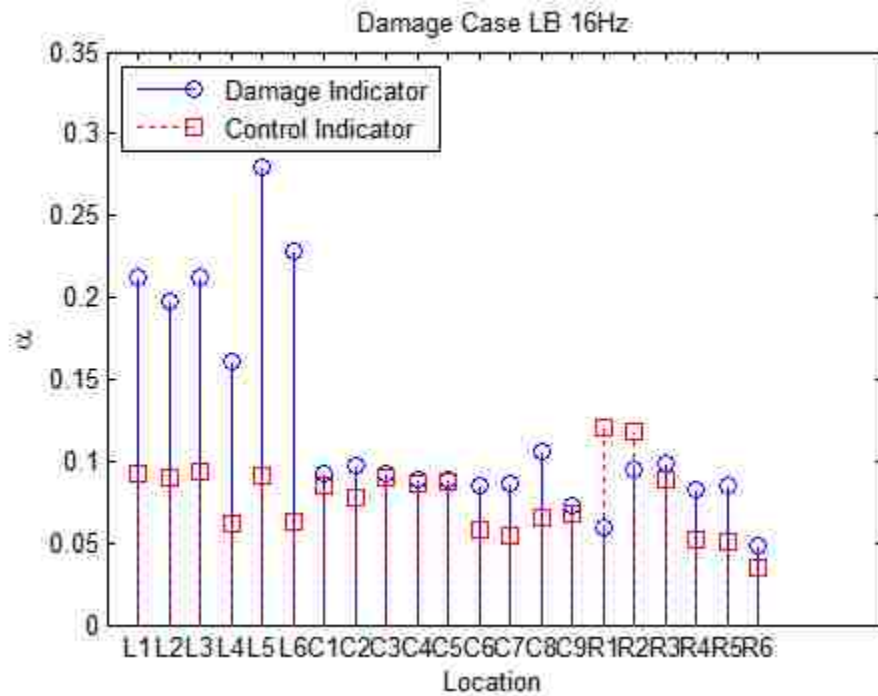
Figure 3.13b Simulation Damage Scenario LB with 10% Noise
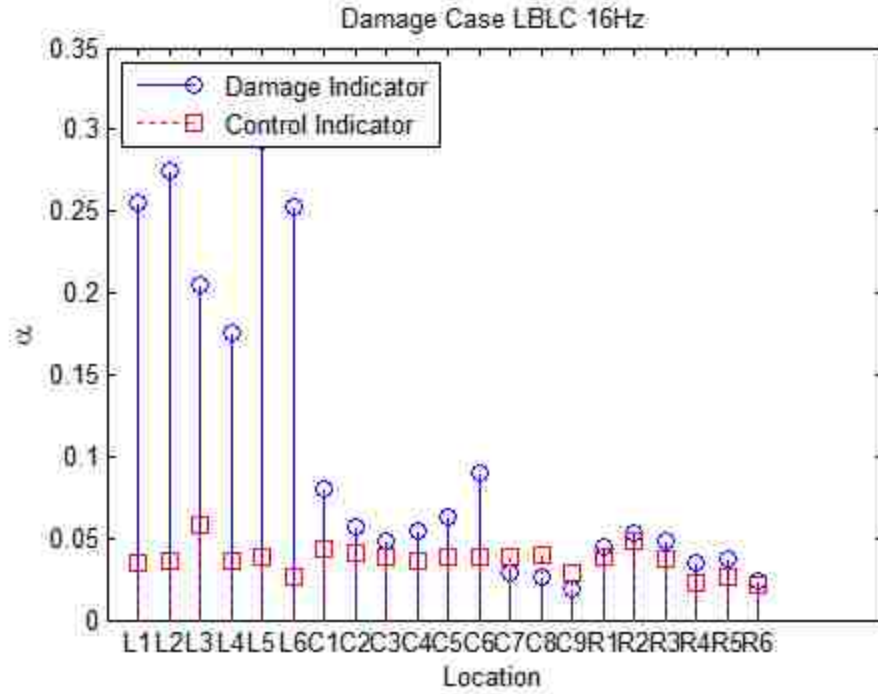
Figure 3.14a Simulation Damage Scenario LBLC with 5% Noise
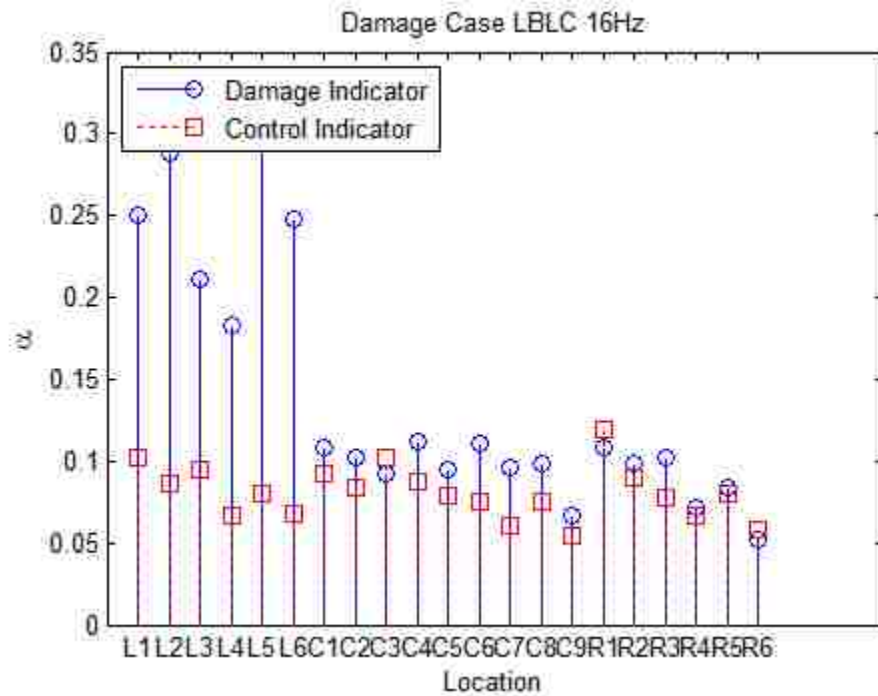
Figure 3.14b Simulation Damage Scenario LBLC with 10% Noise
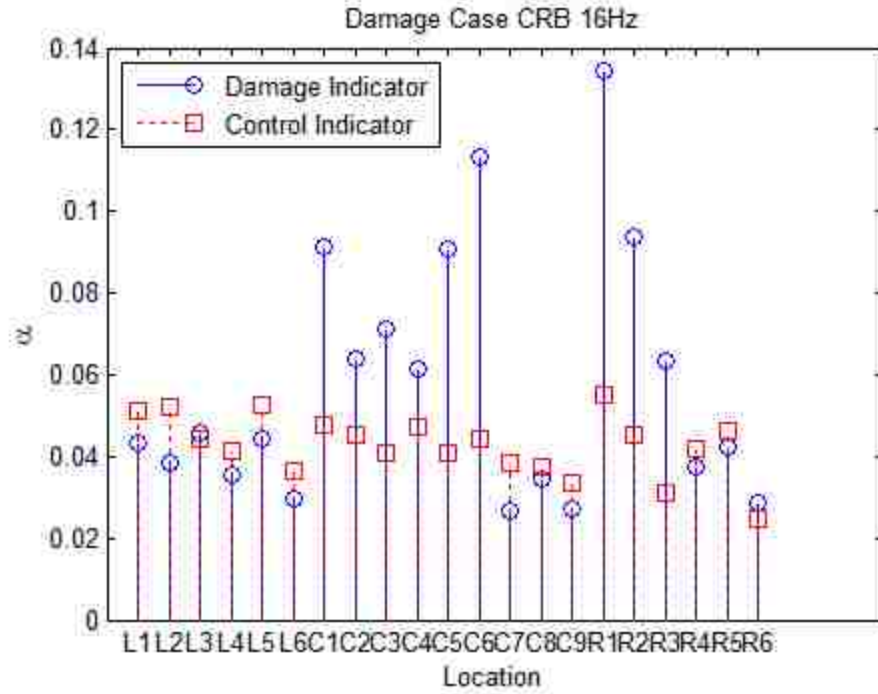
Figure 3.15a Simulation Damage Scenario CRB with 5% Noise
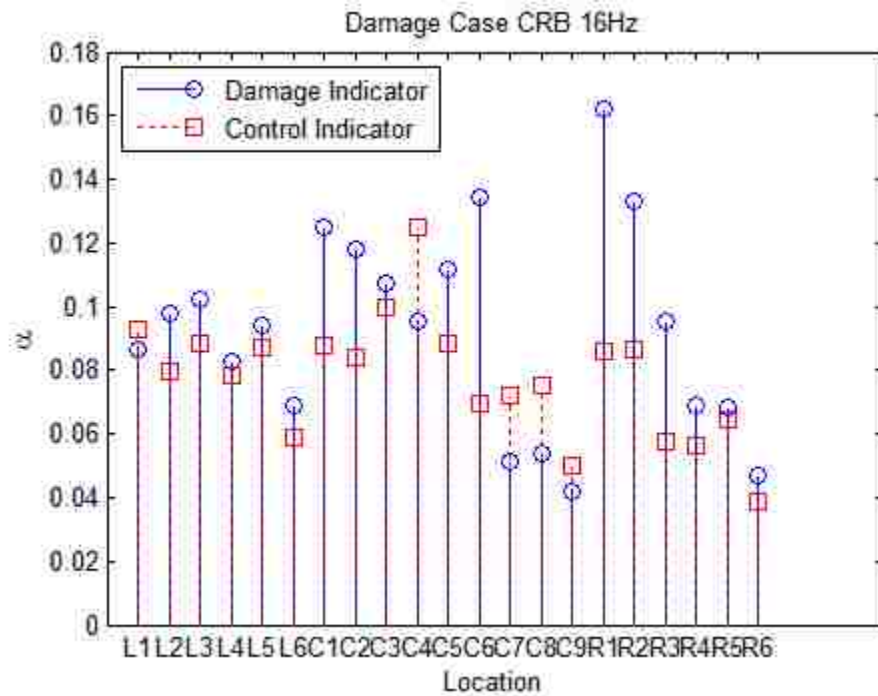
Figure 3.15b Simulation Damage Scenario CRB with 10% Noise
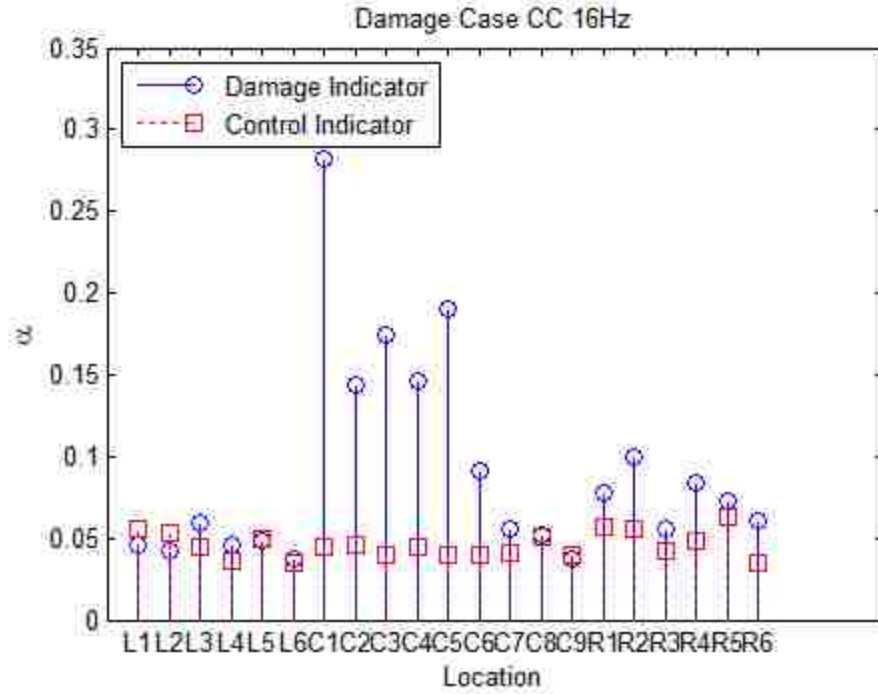
Figure 3.16a Simulation Damage Scenario CC with 5% Noise
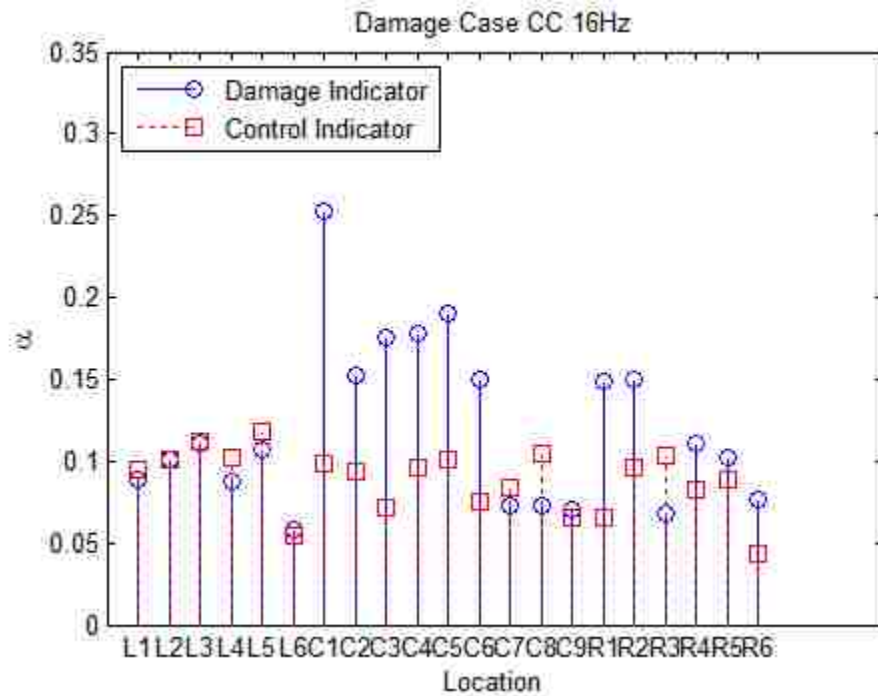
Figure 3.16b Simulation Damage Scenario CC with 10% Noise
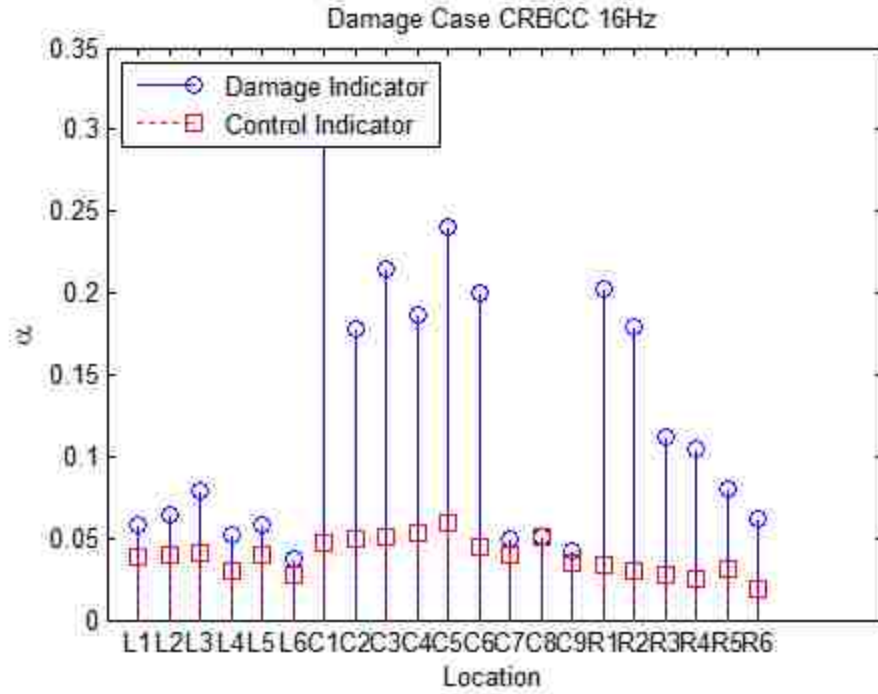
Figure 3.17a Simulation Damage Scenario CRBCC with 5% Noise
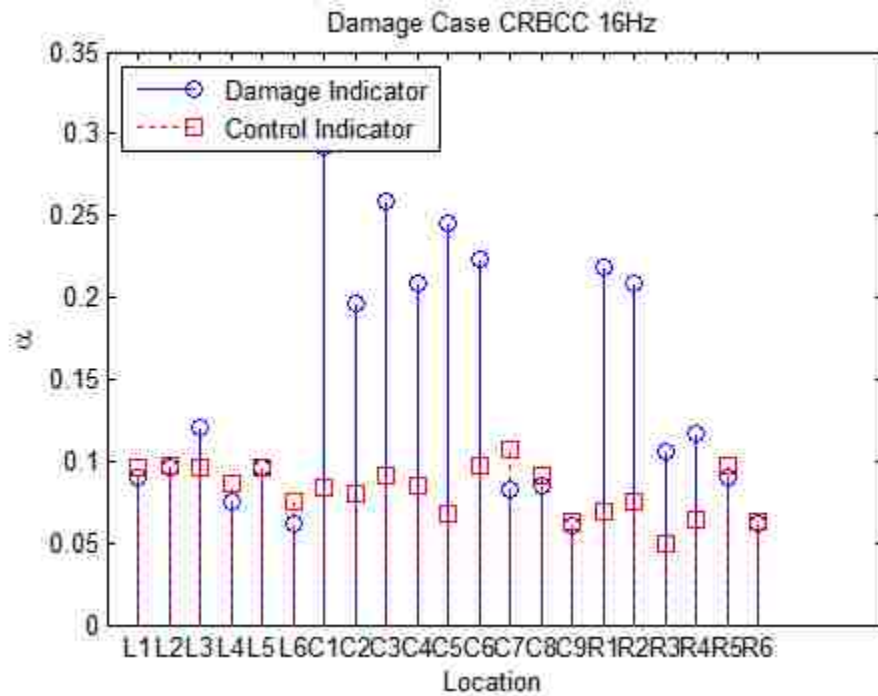
Figure 3.17b Simulation Damage Scenario CRBCC with 10% Noise
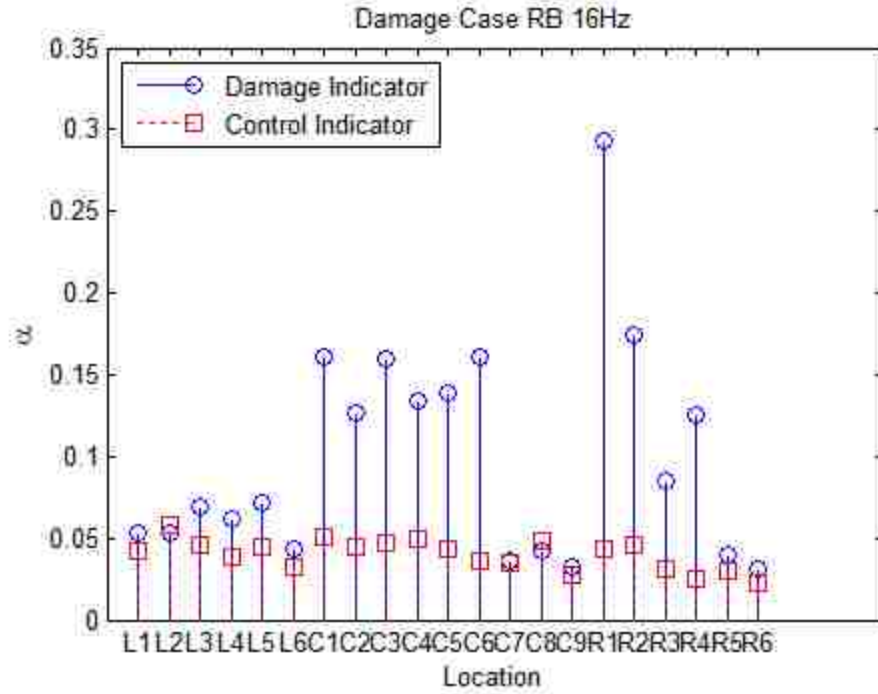
Figure 3.18a Simulation Damage Scenario RB with 5% Noise
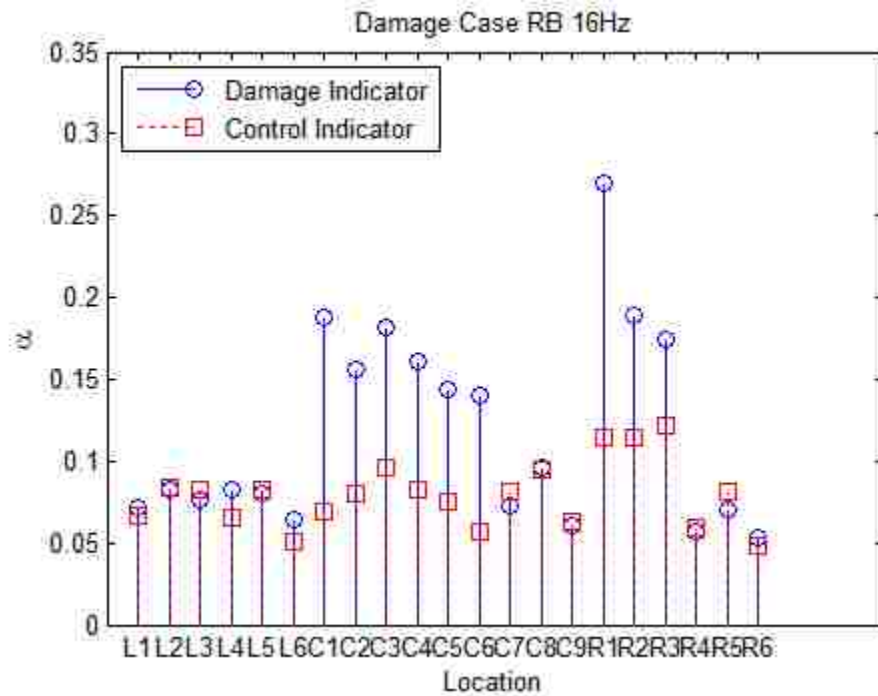
Figure 3.18b Simulation Damage Scenario RB with 10% Noise
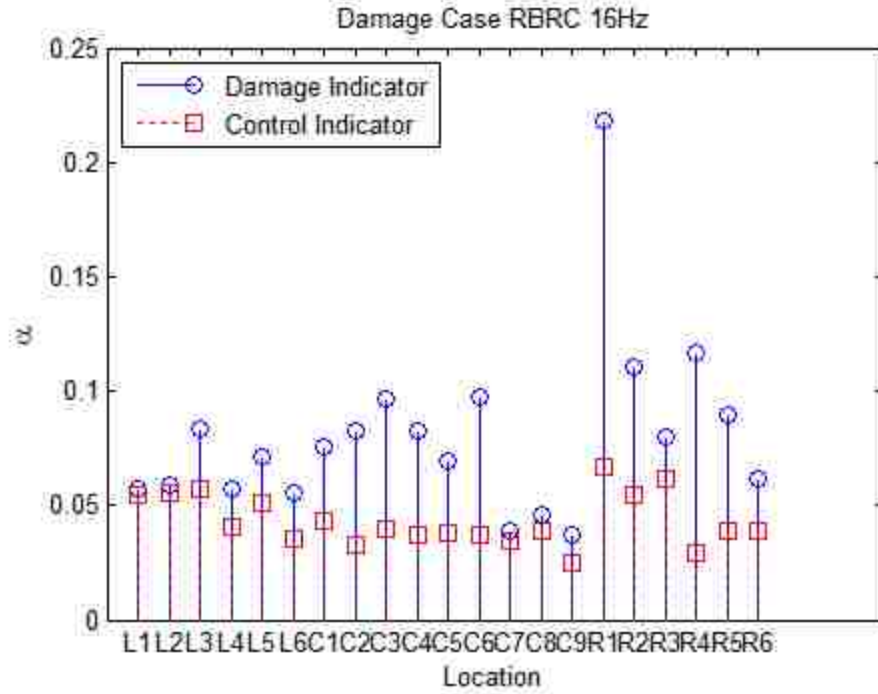
Figure 3.19a Simulation Damage Scenario RBRC with 5% Noise
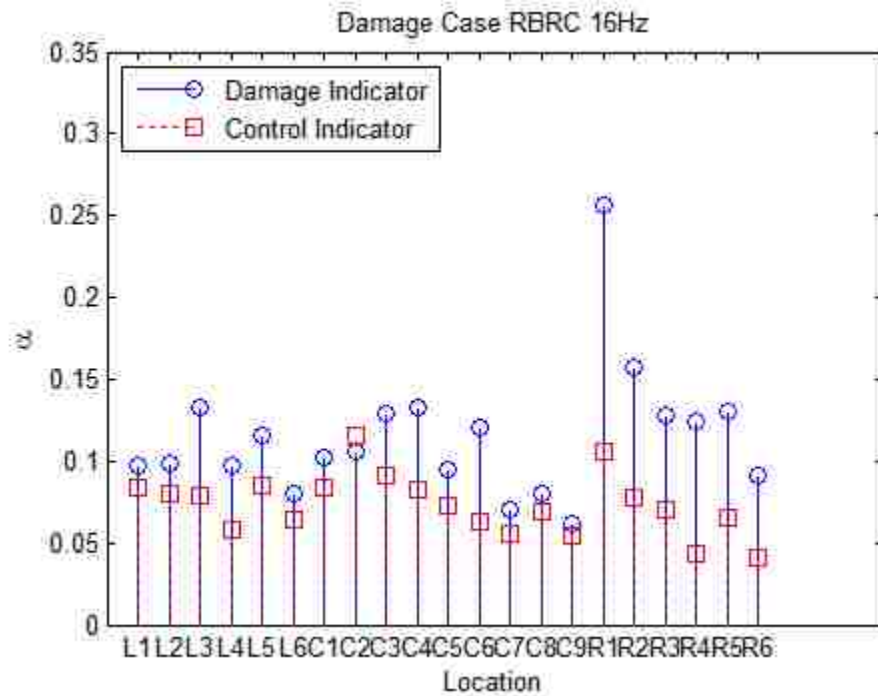
Figure 3.19b Simulation Damage Scenario RBRC with 10% Noise
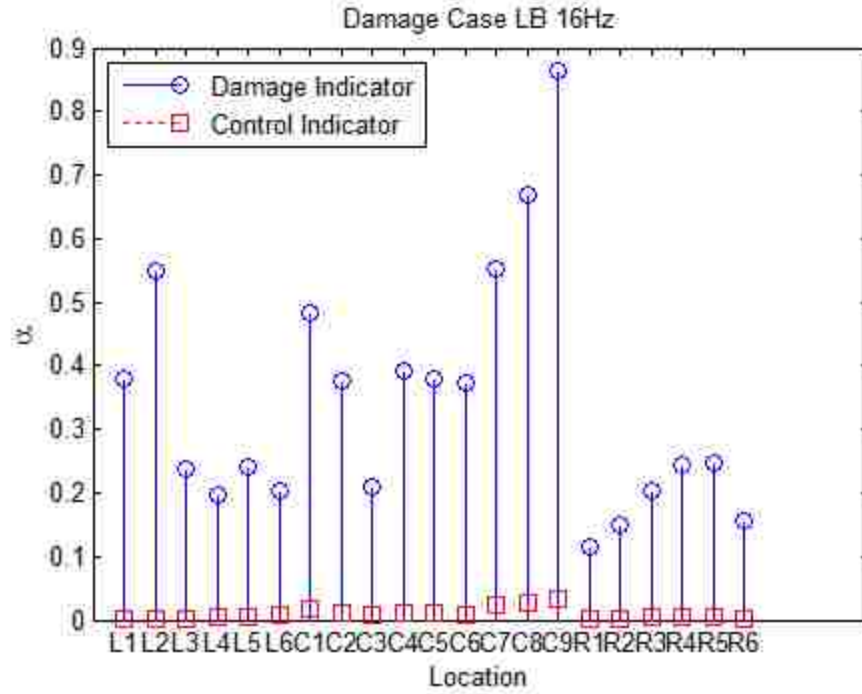
Figure 3.20 Lab Damage Scenario LB with 16Hz Input
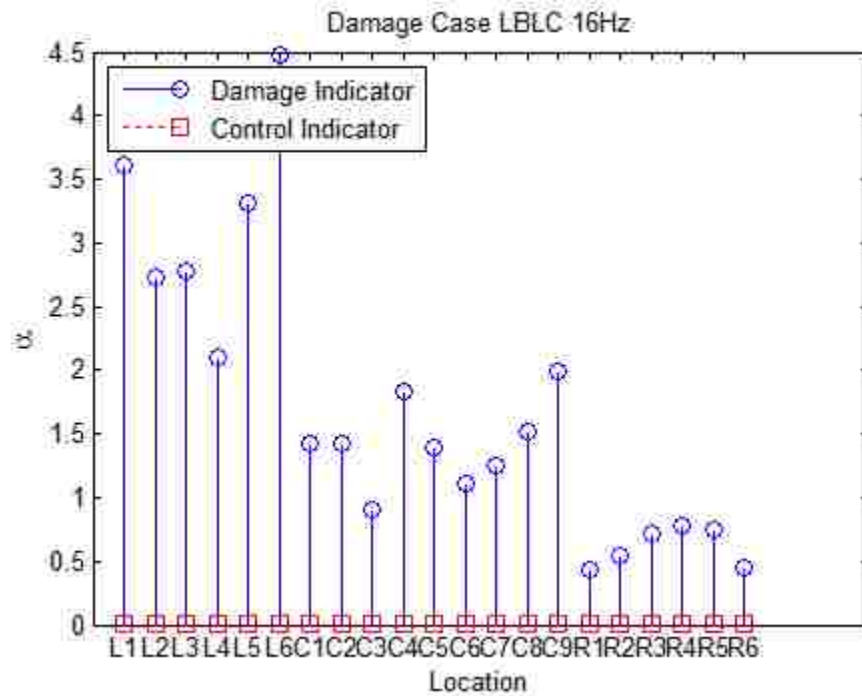
Figure 3.21 Lab Damage Scenario LBLC with 16Hz Input
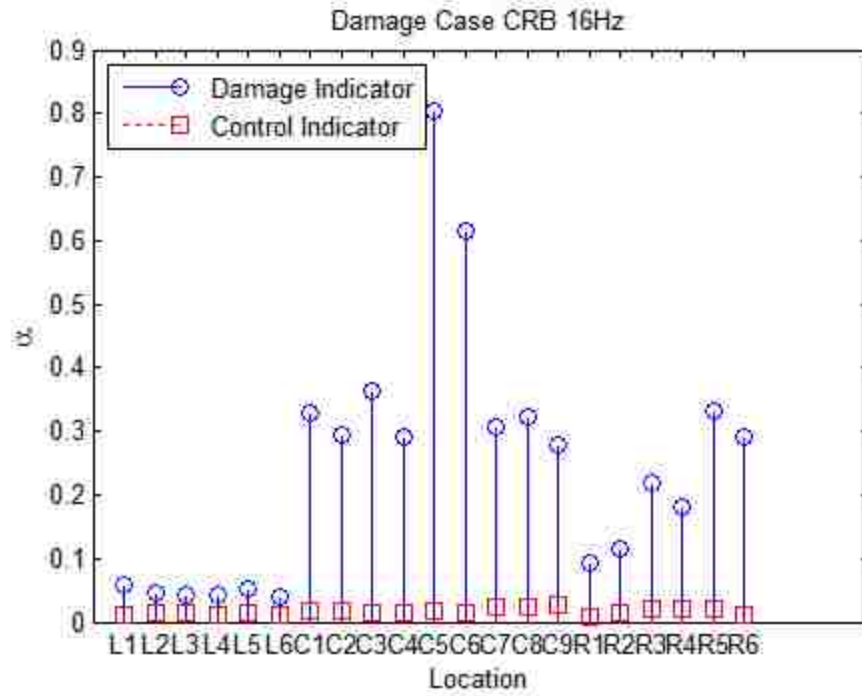
Figure 3.22 Lab Damage Scenario CRB with 16Hz Input
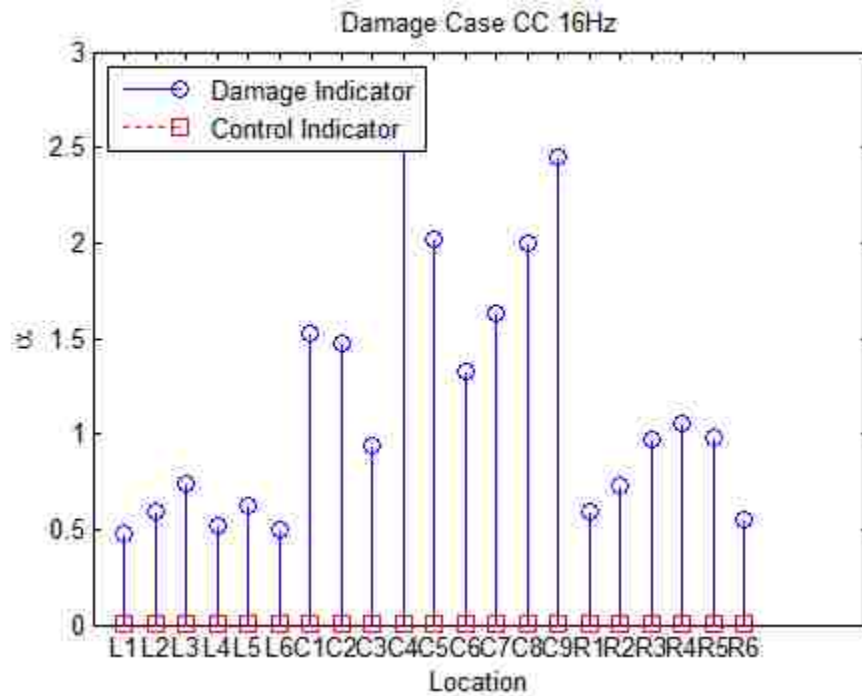
Figure 3.23 Lab Damage Scenario CC with 16Hz Input
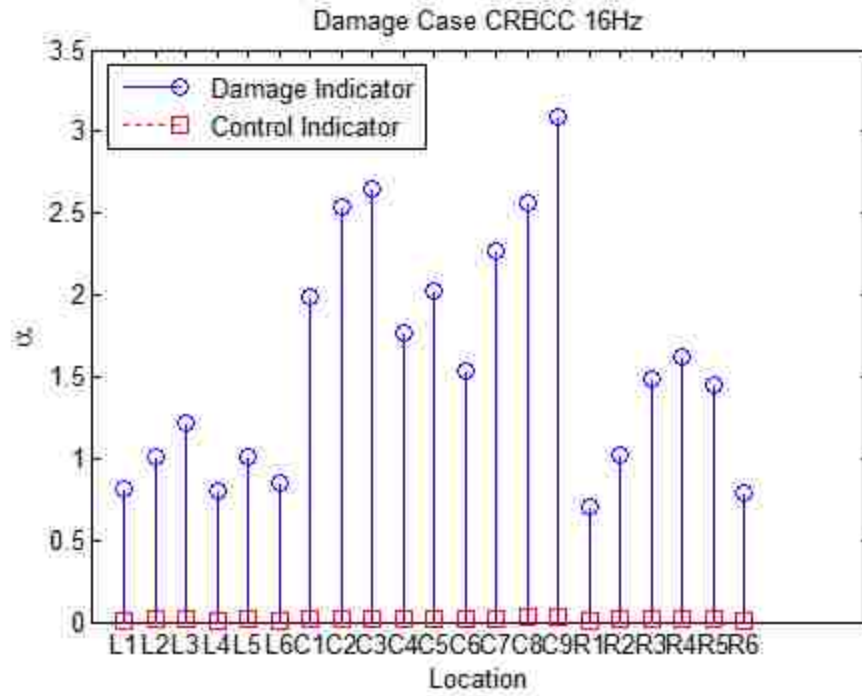
Figure 3.24 Lab Damage Scenario CRBCC with 16Hz Input
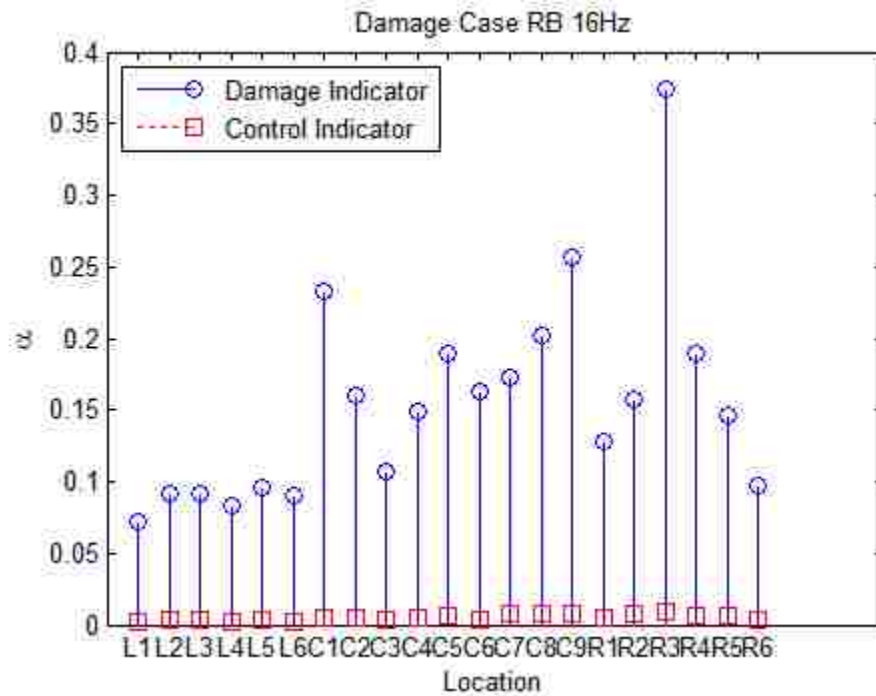
Figure 3.25 Lab Damage Scenario RB with 16Hz Input
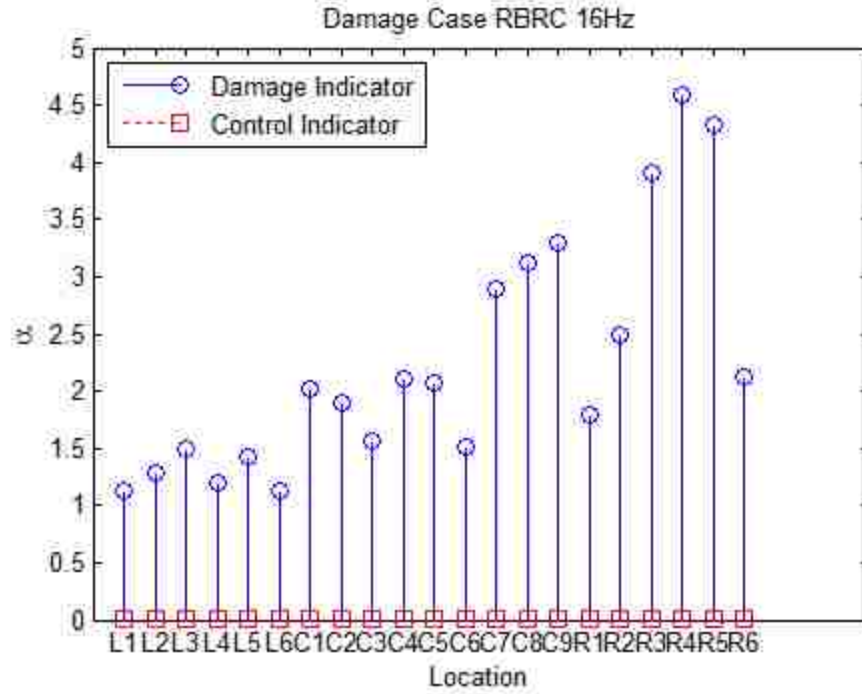
Figure 3.26 Lab Damage Scenario RBRC with 16Hz Input
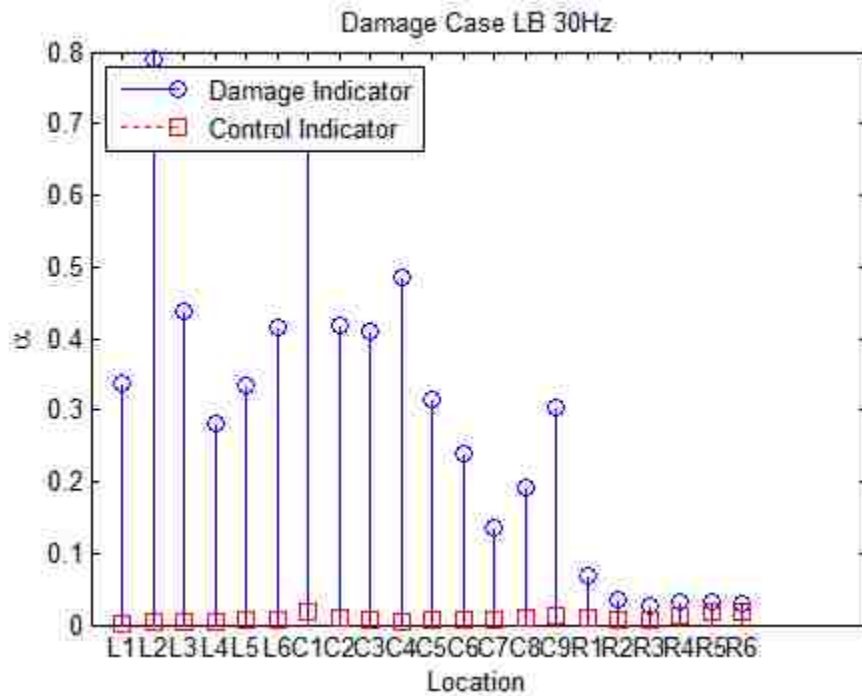
Figure 3.27 Lab Damage Scenario LB with 30Hz Input
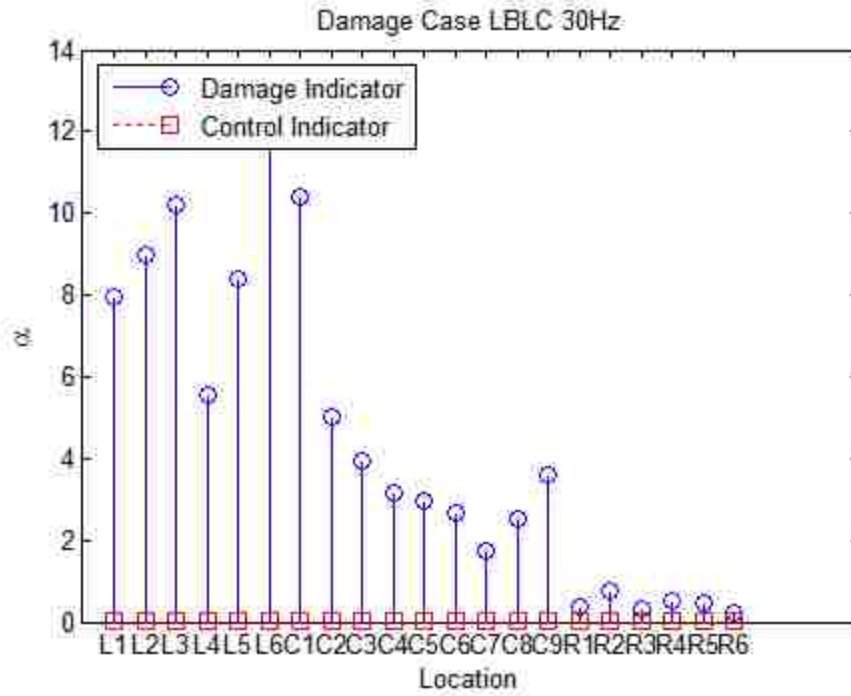
Figure 3.28 Lab Damage Scenario LBLC with 30Hz Input
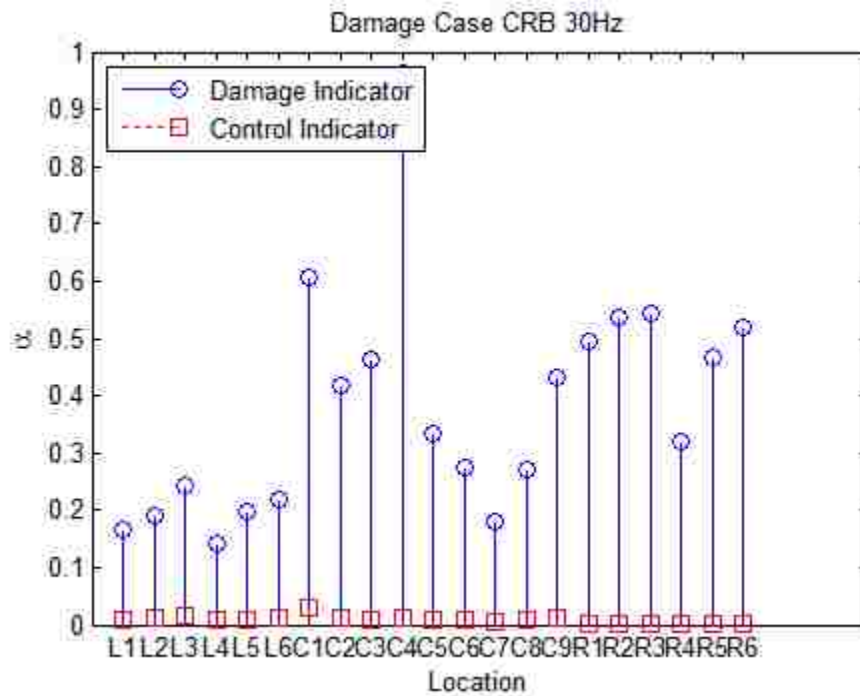
Figure 3.29 Lab Damage Scenario CRB with 30Hz Input
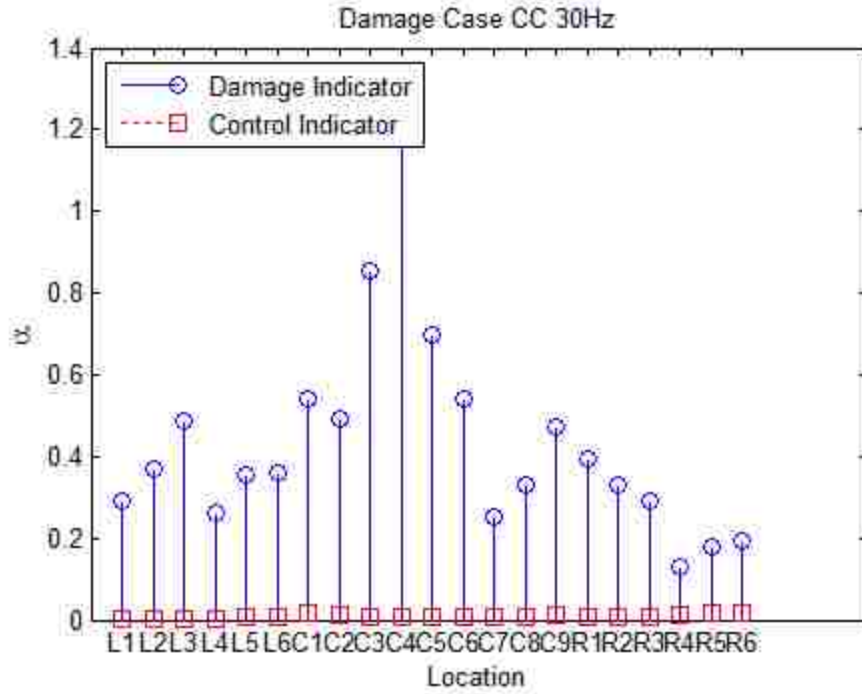
Figure 3.30 Lab Damage Scenario CC with 30Hz Input
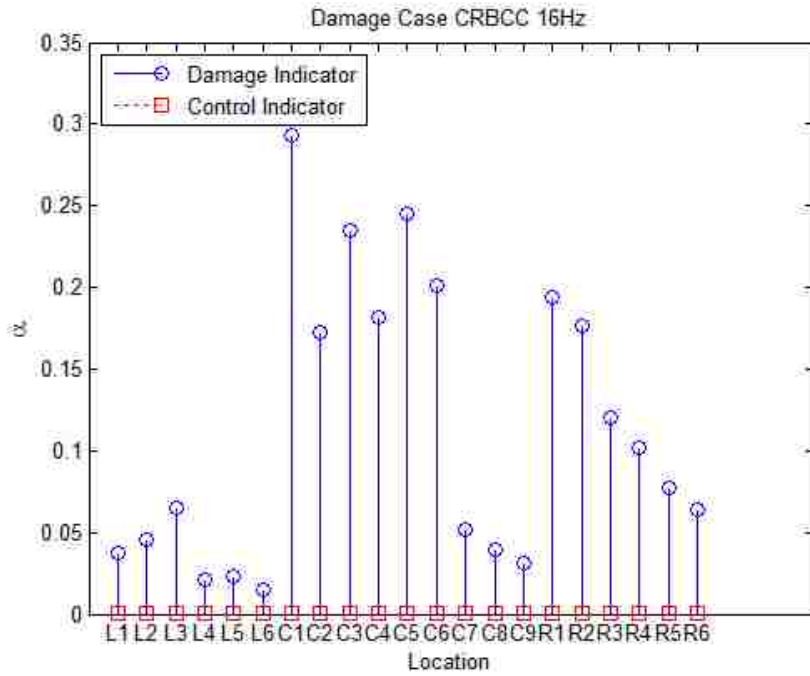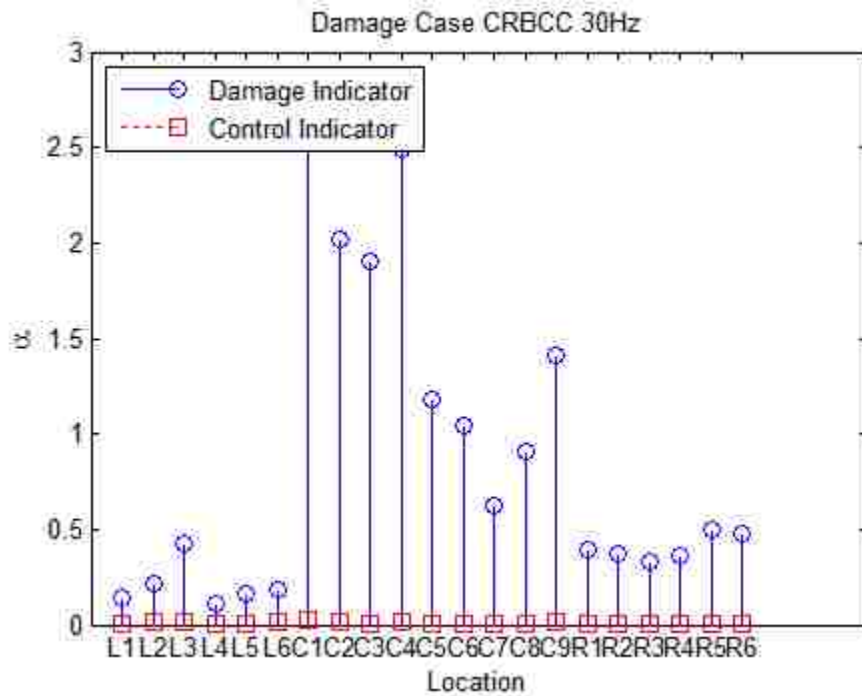

Figure 3.31 Lab Damage Scenario CRBCC with 30Hz Input
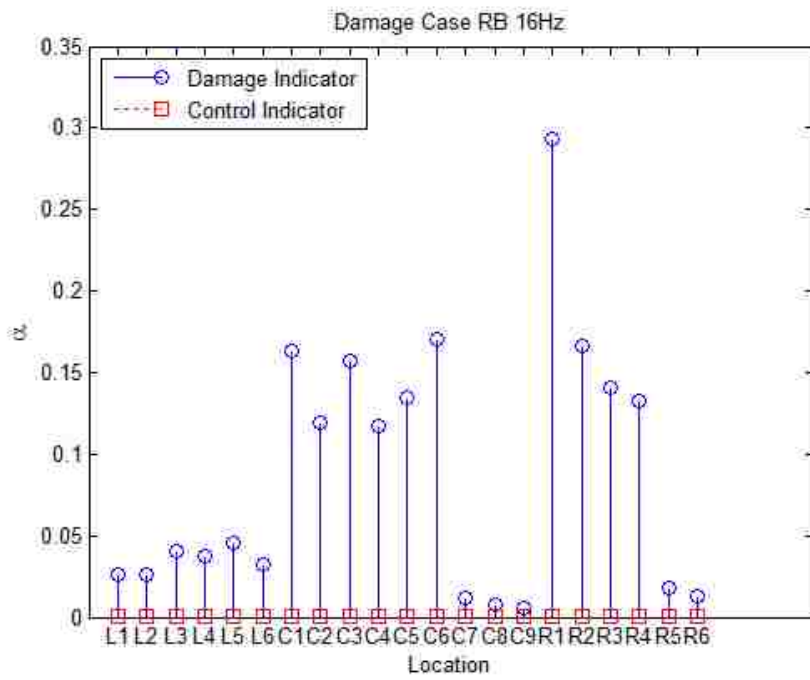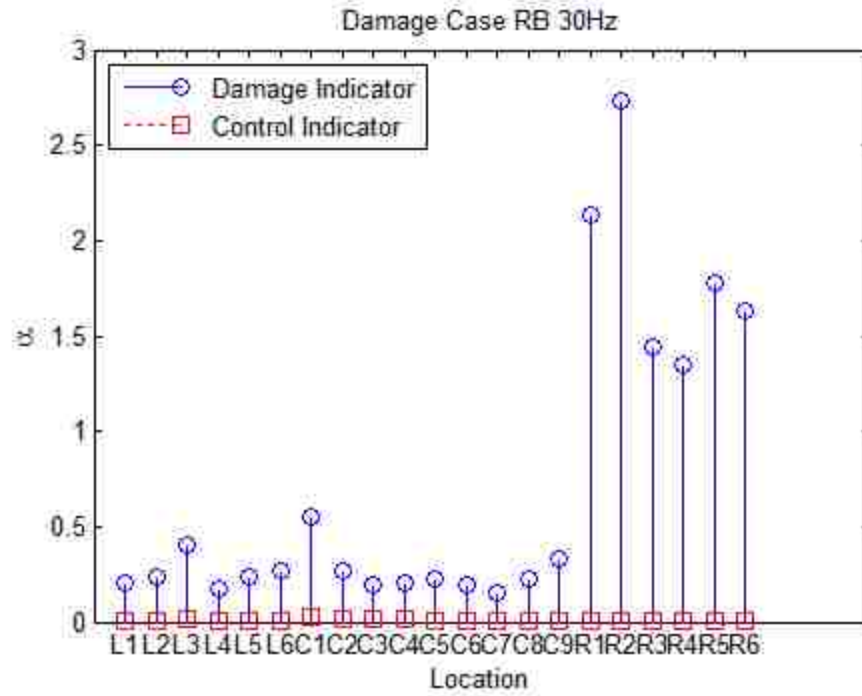
Figure 3.32 Lab Damage Scenario RB with 30Hz Input
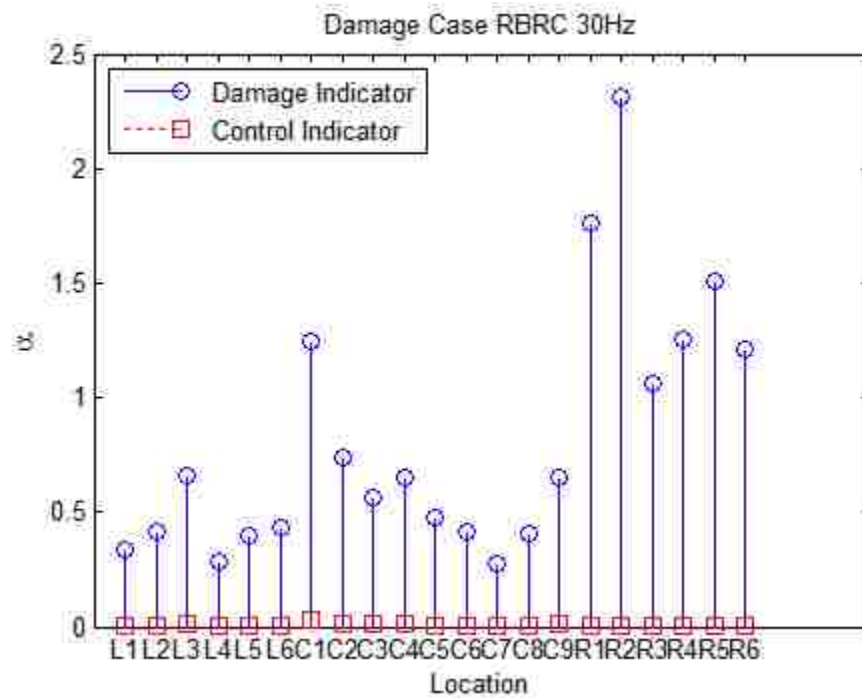
Figure 3.33 Lab Damage Scenario RBRC with 30Hz Input
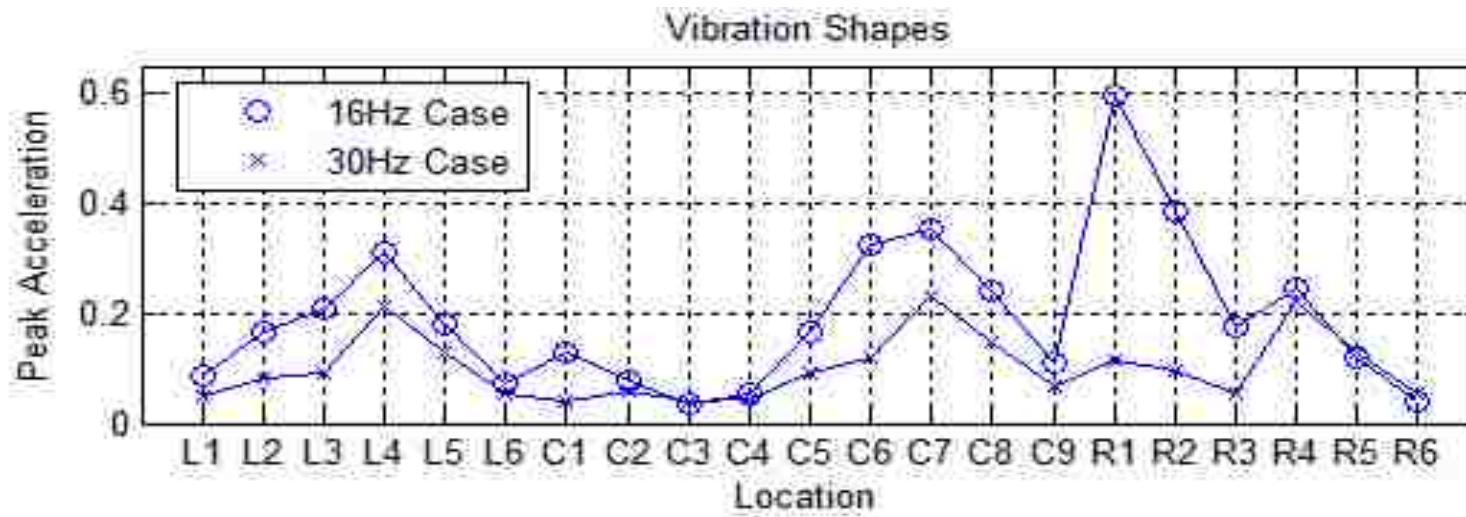
Figure 3.34 Vibration Curves for 16Hz and 30Hz input cases

Chapter 4 Two-Variable Linear Regression Based Damage Detection Algorithm

4.1 Introduction

This chapter presents the application of two-variable linear regression to damage detection. In chapter 3, the input of the system is assumed to be only the harmonic input so that the system responses are proportional to the input. However, as seen in some of the results, damage detection indicators are missing for some nodes. That means the single linear regression is not a perfect simulation. So in this chapter, the ambient vibration from the test environment is also considered as an input (demonstration in Figure 4.1) and two-variable linear regression will be used in the damage detection algorithm to see if it will provide a better simulation of the relationship of dynamic responses between nodes.

First, data from the finite element model tests will be used to verify the performance of the two-variable linear regression method. Then both 5% and 10% noise will be added to the data to test the robustness of the method against noise. At last, data from lab test will be used to perform the damage detection method.

4.2 Two-variable Linear Regression

Instead of having one dependent variable with one independent variable in the single-variable linear regression, two independent variables will be used to express the dependent variable in two-variable linear regression.

$$y = \beta_1 \cdot x_1 + \beta_2 \cdot x_2 + e \qquad \text{(Eq. 4.1)}$$

Equation 4.1 is the general form of a two-variable linear function. The function that will be used in this research is,

$$\widehat{u}_i(n) = \beta_1 \cdot \ddot{u}_j(n) + \beta_2 \cdot \ddot{u}_j(n-1) + \gamma_i + \varepsilon_i, i = 1 \dots m \qquad \text{(Eq. 4.2)}$$

where

$\ddot{u}_j$ = acceleration response from one node used as the independent variables;

$\widehat{\ddot{u}}_i$ = estimated acceleration response of a node other than node i;

β_1, β_2 = regression coefficients;

γ_i = intercept term;

ε_i = error term.

It is a spatio-temporal regression model used in this research. Spatio-temporal regression models are widely used for identifying data sets with strong spatial and temporal relationships (Katanoda et. al 2002; Ichoku et.al 2002). Since the dynamic responses from the same structure are definitely spatial and temporal related, the spatio-temporal regression model is expected to give precise descriptions of such relationships. The regression function used in this chapter only includes two nodes and information from one time step back, which is a very simple form of the spatio-temporal regression model.

4.2.1 Matrix Solution

Matrix solution is again applied on two-variable linear regression to solve for the coefficient matrix. Now the **X** matrix is $n \times 3$ instead of $n \times 2$ and $\widehat{\boldsymbol{\beta}}$ is 3×1.

$$\widehat{\boldsymbol{\beta}} = (\boldsymbol{X}' \cdot \boldsymbol{X})^{-1} \cdot (\boldsymbol{X}' \cdot \boldsymbol{Y}) \qquad \text{(Eq. 4.3)}$$

where

$$\boldsymbol{Y} = \begin{bmatrix} Y_1 \\ Y_2 \\ \vdots \\ Y_{n-1} \end{bmatrix}_{(n-1)\times 1} , \qquad \boldsymbol{X} = \begin{bmatrix} 1 & X_1 & X_2 \\ 1 & X_2 & X_3 \\ \vdots & \vdots & \vdots \\ 1 & X_{n-1} & X_n \end{bmatrix}_{(n-1)\times 3} , \qquad \widehat{\boldsymbol{\beta}} = \begin{bmatrix} \gamma \\ \beta_1 \\ \beta_2 \end{bmatrix}_{3\times 1}$$

4.2.2 Correlation

The same expression of r^2, *coefficient of determination* (CoD), is used for represent the percentage of the dependent variable that is expressed by the two independent variables. And in this chapter the concept of coefficient of determination will be a little complicated than that in Chapter 3. Figure 4.2 demonstrates the meaning of R^2 determination in a two-variable linear regression. In the two-variable linear regression, the variation Y is explained by X_1 and X_2 at the same time. In Figure 4.2, the area covered by shadows represents the portion that is successfully explained by the two independent variables and the r^2 determination is the ratio of this area to the total area. The higher r^2 determination means a better explanation of Y variation.

4.2.3 Variance Inflation Factor

When two or more independent variables are included in the linear regression function, the linear relationship between these independent variables should be considered. In statistics, the variance inflation factor (VIF) quantifies the severity of multicolinearity in

an ordinary least squares regression analysis (Izenman 2008). It can be calculated as follows,

$$\text{VIF} = \frac{1}{1-R^2} \qquad\qquad (\text{Eq. 4.4})$$

R^2 has the same calculation as that shown in the previous section. The only difference is that now it is between one and the rest of the independent variables and the dependent variable is not included. A high value of VIF means a great portion of information that one dependent variable carries overlaps with that of the other dependent variable(s). A demonstration of how the VIF values are related to the amount overlapped information is shown in Figure 4.3. When the factor is 5, the overlapped area is 80% of the area of X_2.

The problem of dependent variable overlapping each other is that it will make the result of linear regression to be unstable. Small alteration in the data can make big difference in the resulting coefficient vector. In the research, the upper bound for VIF is set to be 10, as suggested in Izenman's book.

4.3 Damage Indicator

Eq. 4.3 can be considered as a plane function in the term of geometry and the normal vector the plane is $[\beta_1 \ \beta_2 \ -1]$. Since the assumption is made that the linear relationship will alter after damage occurs on the structure, a new set of coefficients will appear and so will a new plane. The two planes in Figure 4.4 represent the linear relationship between three variables before and after damage respectively. The angle α between these two planes is used to indicator the change of such linear relationship. Since normal vectors are perpendicular to their planes, the angle between the two normal vectors is equal to the angle between the two planes. α can be calculated as

$$\alpha = \cos^{-1}\left|\frac{v \cdot v'}{\|v\| \cdot \|v'\|}\right| = \cos^{-1}\left|\frac{\beta_1 \cdot \beta_1' + \beta_2 \cdot \beta_2' + 1}{\sqrt{\beta_1^2 + \beta_1^2 + 1} \cdot \sqrt{\beta_2'^2 + \beta_2'^2 + 1}}\right| \qquad \text{(Eq. 4.5)}$$

Again, control indicators will also be calculated for each damage indicator.

4.4 Test results

The results will be organized in the same order as in Chapter 3. First, simulation test results from the finite element model will be presented, followed by are results with certain percent of noise. At last results from lab tests with different input will be shown.

4.4.1 Simulation Test Results

The same data will be used for performing the two-variable linear regression based damage detection algorithm, in order to see the difference between performances of the two algorithms. As found in Chapter 3, some damage scenarios can only be detected under certain inputs. So in this Chapter, totally 4 inputs with input frequency 16Hz, 18Hz, 20Hz and 30Hz are subjected to the frame. Only the best result among all the results of different the input cases for each damage scenario is shown.

4.4.1.1 Damage Scenario LB

For the damage scenario LB, the detection algorithm works the best with the 20Hz input. In Figure 4.5, one can see that a rough level 1 damage prediction is made to show damage more possible on the left column where the largest damage indicator is found, while the actual damage is on the beam where large damage indicators also exist.

4.4.1.2 Damage Scenario LBLC

Figure 4.6 is the result for damage case LBLC with an 18Hz input. A level one damage prediction is made that damages are around node L2 and L5 which is exactly the damage case.

4.4.1.3 Damage Scenario CRB

A level 2 prediction is made in the result shown in Figure 4.7. When a 30Hz sinusoidal input is subjected on the frame and damage detection algorithm is applied to the simulation data, damage is found around node C1 which is near location CLB. Traditional physical damage detection method are need to find the exact damage location.

4.4.1.4 Damage scenario CC

What can be observed from Figure 4.8, the result of damage scenario CC, is that damage indicators in group C are relatively high. One large damage indicator is seen on node C1 and several less large damage indicators on location L3, C2 and C7 to C9. That means damage is likely on location CRB and location CC. It provides a level 2 prediction since the real damage is on the center column.

4.4.1.5 Damage Scenario CRBCC

The best result that can be found for damage scenario CRBCC is the case with 30Hz input, shown in Figure 4.9. One can see that the shape of the stem plot is very much like the one for damage case CC only with larger damage indicators. A level 2 damage identification is made to indicate damage on the central joint, for that damage indicators the central joint are relatively larger than the rest of the damage indicators.

4.4.1.6 Damage Scenario RB

The result for damage case RB is shown in Figure 4.10. Data is from the 18Hz input tests. The largest damage indicator is seen on node R1 and the rest of the damage indicators in group R are all larger than those in other groups. A level 1 damage prediction can be made from this result showing that damage is on the right end of the right beam.

4.4.1.7 Damage Scenario RBRC

The best result for damage scenario RBRC is the case with a 20Hz input, shown in Figure 4.11. One can easily see that the damage most possibly takes place on the right joint since damage indicators on that joint are much larger than the others. So a level 1 damage prediction is made in this case. But one problem remain is this case is that if one have no idea of the damage numbers, it hard to tell how many damages are there in the case and what are the locations.

4.4.2 Simulation Test Results against Noise

As what was did in Section 3.4.2, the robustness of the damage detection algorithm against noise will be tested. Random 5% and 10% noise will be added to the simulation test data. Since the noise is added randomly, it won't be exactly the same noise that is used in the previous section, but level of the noise will be the same. Then noise will be added to the data from those picked damage cases in the previous section since they provide the best estimations of damage. Totally 25 tests will be made for each damage case and the results will be averages of the 25 test so that they will be representative. Conclusions and discussions will be made based on these picked-out results.

4.4.2.1 Damage scenario LB

Results are shown in Figure 4.12a and b for 5% noise and 10% noise, respectively. One can see that damage indicators in group L haven't increased too much with the effect of noise while damage indicators in the other groups are increasing along with their control indicators. A level 2 damage prediction can be made for the 5% noise case. However for the 10% noise case, the control indicators in group L are too close to the damage indicators. No useful damage detection can be made, so it is a level 4 damage prediction.

4.4.2.2 Damage scenario LBLC

Figure 4.13a and b are results for damage case LBLC with 18Hz input against 5% and 10% noise, respectively. For the case against 5% noise, useful damage indicators are seen on from node L1 to L6 and node C1, which are exactly the larger ones in the case without noise. So the same conclusion can be drawn as in Section 4.4.1.2 that damage are seen around node L2 and L5 for this level of noise providing a level 1 damage detection. However situation is not the same for the case with 10% noise. In Figure 4.13b, the difference between the damage indicator and the control indicators on node L2 to L4 and C1 are not as big as in the previous case. So the damage prediction for the case with 10% noise is only a level 4 damage prediction showing no damage location.

4.4.2.3 Damage scenario CRB

Figure 4.14a is the result of damage case CRB with 30Hz input against 5% noise. While damage indicators in group C, except node C1, are not clearly larger than their corresponding control indicators, those in the other two groups are all at the same level

with their control indicators. It means that if there is one damage location, it is most possibly on the left beam of the central joint. But it is not the correct damage location. So a rough level 3 damage prediction is given for this case. And in Figure 4.14b, the result against 10% noise, almost all damage indicators are almost covered by their control indicators except the one on node C1. Since there is only one useful damage indicator, even the existence of damage is uncertain in this case. A level 4 damage prediction is made for this case.

4.4.2.4 Damage Scenario CC

Figure 4.15a and b present the results of damage case CC against 5% and 10% noise. The differences between damage indicators and control indicators in the case with 5% are bigger than those in the case with 10% noise in which most of the control indicators are even larger than the damage indicators. But the it is not enough to say the damage indicators in the 5% noise case are useful and reliable to be used to identify damages, because the differences between control indicators and damage indicators in the 5% noise case are not large enough. Generally speaking, level 4 predictions, no damage is predicted, are made for both cases.

4.4.2.5 Damage Scenario CRBCC

For the damage case against 5% noise, the first damage is easily predicted around location CLB which is neither of two actual damage locations. The second damage prediction in this case is vague because large and useful damage indicators are seen in both group L and group C. According to the two conclusions above, a level 2 damage prediction can be made in this case. And in the case with 10% noise, since the only useful

damage indicator is the one on node C1 which indicates that damage is around that node, a level 4 prediction is the only prediction that can be made.

4.4.2.6 Damage Scenario RB

Figure 4.17a gives the result of damage case RB with 18Hz input against 5% noise. As one can see, in this case, the noise has really little effect on the damage indictors in group C and group R which makes the case clear for damage detection. A level 1 damage prediction shows that the damage is most likely on location RB. In the case that has a 10% noise, shown in Figure 4.17b, while the noise level raises, damage indicators in group C become unreliable. However it doesn't change the result of damage prediction that damage is on the beam within the right joint.

4.4.2.7 Damage Scenario RBRC

In Figure 4.18a and 4.18b are the results for damage scenario RBRC with 20Hz input against 5% and 10% noise respectively. Despite the different levels of control indicators in the two cases, the damage prediction results are the same since damage indicators in group R remain almost the same and unaffected by the noise. For both cases, a level 1 damage prediction can be made that damage is on both the beam and the column on the right joint.

4.4.3 Lab Test Results

In this section, totally 28 combinations of damage case are tested in the lab frame in ATLSS, 7 damage scenarios with 4 kinds of input. For each damage scenario, the best result amount the results with the 4 inputs will be shown in the following sections.

4.4.3.1 Damage Scenario LB

The best result got for this damage scenario is the ones with a 20Hz sinusoidal input, shown in Figure 4.19. One can see the largest damage indicator is on location L2 which is exactly the damage location and also the rest of the damage indicators in group L are also relatively large. One imperfection about this result is that some of the damage indicators in group R are also large, which leads to a suspicion that a slighter second damage may also be found on the right joint. However the result can still be considered to be a level 1 prediction of the damage.

4.4.3.2 Damage Scenario LBLC

Best result for this damage case in Figure 4.20 came from the tests with 16Hz input. Large α values are found on location L1, L5 and L6, which means damages may locate both on the left column and near the left end of left beam. It provides a level 1 prediction of damage for this case.

4.4.3.3 Damage Scenario CRB

Figure 4.21 presents the best result for damage scenario CRB. In this set of tests, a 16Hz sinusoidal input was subjected onto the frame. Result shows that damage is most like around node C5 and C6, but the possibility of damage locating on the center column, the place where node C7 and C8 locate, cannot be completely ruled out. So this result gives a controversial level 2 prediction.

4.4.3.4 Damage Scenario CC

Tests with 16Hz input produced the best damage prediction in this damage scenario. In Figure 4.22, one can see that the two possible damage locations are location CRB and location CC since damage indicators on these two locations are larger than any others. Because the real damage is on the center column only which means the prediction of damage on the beam is a false alarm, the result is a level 2 prediction of damage.

4.4.3.5 Damage Scenario CRBCC

In Figure 4.23 is the result for damage scenario CRBCC with 16Hz input. It is obvious that damage indicators in group C are larger than those in the other two groups. And within group C, larger damage indicators are found on the column and the right end of the left beam. It is a the exact prediction of the damage scenario, but considering the fact that the two out of three members of the center joint are weakened, it is possible that the behavior of the member that has no damage on it will be significantly altered under the influence of the two damaged sections. Further detection is needed for detailed damage location information. A rough level 1 prediction is made in the case.

4.4.3.6 Damage Scenario RB

Damage indicators from test with damage on the right end of the right beam and a 30Hz input are presented in Figure 4.24. Damage is predicted to be around node R1 and R2 which gives a level 1 prediction of this damage case.

4.4.3.7 Damage Scenario RBRC

In this damage case, damages both on the right column and the right beam with a 30Hz input onto the frame, one damage is predicted on location RB because of the two large

damage indicators seen on node R1 and R2. However the sign for the damage that exists on the column is vague. If the relatively large damage indicator on node R5 is considered as a sign of damage on the right column, then damage may also be predicted around node C1 since the damage indicator for node C1 is almost as large as the one for node C5. So only a level 2 prediction of damage can be made for this damage scenario.

4.5 Conclusions

In this chapter, a damage detection method based on two-variable linear regression is used to perform damage prediction on both a finite element model and a lab frame. Also the robustness of such method against test noise is discussed. The results are organized in Table 4.1. A success in damage detection in some level is achieved. Several conclusions are drawn by analyzing the test results in this chapter and comparing them with results in the previous chapter.

1) Results in Section 4.4.1 and Section 4.4.3 verify a conclusion got in Chapter 3 that with different input frequencies, the finite element model or the real frame will be excited in different ways. And a specific damage scenario can be identified more easily with a perticular input. And in this chapter, this rule has been revealed more. Looking at Figure 4.5 to Figure 4.11, one can see that when damage is location on the two side joints, the right joint and the left joint, an input with frequency 18Hz or 20Hz can reveal it more clearly; when damage is on the central joint, a 30Hz input is a better choice. And this situation also happens in the results from the lab frame tests. However, due to the imperfectness of the finite element model, the excited the pattern of the

real frame is not exact the same as the finite element model. For the real frame, damage on LB is revealed by a 20Hz input, but when a column-damage is added, the damage scenario is revealed by a 16Hz input. And damages on the central joint are detected in the case with the 16Hz input and those on the right joint are detected in the case with the 30Hz input. Further studies are needed to find the relationship between the best prediction of damage and input force frequency.

2) The robustness of the damage detection method based on two-variable linear regression is worse than that of the method based on single-variable linear regression. Take the example of damage case CC. when applying the single-variable linear regression method to simulation data with 10% noise, damage indicators in Figure 3.16b on node C1 to node C6 stand out clearly from an averaging control indicator of 0.11; when applying the two-variable linear regression method to the same damage case with same amount of noise, damage indicators in Figure 4.15b are all less than their corresponding control indicators, except for the one on node C1. And no helpful damage prediction is provided in this case. The reason to cause this situation is that when two variables are included in the linear regression, more noise is added to the regressing process than that when only one variable is employed, since each variable has theoretically the same amount of noise.

3) By comparing the results in Section 4.4 where two-variable linear regression is applied on test data from the lab specimen with results in Section 3.4 where single-variable linear regression is applied, one can see that, for some of the

cases, the results haven't been improved much by adding another variable into the regression function. The damage case RB with a 30Hz input is taken as an example here. Putting Figure 3.32 and Figure 4.24 together, it is observed that both the shape of plot and the values of the damage indicators are almost the same. Table 4.1 represents all the damage indicators for every node pair in group R. The damage indicator got from the single-variable method is on the left side of the slash and that from the two-variable method is on the right in each cell. To explain this, coefficients are pulled out from both tests using single-variable method and those using two-variable method, shown in Table 4.2 and Table 4.3 and linear regression functions are recalled as below,

$$y(n) = \beta \cdot x(n) + \alpha \qquad \text{(Eq 4.6)}$$

$$y(n) = \beta_1 \cdot x(n) + \beta_2 \cdot x(n-1) + \alpha \qquad \text{(Eq 4.7)}$$

Coefficients in Table 4.2 are the coefficient, β, in Equation 4.6 and Coefficients in Table 4.3 are the ones in Equation 4.7 with the one before semicolon to be β_1 and the one after semicolon to be β_2. Comparing Table 4.2 with Table 4.3, one can see that the β and β_1 for each node pair are very close while β_2 is very small compared with β_1. This means that the second term in Equation 4.7 actually contributes little in expressing the *y(n)* data in this damage case. However, in some other cases, a second independent variable did provide a better result. For example, the results shown in Figure 4.26a and Figure 4.26b are damage detection predictions for damage scenario CC with 18Hz input from single-variable linear regression and two-variable linear regression. As one can see, that the result from the single-variable regression

algorithm actually shows that damage is on location RB which is certainly not the real damage location. In the result shown in Figure 4.26b, although large damage indicators are still seen on location RB, their corresponding control indicators are also large, so the damage prediction is made to be on the central joint, which is a better damage prediction than the previous one.

So a conclusion can be drawn that a linear regression that contains more independent variables doesn't necessarily provide a better results. For different node pairs, the proper number of independent variables that shall be included in the regression function is different.

Table 4.1 Damage Prediction Using Two-variable Linear Regression Based Algorithm Results Summary

Level of Damage Prediction		Damage Scenarios						
		LB	LBLC	CRB	CC	CRBCC	RB	RBRC
Simulation Tests		1	1	2	2	2	1	1
Simulation tests With noise	5%	2	1	3	4	2	1	1
	10%	4	4	4	4	4	1	1
Lab tests		1	1	2	2	1	1	2

Table 4.2 Damage Indicators for Group R in Damage Case RB with 30Hz Input

	R1	R2	R3	R4	R5	R6
R1		0.84/0.83	1.32/1.32	2.65/2.65	3.32/3.31	2.55/2.54
R2	0.84/0.83		2.21/2.22	3.02/2.98	4.05/4.03	3.57/3.60
R3	1.32/1.32	2.21/2.22		0.71/0.70	1.23/1.22	1.78/1.77
R4	2.64/2.64	3.01/2.98	0.71/0.70		0.18/0.18	0.17/0.17
R5	3.31/3.30	4.04/4.02	1.22/1.22	0.18/0.18		0.11/0.11
R6	2.54/2.54	3.57/3.59	1.77/1.77	0.16/0.17	0.11/0.11	

Table 4.3 Coefficients for Node Pairs in Group R in Damage Case RB with 30Hz Input When Single-Variable Linear Regression Is Applied

	R1	R2	R3	R4	R5	R6
R1		1.23	2.02	0.53	0.90	2.15
R2	0.81		1.65	0.43	0.73	1.75
R3	0.49	0.61		0.26	0.44	1.06
R4	1.89	2.32	3.83		1.70	4.08
R5	1.11	1.37	2.26	0.59		2.40
R6	0.46	0.57	0.94	0.25	0.42	

Table 4.4 Coefficients for Node Pairs in Group R in Damage Case RB with 30Hz Input When Two-Variable Linear Regression Is Applied

	R1	R2	R3	R4	R5	R6
R1		[1.25;0.07]	[2.03;0.03]	[0.53;0.00]	[0.90;0.00]	[2.16;0.01]
R2	[0.80;-0.04]		[1.63;-0.07]	[0.42;-0.02]	[0.72;-0.04]	[1.73;-0.09]
R3	[0.49;-0.01]	[0.61;0.02]		[0.26;-0.00]	[0.44;-0.00]	[1.06;-0.01]
R4	[1.89;-0.01]	[2.36;0.11]	[3.84;0.03]		[1.70;-0.01]	[4.08;-0.01]
R5	[1.11;-0.00]	[1.39;0.07]	[2.27;0.02]	[0.59;0.00]		[2.40;0.01]
R6	[0.46;-0.00]	[0.58;0.03]	[0.94;0.01]	[0.25;0.00]	[0.42;-0.00]	
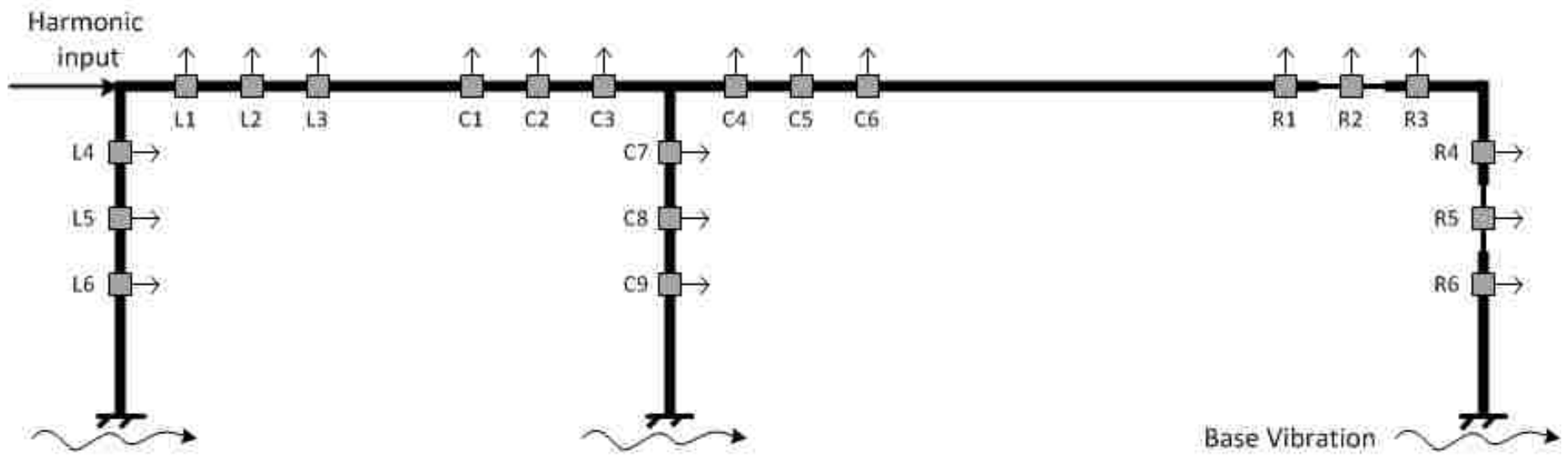
Figure 4.1 Base Vibration Considered as A Second Input

Total variation in Y

Variation in Y explained by X1

Variation in Y explained by X2

Variation in Y explained by X1 and X2 redundantly

Variation in Y explained by neither X1 nor X2
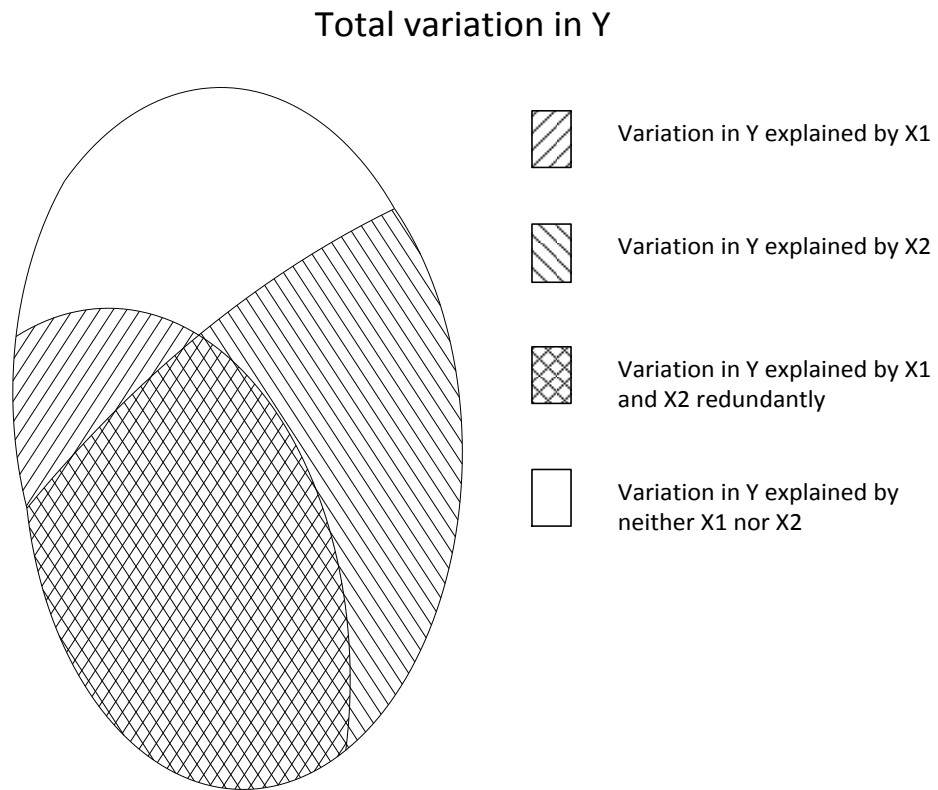
Figure 4.2 Relationship of the Dependent Variable and the Independent Variables in a Two-variable Linear Regression

X_2

X_1

VIF = 5

80% overlapping
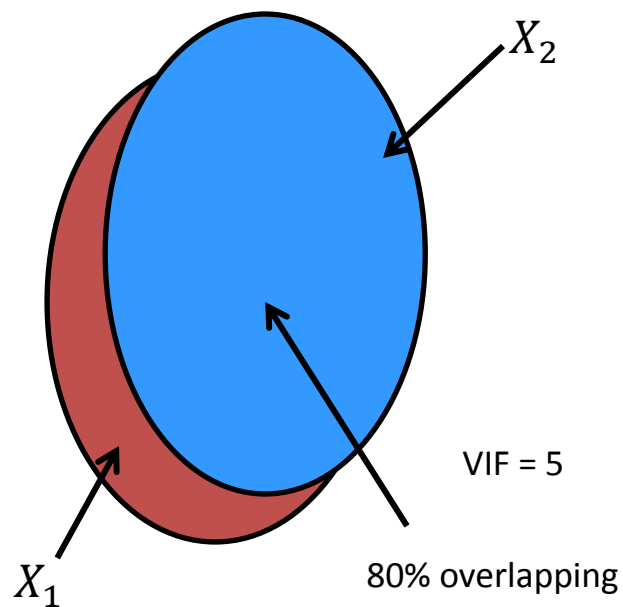
Figure 4.3 Demonstration of Variance Inflation Factors
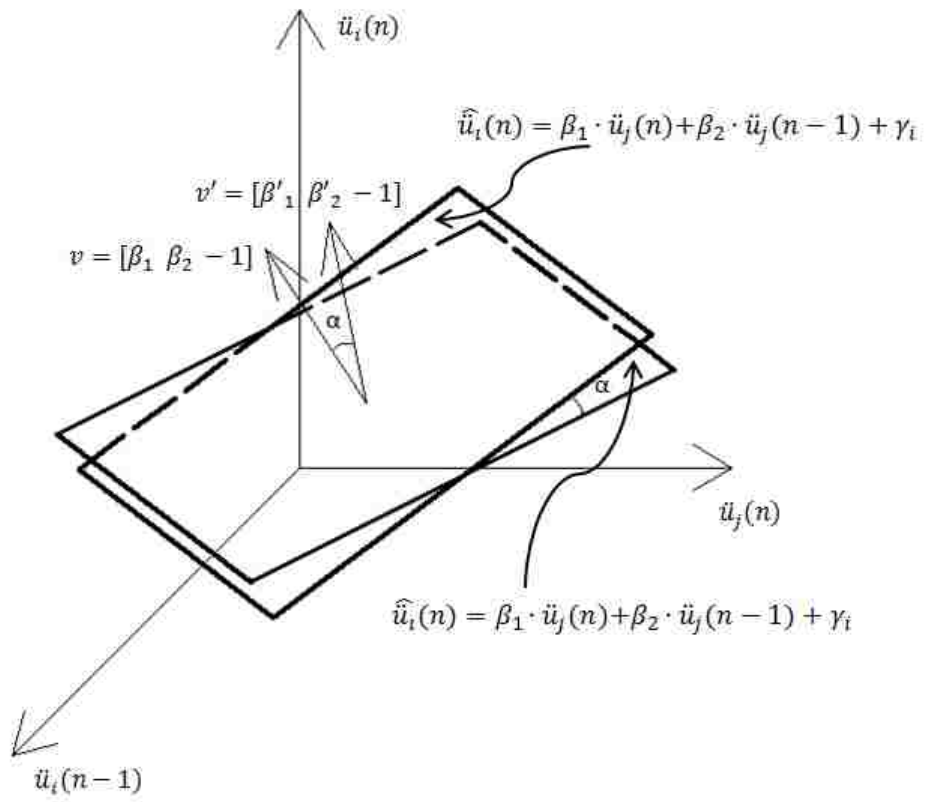
Figure 4.4 Geometry Meaning of the Damage Indicator
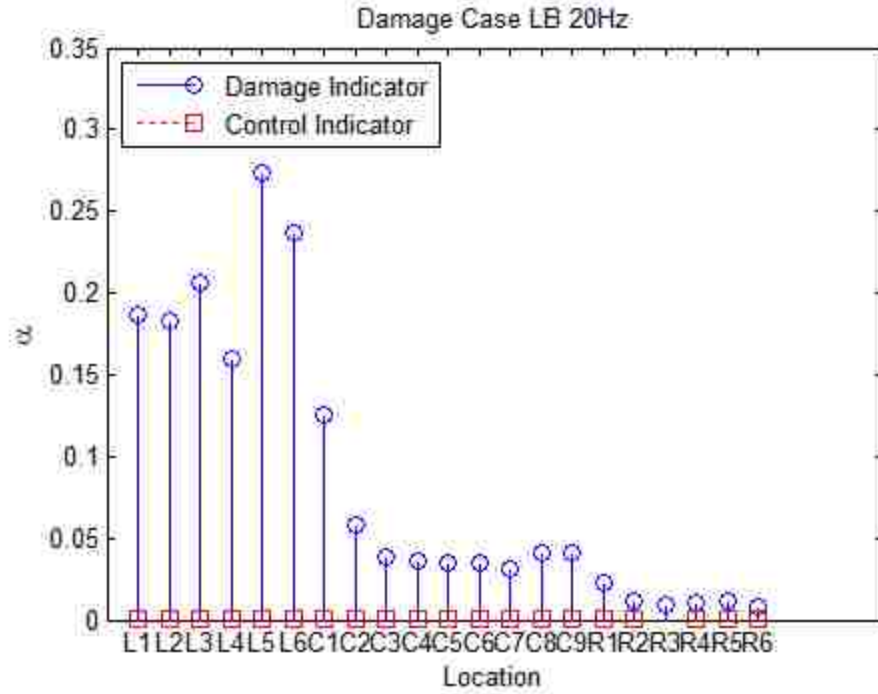
Figure 4.5 Simulation Damage Scenario LB with 20Hz Input
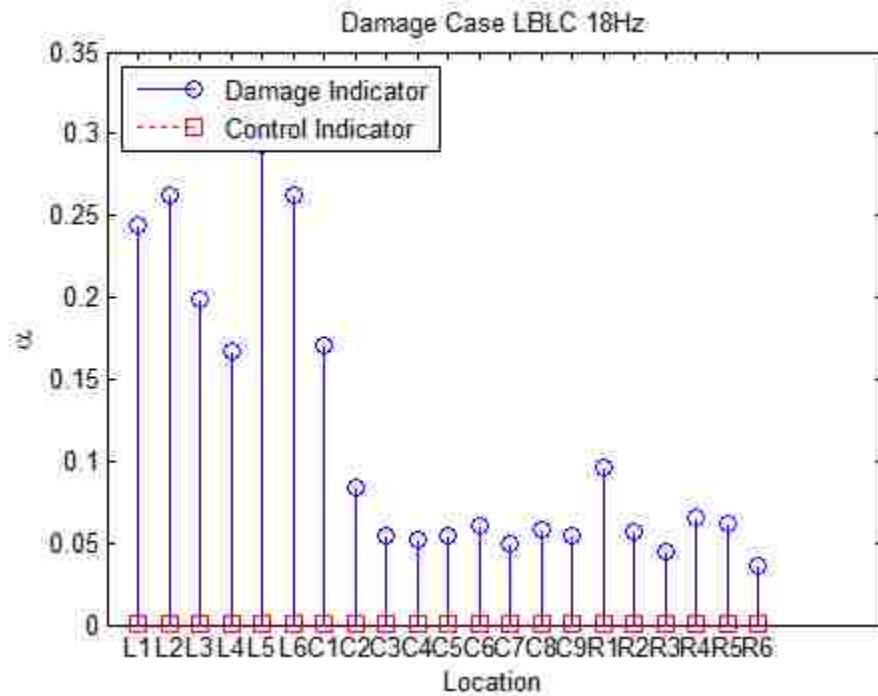
Figure 4.6 Simulation Damage Scenario LBLC with 18Hz Input
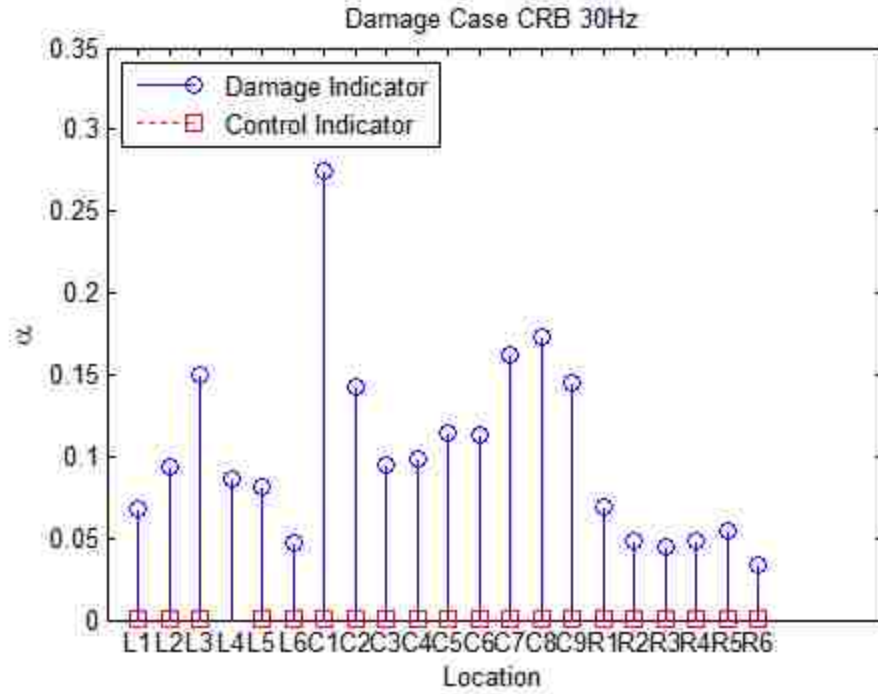
Figure 4.7 Simulation Damage Scenario CRB with 30Hz Input
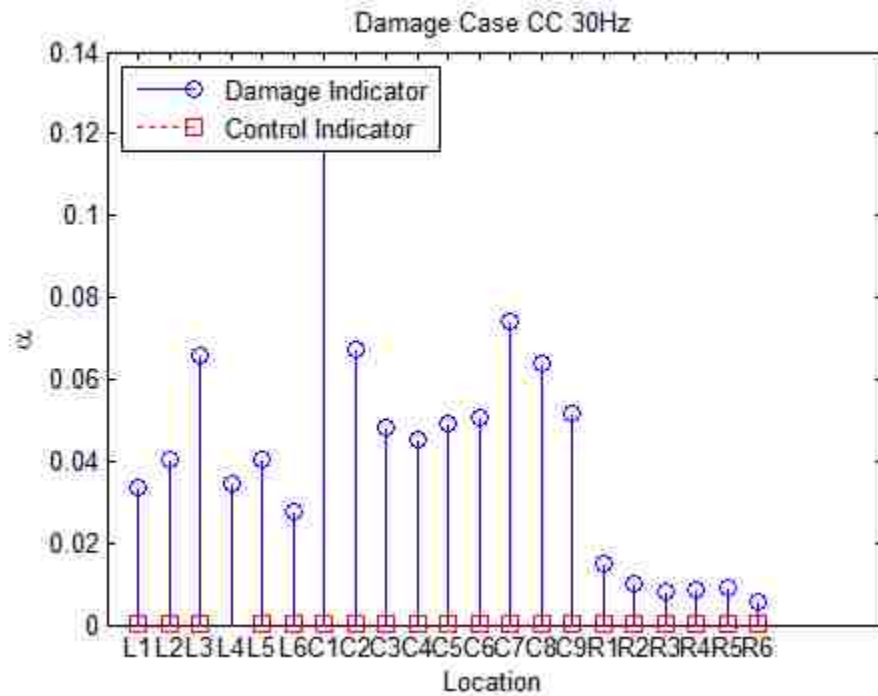
Figure 4.8 Simulation Damage Scenario CC with 30Hz Input
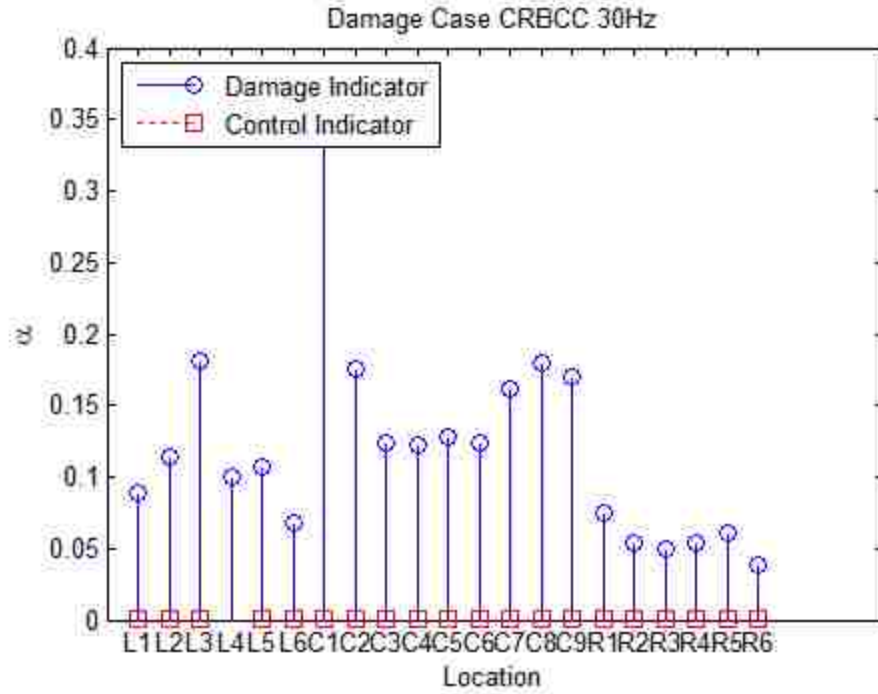
Figure 4.9 Simulation Damage Scenario CRBCC with 30Hz Input
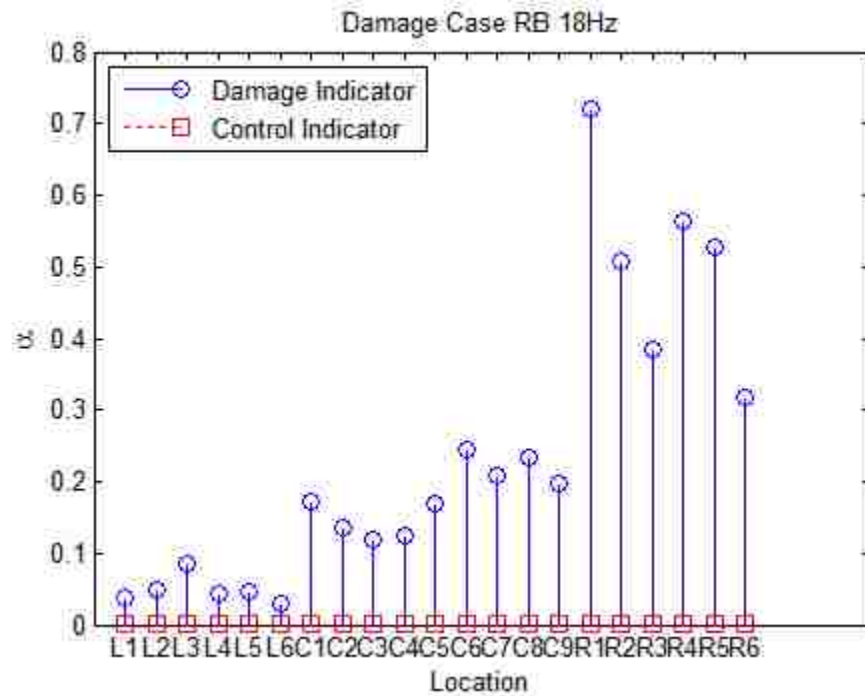
Figure 4.10 Simulation Damage Scenario RB with 18Hz Input
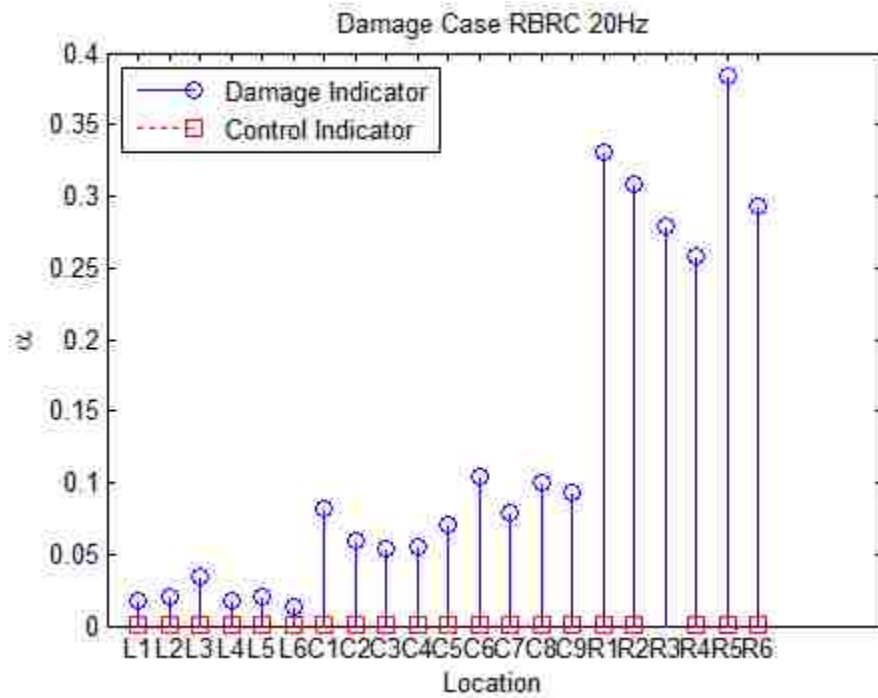
Figure 4.11 Simulation Damage Scenario RBRC with 20Hz Input
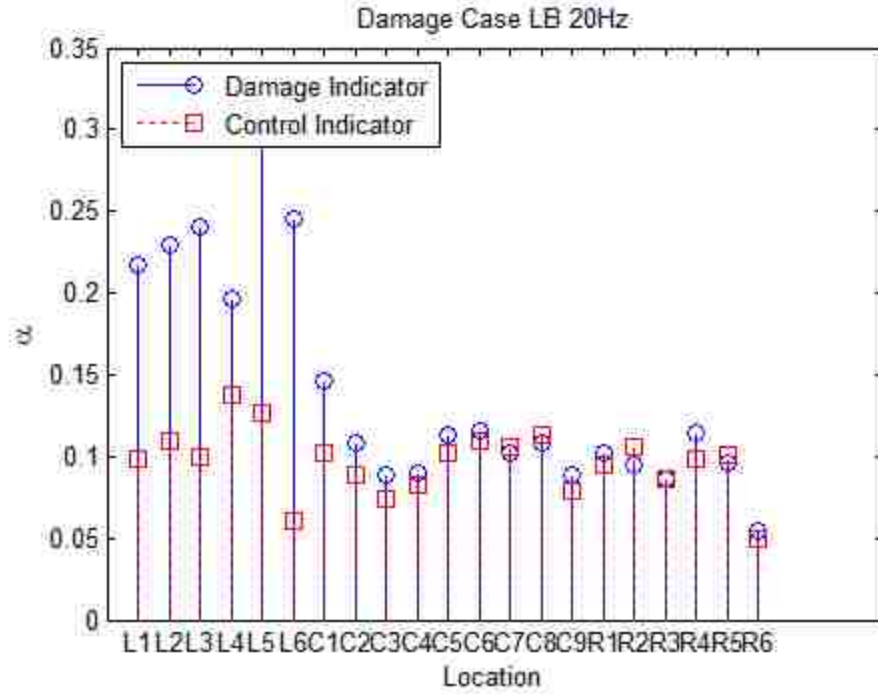
Figure 4.12a Simulation Damage Scenario LB with 20Hz Input Plus 5% Noise
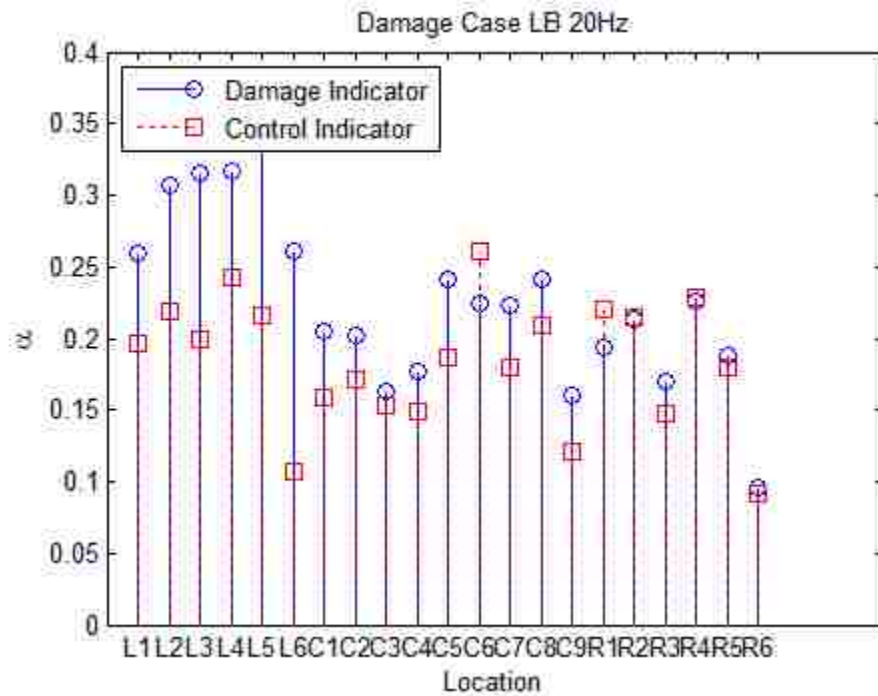
Figure 4.12b Simulation Damage Scenario LB with 20Hz Input Plus 10% Noise
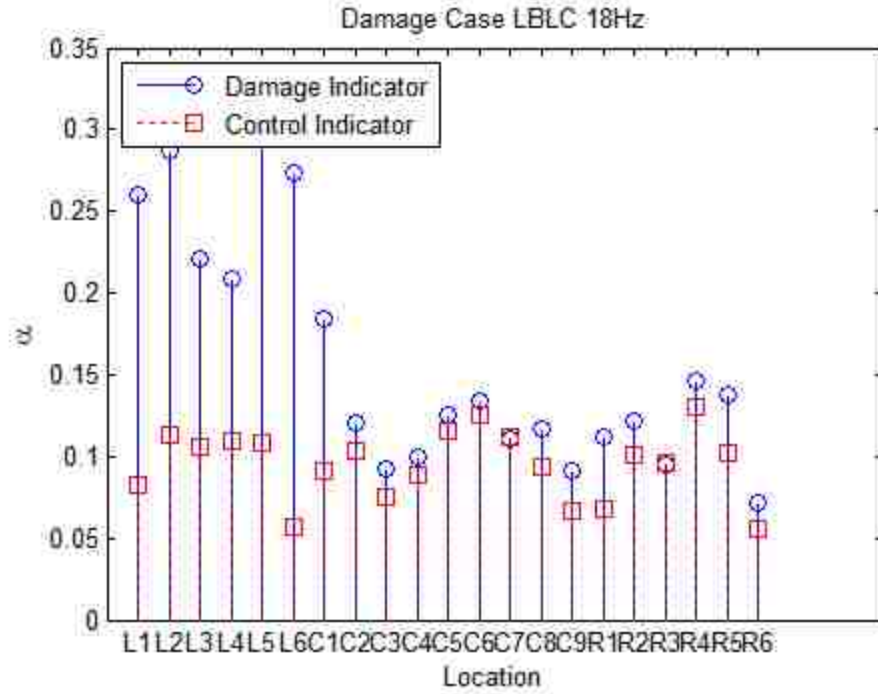
Figure 4.13a Simulation Damage Scenario LBLC with 18Hz Input Plus 5% Noise
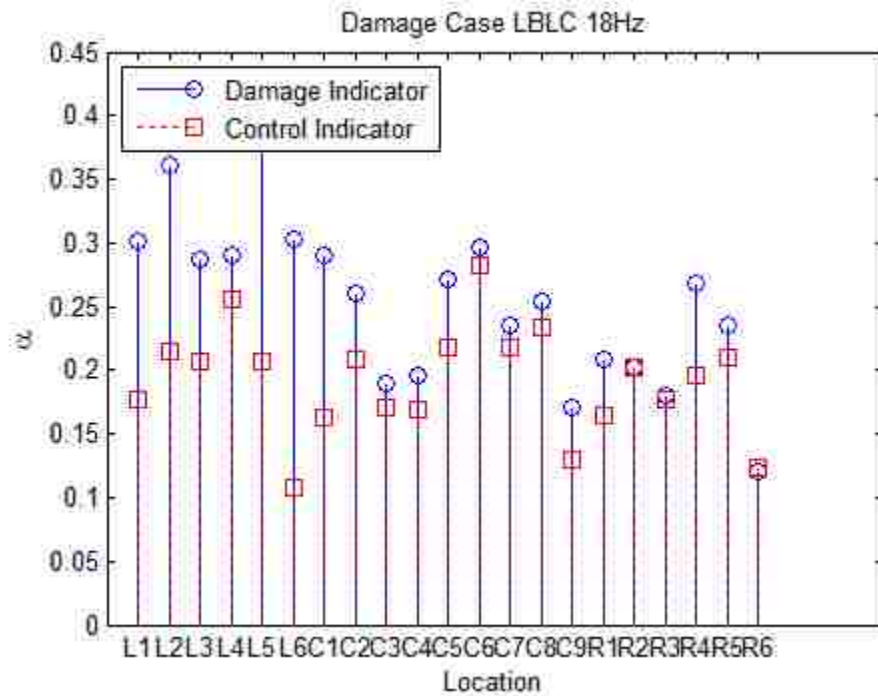
Figure 4.13b Simulation Damage Scenario LBLC with 18Hz Input Plus 10% Noise
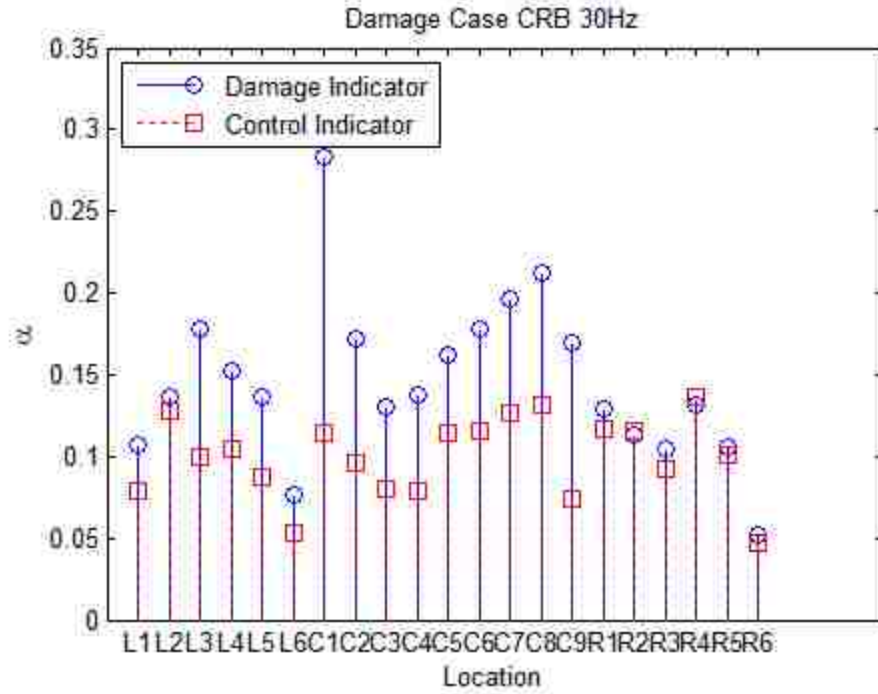
Figure 4.14a Simulation Damage Scenario CRB with 30Hz Input Plus 5% Noise
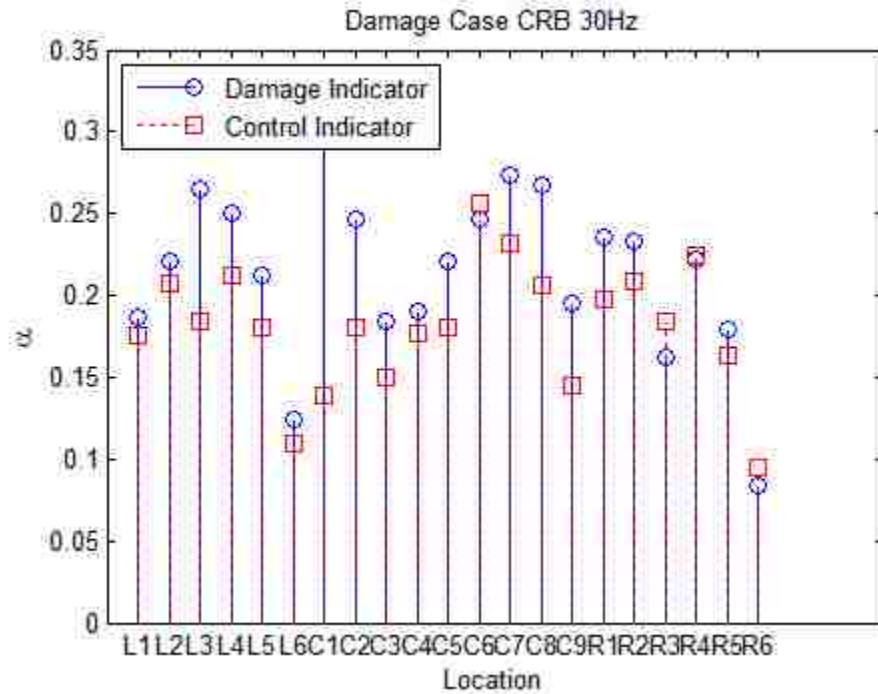
Figure 4.14b Simulation Damage Scenario CRB with 30Hz Input Plus 10% Noise
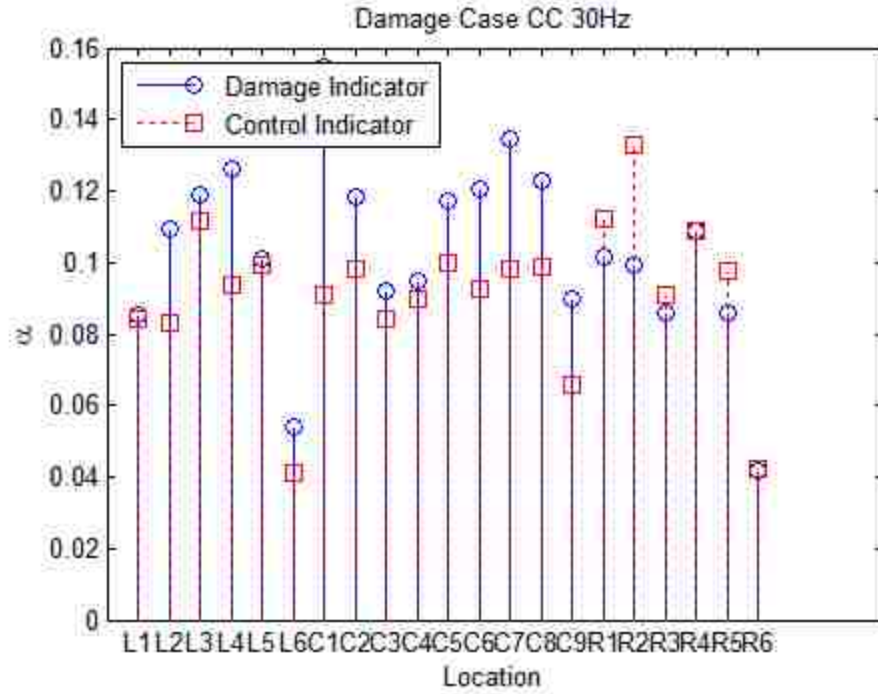
Figure 4.15a Simulation Damage Scenario CC with 30Hz Input Plus 5% Noise
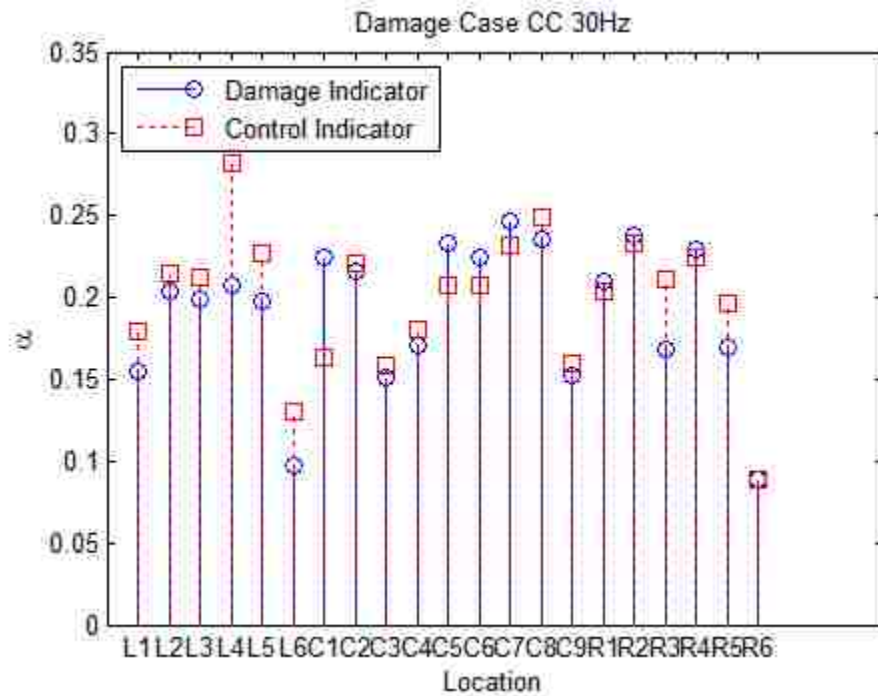
Figure 4.15b Simulation Damage Scenario CC with 30Hz Input Plus 10% Noise
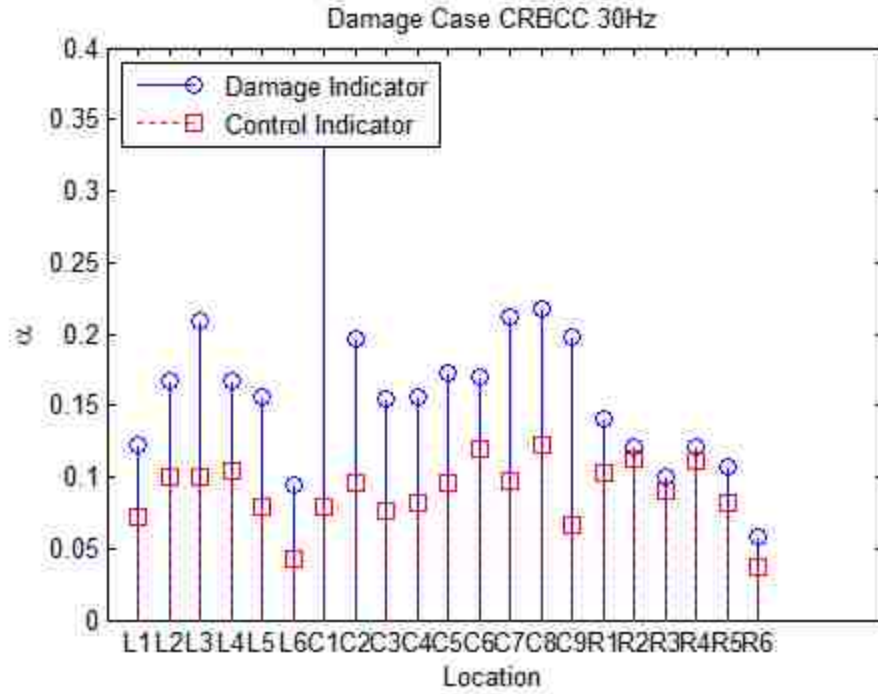
Figure 4.16a Simulation Damage Scenario CRBCC with 30Hz Input Plus 5% Noise
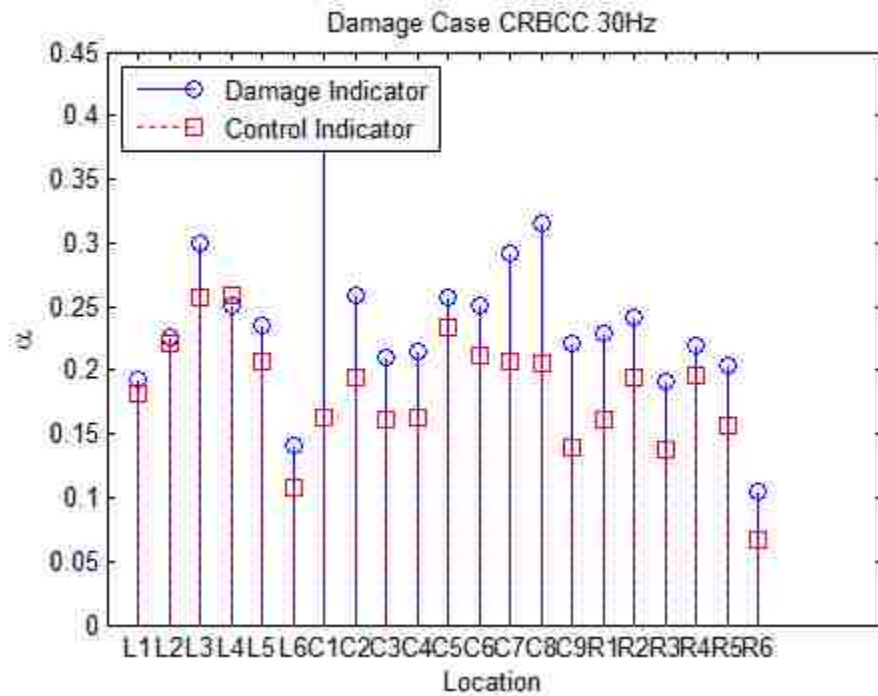
Figure 4.16b Simulation Damage Scenario CRBCC with 30Hz Input Plus 10% Noise
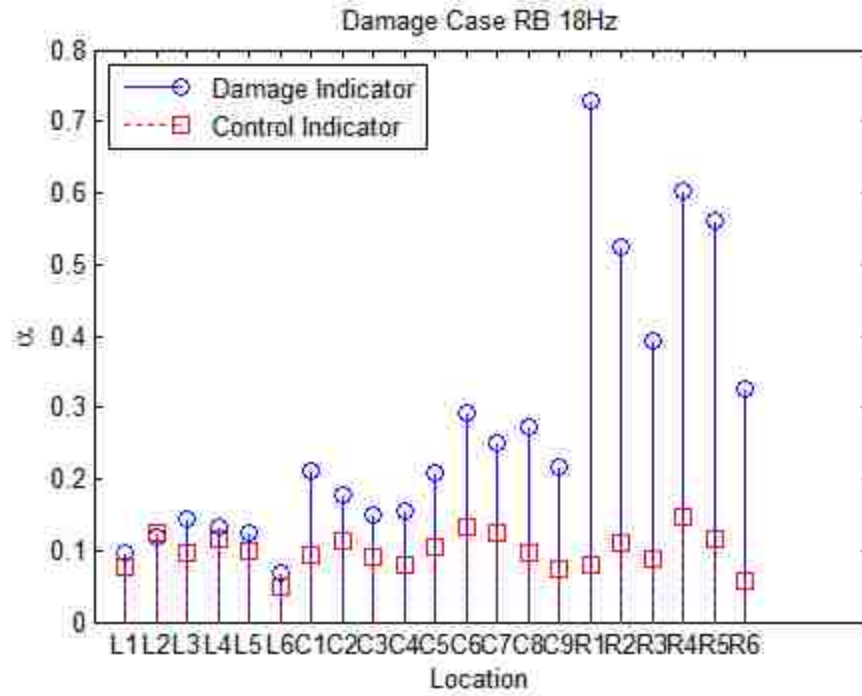
Figure 4.17a Simulation Damage Scenario RB with 18Hz Input Plus 5% Noise
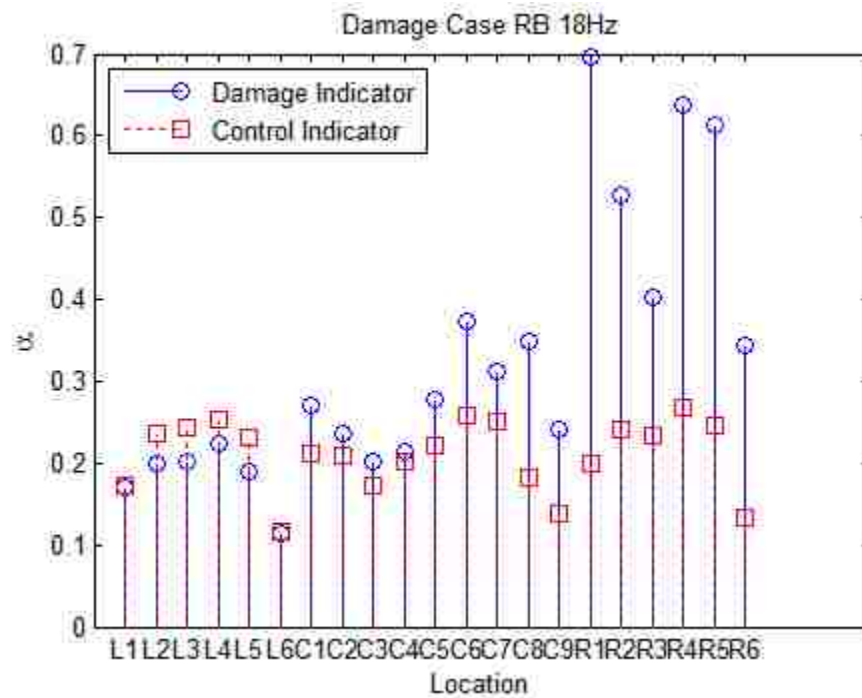
Figure 4.17b Simulation Damage Scenario RB with 18Hz Input Plus 10% Noise
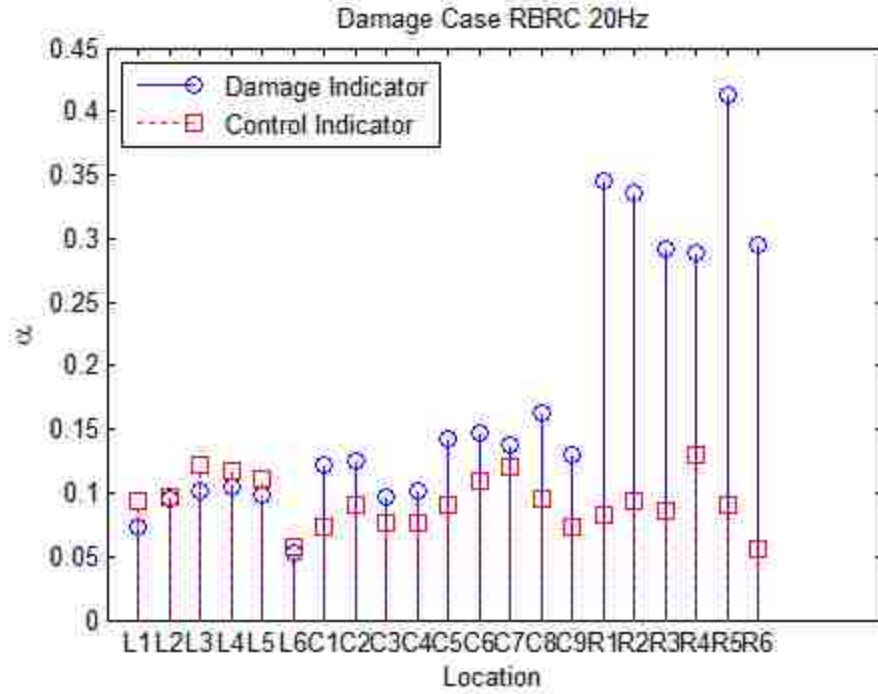
Figure 4.18a Simulation Damage Scenario RBRC with 20Hz Input Plus 5% Noise
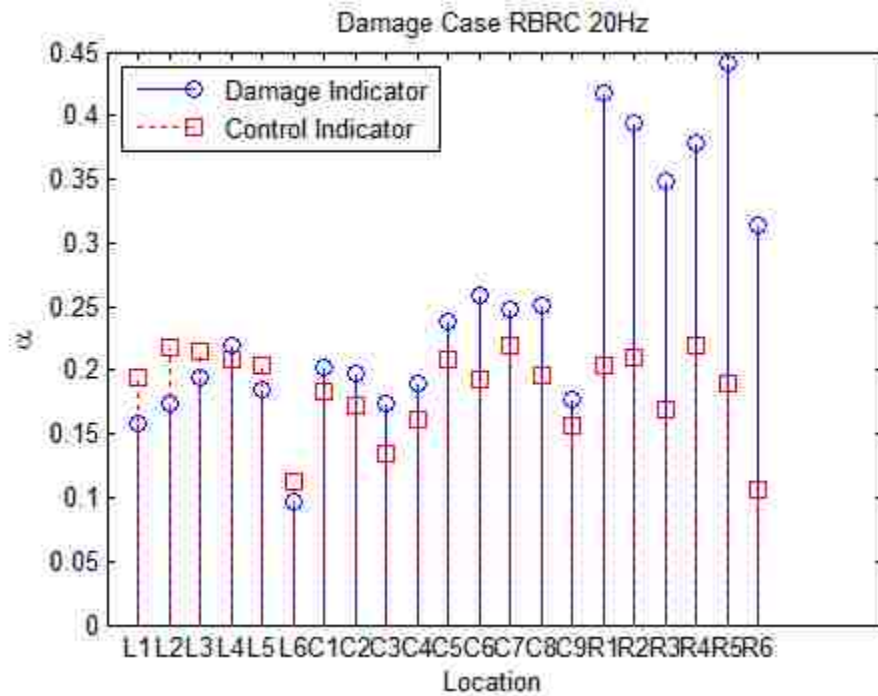
Figure 4.18b Simulation Damage Scenario RBRC with 20Hz Input Plus 10% Noise
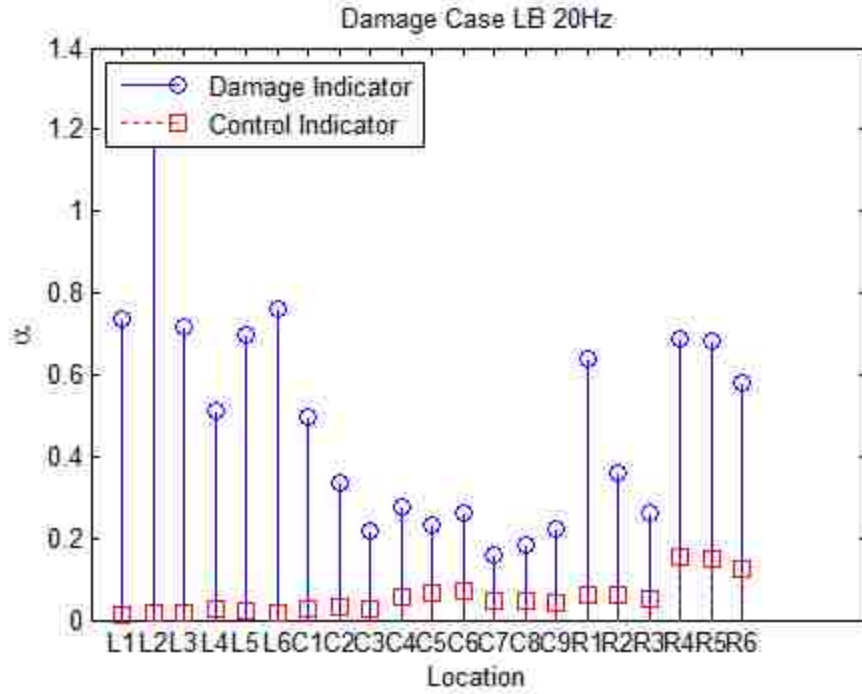
Figure 4.19 Lab Damage Scenario LB with 20Hz
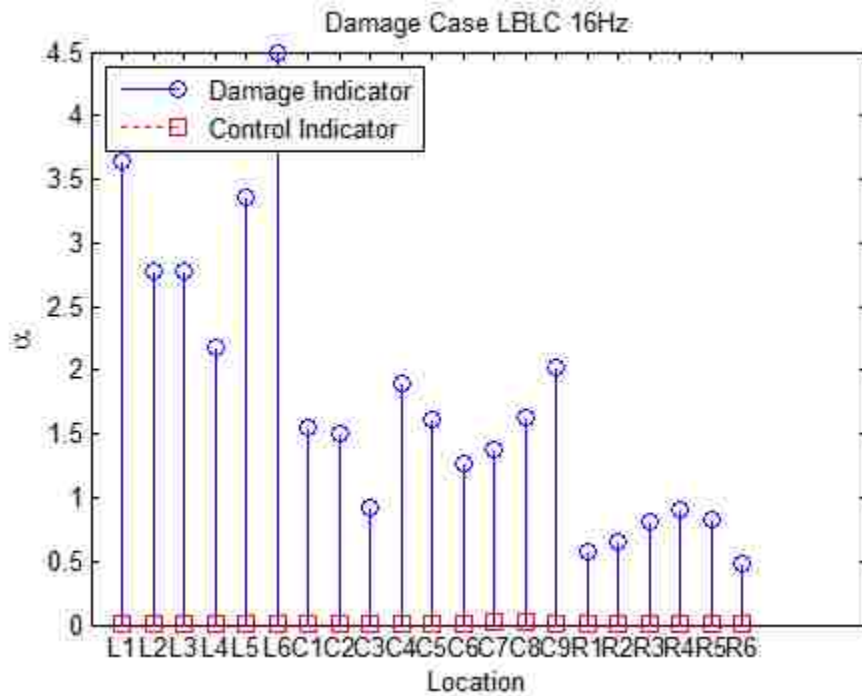
Figure 4.20 Lab Damage Scenario LBLC with 16Hz
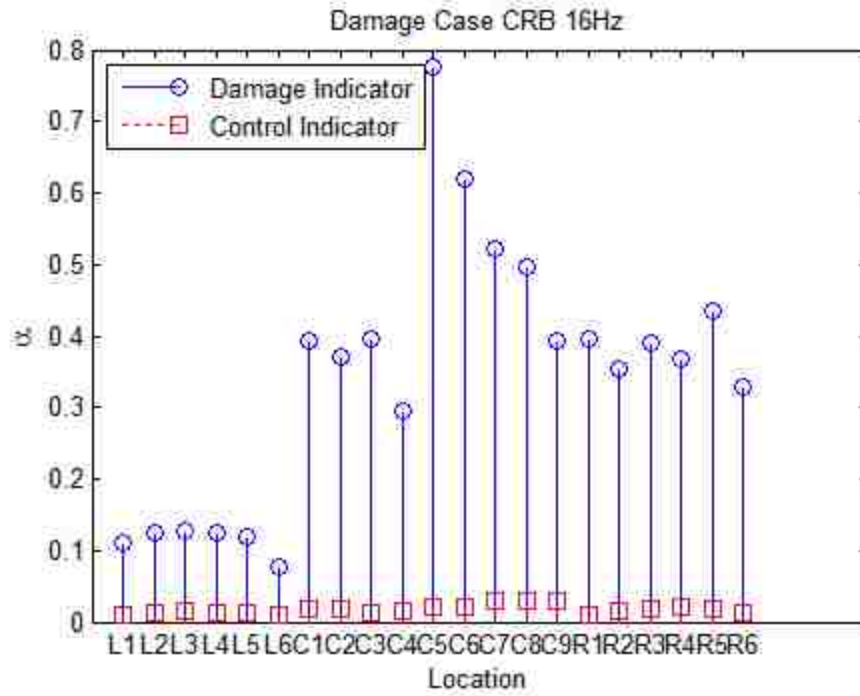
Figure 4.21 Lab Damage Scenario CRB with 16Hz
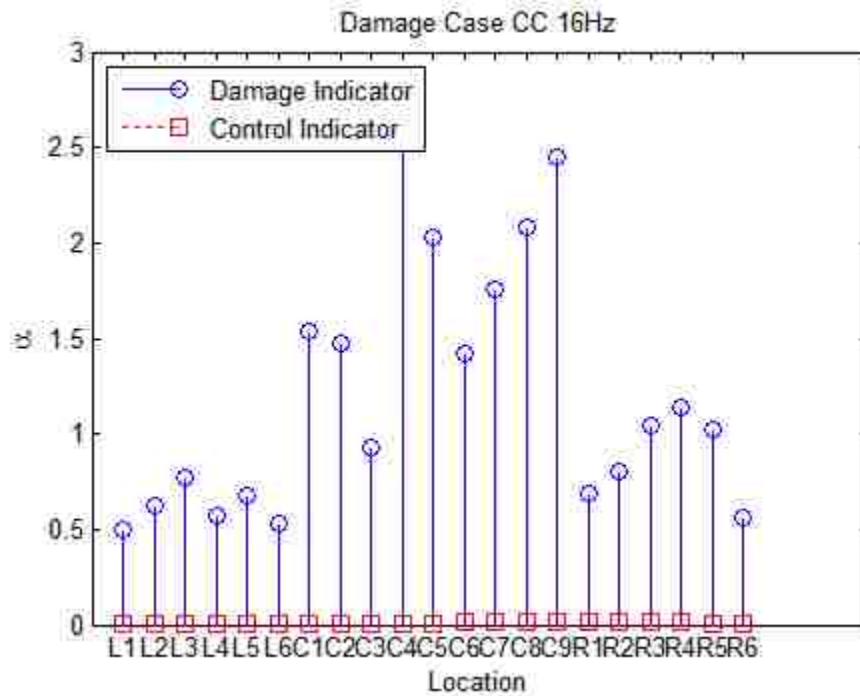
Figure 4.22 Lab Damage Scenario CC with 16Hz
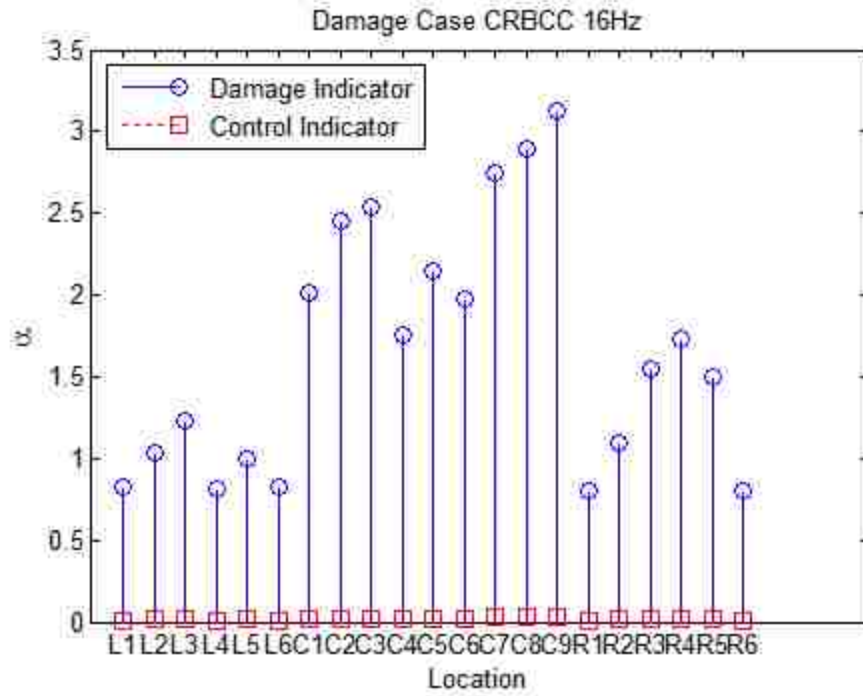
Figure 4.23 Lab Damage Scenario CRBCC with 16Hz
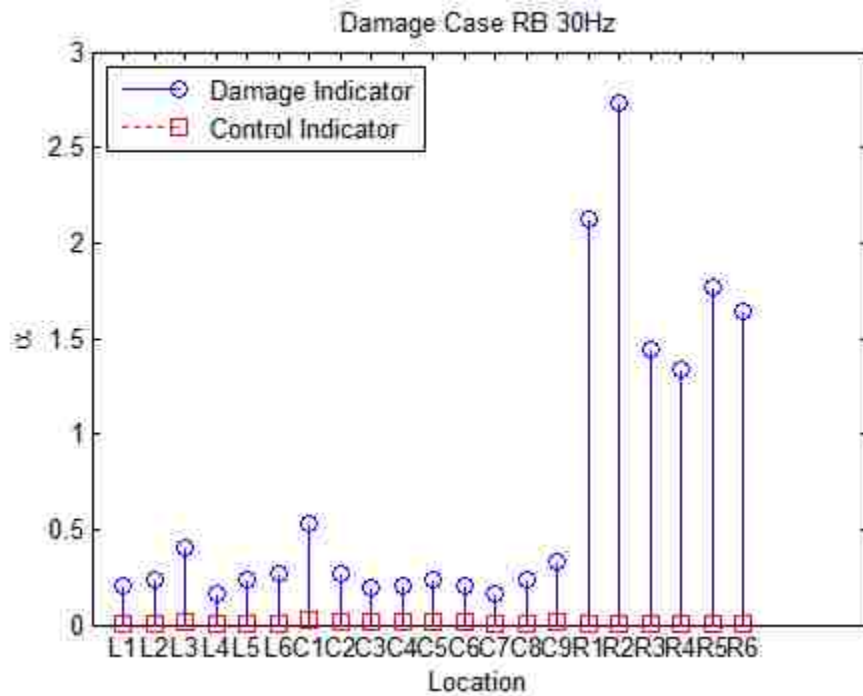
Figure 4.24 Lab Damage Scenario RB with 30Hz
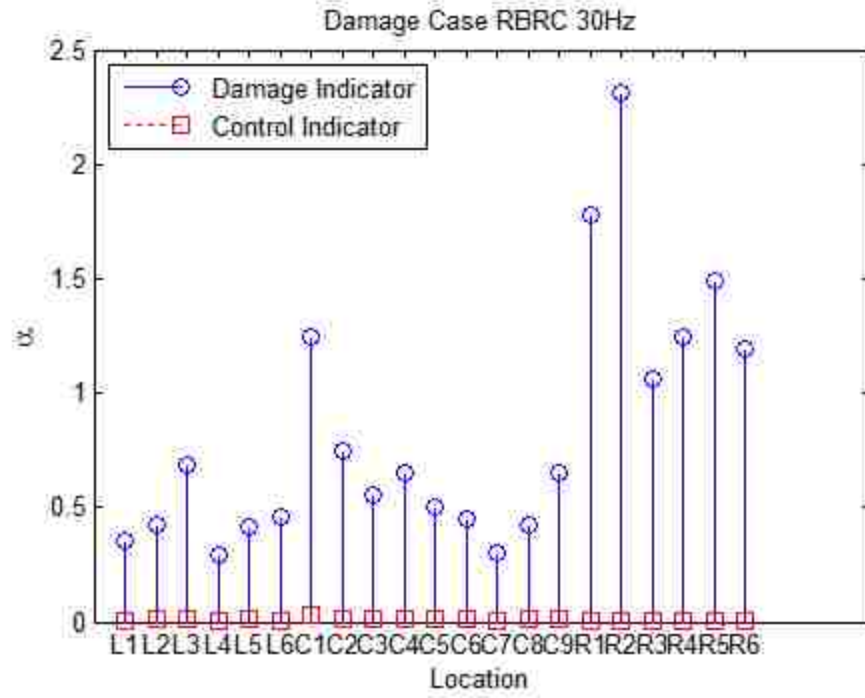
Figure 4.25 Lab Damage Scenario RBRC with 30Hz
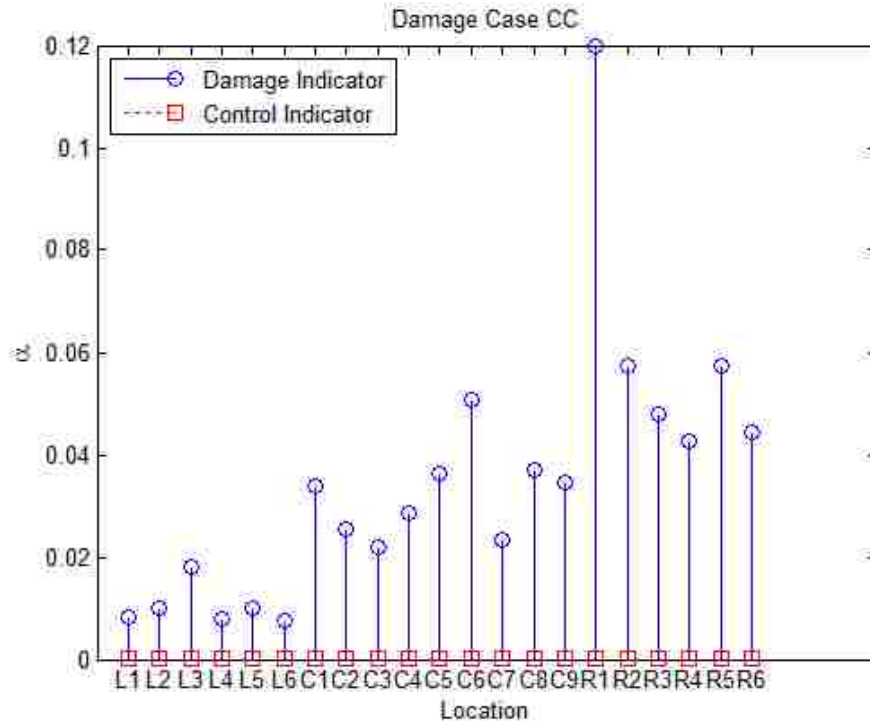
Figure 4.26a Damage Scenario CC with 18Hz Input Using Single-variable Linear Regression Based Algorithm
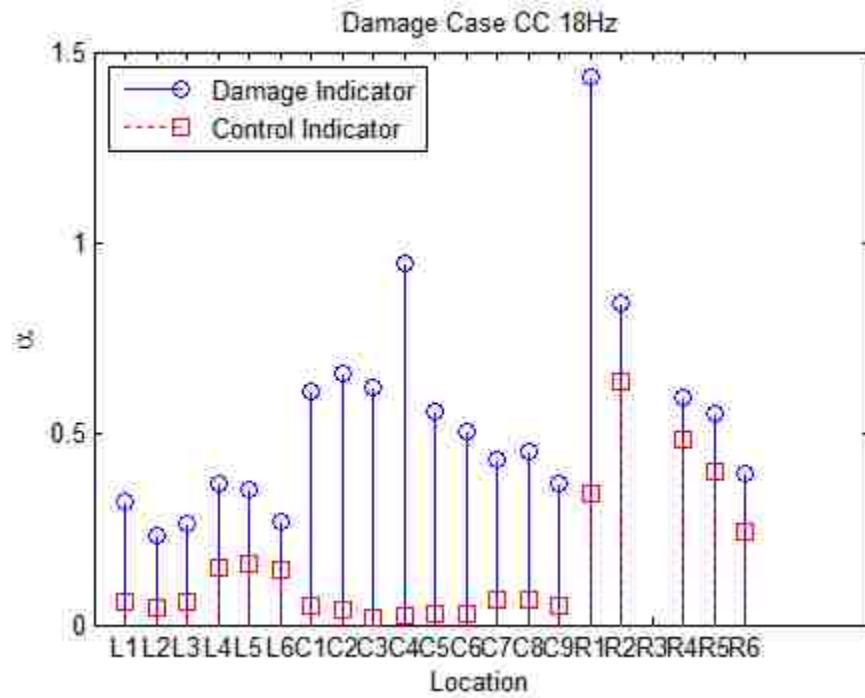
Figure 4.26b Damage Scenario CC with 18Hz Input Using Two-variable Linear Regression Based Algorithm

126

Chapter 5   Multi-Variable Linear Regression Based Damage Detection Algorithm and Random Input Tests

The single-variable linear regression method and the two-variable linear regression method are introduced and results from both the finite element simulation tests and the lab specimen tests are discussed in the previous chapters. They are proved to be useful when the inputs are harmonic, especially with some particular input frequency. However there are still two problems for applying this linear regression based damage detection algorithm. The first one is how to determine the proper number of independent variables to include in the regression function. From the previous sections, one knows that for different cases, even for different node pairs in the damage case, the number of variables that shall be used to provide a precise regression is different. The second problem is that in the real damage detection case, the input of the system will not always be harmonic. In most of the cases, the input will be ambient because, for large structures, it's almost impossible or too costly to excite the whole structure with one or multiple actuators. In this chapter, test data from random input tests will be processed with a new kind of multi-variable linear regression based damage detection method to see the possible performance of such method for the real cases.

5.1   Lab Tests with Random Input

Since in the real world dynamic loads on the structures are ambient and sometimes impulse input, test results from harmonic tests cannot prove the workability of the method for real damage detection cases. To simulate the real input on a structure, random

inputs are subjected onto the lab specimen. The character of this random input is that the power spectrum of the input has an approximate uniform distribution within a certain frequency range. In this research, this distribution will be from 0Hz to 50Hz. A part of the random input in time series is shown in Figure 5.1 and the power spectrum density plot of the input is shown in Figure 5.2.

5.2 Multi-Variable Linear Regression

Multi-variable linear regression function which is going to be used is written below.

$$\widehat{u}_i(n) = \sum_k \beta_k \cdot \ddot{u}_j(n - k + 1) + \alpha_i + \varepsilon_i \qquad \text{(Eq. 5.1)}$$

where

$\ddot{u}_j$ = acceleration response from one node used as the independent variables;

$\widehat{u}_i$ = estimated acceleration response of a node other than node i;

β_k = regression coefficients;

α_i = intercept term;

ε_i = error term;

k = number of independent variables that are included.

From the third conclusion got in Chapter 4, it is not true that the more independent variables are included, the better damage prediction is going to show. Sometimes only one regression term in the summary sign is enough. But there are also times that more than two independent variables are needed. In order to find a proper number of independent variables, an iterative linear regression is introduced to linear regression procedure. The general flow chart of this iterative linear regression is shown in Figure 5.3. In this process, the number of independent variables in the linear regression function for

each node pair is not determined until the requirement for CoD is satisfied. Then VIF for this linear regression will be checked when there are two or more independent variables and those don't have a VIF that is less than 10 will be given a 0 for the damage indicator and ruled from the final damage indicator calculation procedure.

There is a problem for applying this multi-variable linear regression. When too many terms are included in the linear regression procedure, the time taken in calculating will be very long. In order to reduce the time on iteration, a 5-term stop principle was applied. That is when more than five terms are needed in the linear regression, the process will stop and 0 will be given for the damage indicator for this node pair. Before this 5-term stop principle was applied, the average time for processing one damage scenario is about 6 hours. After it was applied, the average time taken for one damage scenario is 1 minute and 15 seconds. While the processing time was reduced, the quality of results wasn't compromised too much.

5.3   Test Results of Random Input Cases

The multi-variable linear regression based damage detection was applied on test data from random input tests. Figure 5.4 to Figure 5.10 are the results. One can see that, of all the seven damage scenarios, damage can only be successfully detected in the RB damage scenario. The results for the other six damage scenarios are either having large control indicators or vague indication of damage location.

5.4   Results from Filtered Test Data

According to conclusions got from Chapter 3 and Chapter 4, one can see that when the time-history nodal response is in some particular frequency, it is easier to identify the damage location. Based on this idea, data from random input tests will go through a band-pass filter, shown in Figure 5.11 so that only information within a particular bandwidth will be used to perform the damage detection process.

5.4.1 Band-Pass Filter Design

In the process of designing a good filter, one problem occurred: what passing frequency shall be chosen, since the relationship between the input frequency and a good damage detection result has not been cleared. The best way to bypass this problem under current situation is to try every possible passing frequency. Since the frequency content of the test data is within the range of 0Hz to 50Hz, total 50 filters will be applied. The passing band for each filter will be centered on an integer frequency and cover the adjacent ±n Hz range. For example, a 10Hz band-pass filter will let all the frequency content from (10-n) Hz to (10+n) Hz pass and zero all the other frequency content.

5.4.2 Results with ±0.3Hz Band-Pass Filter

First ±0.3Hz band-pass filters were designed and applied to the original data; examples are shown in Figure 5.12. A part of the filtered data is shown in Figure 5.13 in time series. The general shape of the plotted data is quite smooth. For these filters, the passed frequency content won't be overlapping with each other. Since 50 filters were applied onto the data for each damage scenario and there are 7 damage scenarios, it is impossible to discuss total 350 cases one by one. Table 5.1 is a summary of all 350 test results. Label 'X' means a null case that no clear prediction of damage is made. It may be caused by

high control indicators for most of the nodes or no outstanding damage indicators to show damage location; examples for both situations are given in Figure 5.14 and Figure 5.15. Label 'L', 'C' or 'R' means a single prediction case that shows the most possible damage location among the three joints; examples are given in Figure 5.16, Figure 5.17 and Figure 5.18. There is another kind of cases which are called the uncertain cases, the chance of damage appears on two of the joints is almost equal. An example of the uncertain case, 'L/ C', is placed in Figure 5.19. The numbers of cases that reveal a certain damage location, N_L, N_C and N_R, are added up to give a statistical prediction of the damage location. Each single prediction case counts for 1 and each uncertain case counts for 0.5 for each possible damage location in that case. A statistical damage prediction is now made based on the fact of which damage location is predicted in most of the cases. As shown in Table 5.4 and Figure 5.20, correct predictions are made for all seven damage scenarios without knowing the damage location. Take the damage scenario LBLC as an example, the number of cases that identify damage on the left joint is 26.5, much larger than the rest two. And by looking into Table 5.1, one can see that if most of the cases that identify the damage locating on the left joint are next to each other, almost all the way from 7Hz to 34Hz. However the damage detection results for predicting damage in scenario RB and RBRC are less reliable because the number of valid cases is small.

5.4.3 Results with ±1.0Hz Band-pass Filter

This time filters that letting a range of ±1.0Hz frequency content pass will be subjected onto the original data. Examples of the filters are shown in Figure 5.21. As one can see, adjacent filters now have the same frequency content within 1Hz. The filter the data is shown in Figure 5.22. Compared with the one shown in Figure 5.13, the general shape of

plot is sharpened, which is because more frequency content is included. The damage prediction procedure is the same as in the previous section. Table 5.5 and Figure 5.23 give the summary of the results. All 7 damage scenarios are given right damage predictions. As one can see that the valid cases in damage scenario RBRC increased a lot, useful damage prediction can be made in this scenario.

5.4.4 Results with ±2.0Hz Band-pass Filter

The band of the filters is again enlarged, from ±1.0Hz range to ±2.0Hz range. This time more frequency content was contained in the filtered data and the effectiveness of the algorithm was checked. Figure 5.24 shows the some examples of the filters. The passing band of Filter 1.0 is from 0Hz to 3Hz instead of -1Hz to 3Hz, because negative frequencies have no real meanings. Figure 2.25 shows the data in time series. Again, the shape of the plot is further sharpened. Table 5.6 and Figure 5.26 are the results. Although more information was used, the number of valid cases for damage scenario LB, LBLC, CRBCC, CC and RBRC didn't increase too much. For damage scenario CRB, the damage prediction had become better. In the previous two cases, the cases that predicting damage on the central joint were not much more than those that predicting damage on the right joint. The damage prediction results were not very convincing. However in this case, the number of cases that showing damage on the central joint is 1.74 times the one that showing damage on the right joint. Now solid conclusion can be made that damage is on the central joint.

5.5 Conclusion

In this section, test data from random input tests was processed with an upgraded linear regression based damage detection method. First the raw data was directly used without any pre-processing on it. The results from the raw data can't reveal the real damage location or any possible damage location. Then based on some conclusions got from the previous chapters, 3 kinds of filters were designed and applied to the raw data. Each kind of them let a certain range of frequency content in the raw data pass. After the results were organized and summarized, statistic-bases damage location predictions were presented for each damage scenario in each filtering case. And correct damage predictions were made for all the cases. Besides, there are also some useful conclusions that can be drawn from the test result.

1) Data coming out of low frequency band-pass filters always gives null damage prediction. For example, the first five cases showed in Table 5.1, for damage scenario LB, LBLC, CRB, CC, RB and RBRC. There is one explanation for this situation to happen. Low vibration frequency means low change of velocity, i.e. acceleration. Small system acceleration can be easily mixed with noise caused by ambient vibration. Thus the damage identification results will be showing nothing.

2) When the passing band of the filter increases from ±0.3Hz to ±1.0Hz, the damage prediction becomes clearer due to the larger number of valid prediction cases. The valid cases rate in damage scenario LB rises from 23/50 to 33/50. However when the passing band increases ±1.0Hz to ±2.0Hz, this valid case rate doesn't change too much. So it seems that within some passing band width, enlarging the band width actually helps producing a better

damage prediction. But if the band width goes larger than that limit, the damage prediction result won't be improved greatly. Revealing the pattern of choosing a proper passing band width needs some further research.

Table 5.1 Results Summary of Damage Detection with ±0.3Hz Filters

±0.3Hz	LB	LB&LC	CRB	CC	CRB&CC	RB	RB&RC	LB&RB
1	X	X	X	X	L	X	X	X
2	X	X	X	X	X	X	X	C/R
3	X	X	X	X	C	X	X	R
4	X	X	X	X	C	X	X	R
5	X	X	X	X	C	X	X	X
6	X	X	R	C	R	X	X	C
7	X	L	X	R	X	X	X	X
8	X	L	X	C/R	X	X	X	X
9	C	L	X	R	X	X	X	X
10	X	L	X	X	X	X	X	X
11	X	L	C	R	C	X	X	C
12	X	R	X	X	X	X	X	X
13	C/R	L	X	X	X	X	X	X
14	X	X	X	X	X	X	X	X
15	X	L	C	C/R	X	X	X	X
16	X	L	X	X	X	X	X	R
17	X	L/R	X	X	X	X	X	X
18	X	L	X	X	X	X	X	R
19	L	L	X	C	C	X	R	R
20	L	L	R	C	C/R	R	R	R
21	L	L	R	C	C/R	R	R	R
22	L	L	R	C/R	C/R	X	X	C/R
23	L	L	X	C	X	X	X	C/R
24	L	L	X	X	X	X	X	X
25	X	L/C	R	X	X	X	R	L
26	X	X	X	X	X	X	X	C/R
27	X	X	X	C/R	X	X	X	X
28	L	L	X	X	X	X	L	R
29	L	L	X	X	C/R	X	X	R
30	L	L	C	C	R	X	X	C/R
31	L	L	C	L	C	X	X	X
32	X	C	C	X	X	X	X	X
33	X	L	C/R	L	X	X	X	X
34	X	L	X	C/R	C/R	X	X	C
35	X	C	C/R	C	C	X	R	X
36	X	X	X	L/C	X	X	X	X
37	X	C/R	X	C/R	L	X	X	X
38	L/C	L/C	L/C	L/C	L/C	X	X	X
39	L	L/C	X	L	L/C	X	X	C
40	L	L/C	C	L/C	C	X	X	X
41	L/C	L/C	X	C	C	X	X	X
42	L	L/C	X	C	C	X	X	X
43	L	L/C	X	X	C	X	X	X
44	X	L/C	X	X	C	X	X	X
45	C	L/C	C	C	C	X	X	C
46	C	L/C	X	X	C	X	X	X
47	X	X	L	X	C	X	X	X
48	L/C	X	C	X	C	X	X	X
49	L	C	X	X	X	X	L	X
50	L	X	X	X	X	X	X	X

+

135

Table 5.2 Results Summary of Damage Detection with ±1.0Hz Filters

±1Hz	LB	LB&LC	CRB	CC	CRB&CC	RB	RB&RC
1	C	X	X	X	R	X	X
2	X	X	X	X	C/R	X	X
3	X	X	X	X	C	X	X
4	X	X	X	X	C	X	X
5	X	L/C	R	C/R	C	X	X
6	X	L	X	C	X	X	X
7	C	L/C	C	X	C	X	X
8	X	L	C/R	C	C	X	X
9	C	L	X	C/R	X	X	X
10	X	L	R	R	X	X	X
11	X	L	X	X	C	X	X
12	X	L	C/R	X	C	X	X
13	X	L	X	C	X	X	X
14	X	L	R	X	C	X	X
15	X	L	C	X	L/C	X	C
16	X	L	C	X	C	C	C
17	X	L	X	X	X	X	L/C
18	L	L	X	X	C	C	C
19	L	L	R	C	C	C/R	R
20	L	L	R	C	C/R	R	R
21	L	L	R	C	R	R	R
22	L	L	R	C	C/R	R	R
23	L	L	X	C	C	R	C/R
24	L	L	C/R	C	R	C	X
25	L	L	R	X	R	X	C/R
26	L	L/C	X	X	X	X	R
27	L	L	X	X	L/C	X	R
28	L	L	R	X	X	X	R
29	L	L	C/R	C	C	X	R
30	L	L	C	L/C	C	X	R
31	L	L	C	L	C	X	R
32	L	L	X	X	X	X	R
33	L	L/C	C	L/C	X	X	C/R
34	X	L	C	X	C	X	R
35	L	R	X	L	C/R	X	X
36	C/R	C/R	C/R	X	C/R	X	X
37	X	C/R	X	C	X	X	X
38	L	L/C	L	C	X	X	L/C
39	L	L/C	X	L/C	L/C	X	R
40	L/C	L/C	C	L/C	C	X	R
41	L/C	L/C	X	L/C	C	X	R
42	L/C	L/C	X	C	C	X	X
43	L/C	L/C	C	C	C	X	R
44	L/C	L/C	C	C	C	X	R
45	C	L/C	C	C	C	X	R
46	C	L/C	C/R	X	C	X	R
47	X	X	X	X	X	X	R
48	L	L/C	L/C	X	X	X	X
49	X	C	R	R	C/R	X	L/C
50	L/C	C	L/C	L/C	L	X	X

Table 5.3 Results Summary of Damage Detection with ±2.0Hz Filters

±2Hz	LB	LB&LC	CRB	CC	CRB&CC	RB	RB&RC
1	X	X	X	X	R	X	X
2	X	X	X	X	R	X	X
3	X	X	X	X	C	X	X
4	X	L	C	X	C	X	X
5	X	L	C	C	C	X	X
6	C	L	X	C	C	X	X
7	C	L	C	X	C	X	X
8	C	L	C	X	C	X	X
9	X	L	C	X	X	X	X
10	X	L	C/R	C	X	X	X
11	X	L/C	R	X	C	X	X
12	X	L/C	X	C	C	X	X
13	X	L	X	X	X	X	X
14	C	L	R	X	L/R	X	C/R
15	X	L	C	X	X	C/R	C
16	L	L	X	X	X	X	L/C
17	L	L	X	X	X	L	X
18	L	L	X	X	X	C/R	C/R
19	L	L	R	C	C	R	R
20	L	L	R	C	C/R	R	R
21	L	L	R	C	R	R	R
22	L	L	R	C	R	R	R
23	L	L	C/R	C	C/R	C/R	R
24	L	L	R	X	R	X	R
25	X	L	L/R	X	C/R	X	R
26	X	L	X	X	X	X	R
27	X	L	L	X	X	X	R
28	X	L	R	C	X	X	R
29	L	L/C	X	X	X	X	R
30	L	L/C	L/R	X	C	X	R
31	L	L/C	C	L	C	X	R
32	L	L/C	X	L/C	X	X	R
33	L	C	X	L/C	X	X	R
34	L	C	L/C	L/C	C/R	X	R
35	X	C/R	C	L/C	C	X	X
36	X	C/R	C	X	X	X	C/R
37	X	C/R	C	C	X	X	C
38	L	C	C	L	L	X	X
39	L	L/C	C	C	C	X	R
40	L/C	L/C	C	L/C	C	X	R
41	L/C	L/C	C	C	C	X	R
42	L/C	L/C	C	C	C	X	R
43	L/C	L/C	C	C	C	X	X
44	C	L/C	C	C	C	X	R
45	C	L/C	C/R	C	C	X	R
46	L/C	L/C	C	X	C	X	R
47	L/C	L	L/C	R	C	X	R
48	C	C	R	X	X	X	C
49	X	X	L	L	X	X	C/R
50	X	C	X	C	X	X	X

Table 5.4 Summary of Damage Detection for Random Input Case with ±0.3Hz Band-pass Filters

	LB	LBLC	CRB	CRBCC	CC	RB	RBRC
N_L	17.5	26.5	1.5	3	4.5	0	2
N_C	5	8.5	9.5	19.5	14	0	0
N_R	0.5	2	6	4.5	6	2	5
Damage Predication	L	L	C	C	C	R	R

**Table 5.5 Summary of Damage Detection for Random Input Case with ±1.0Hz Band-pass Filters**

	LB	LBLC	CRB	CRBCC	CC	RB	RBRC
N_L	23	33	2	5	3	0	1.5
N_C	9.5	10.5	15	20	27	3.5	6
N_R	0.5	1.5	12	2	7	4.5	21.5
Damage Predication	L	L	C	C	C	R	R

Table 5.6 Summary of Damage Detection for Random Input Case with ±2.0Hz Band-pass Filters

	LB	LBLC	CRB	CRBCC	CC	RB	RBRC
N_L	20	31	4	6.5	1.5	1	0.5
N_C	10	13.5	20	20.5	23	1.5	6
N_R	0	1.5	11.5	1	7.5	5	25.5
Damage Predication	L	L	C	C	C	R	R
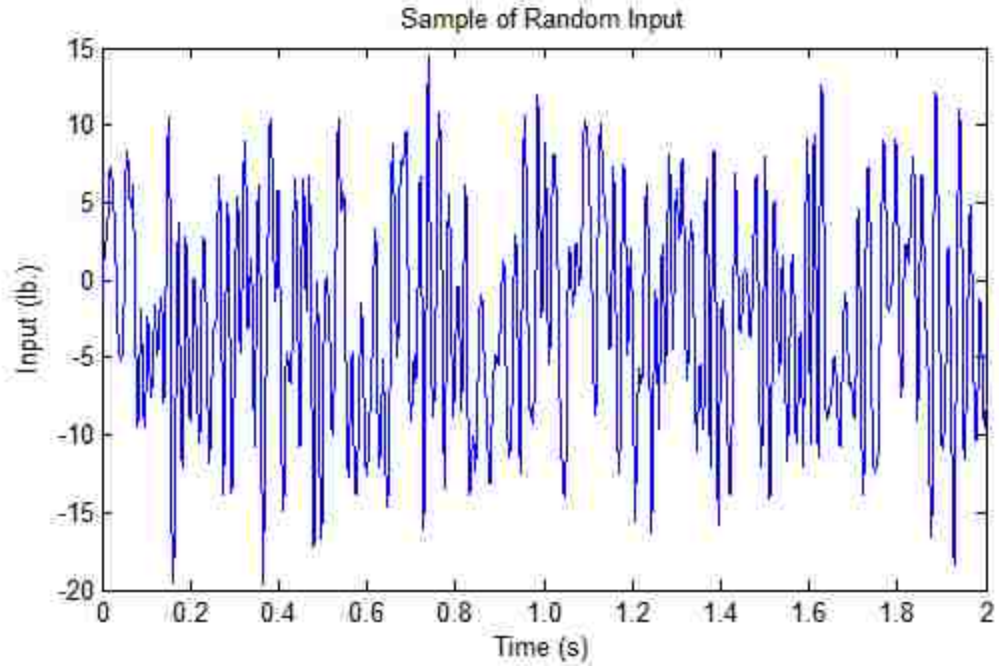
Figure 5.1 A Sample of Random Input
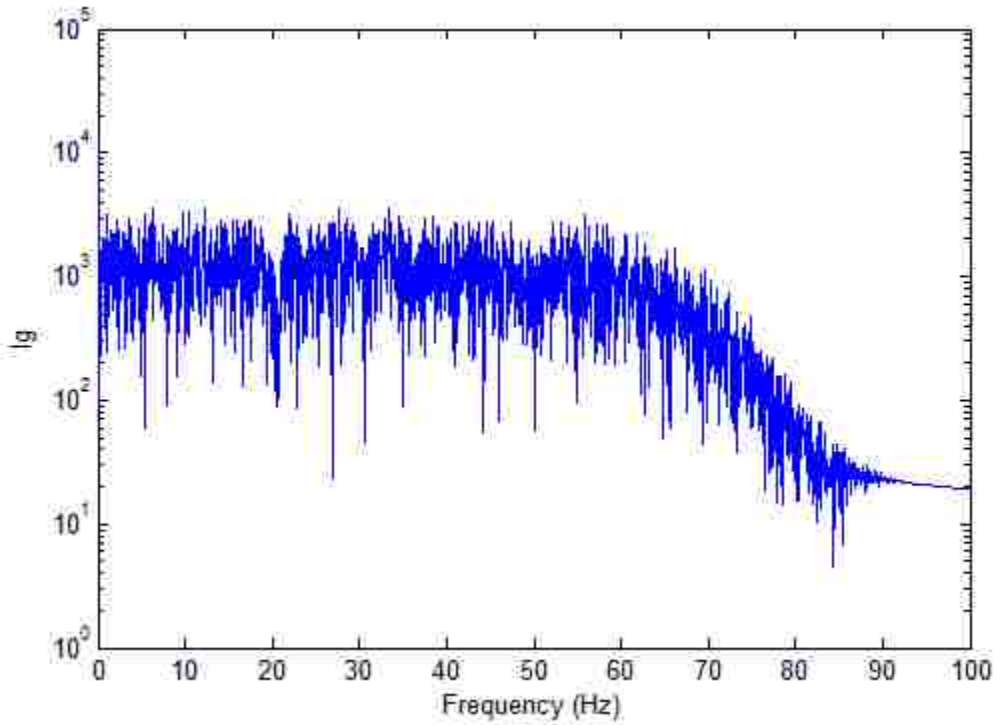
Figure 5.2 Filtering Data in Frequency Domain
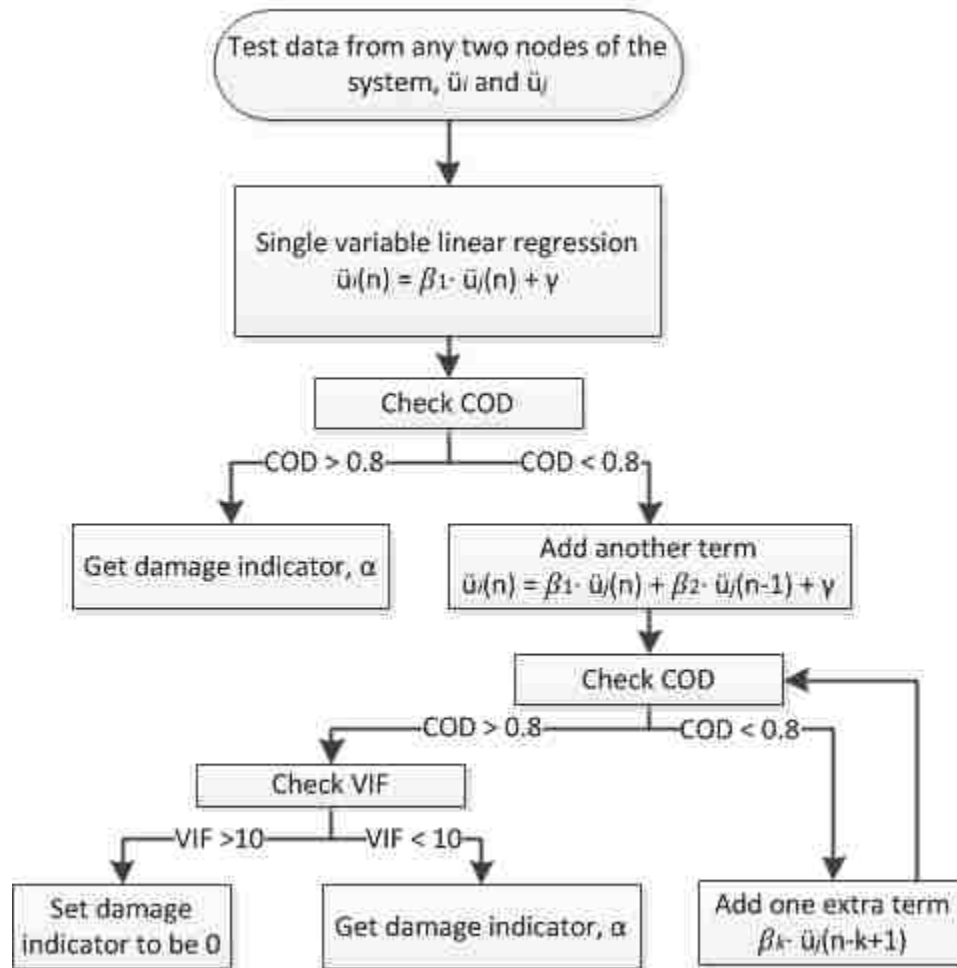
Figure 5.3 Flow Chart of the Multi-variable Linear Regression Based Iterative Damage Detection Algorithm
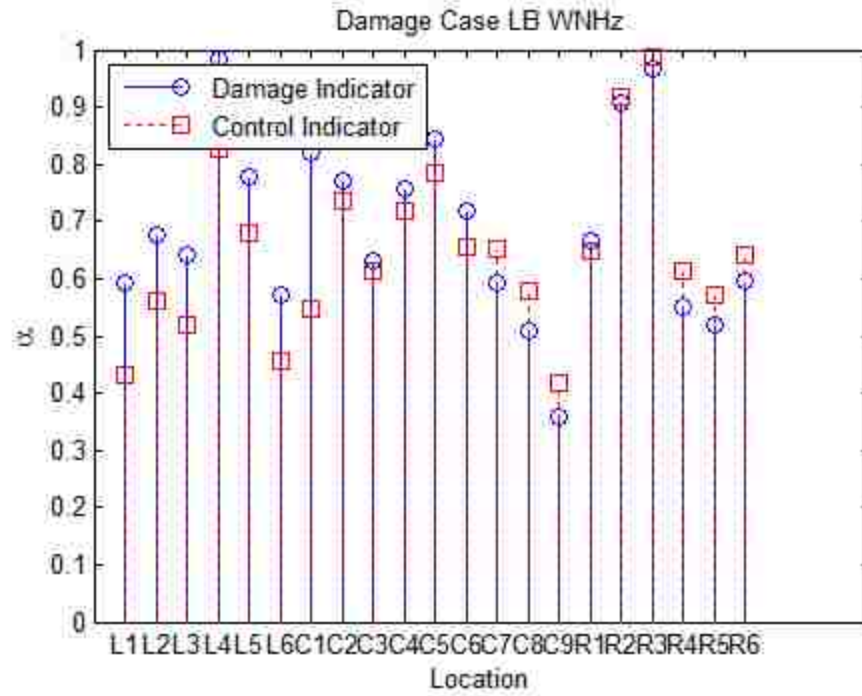
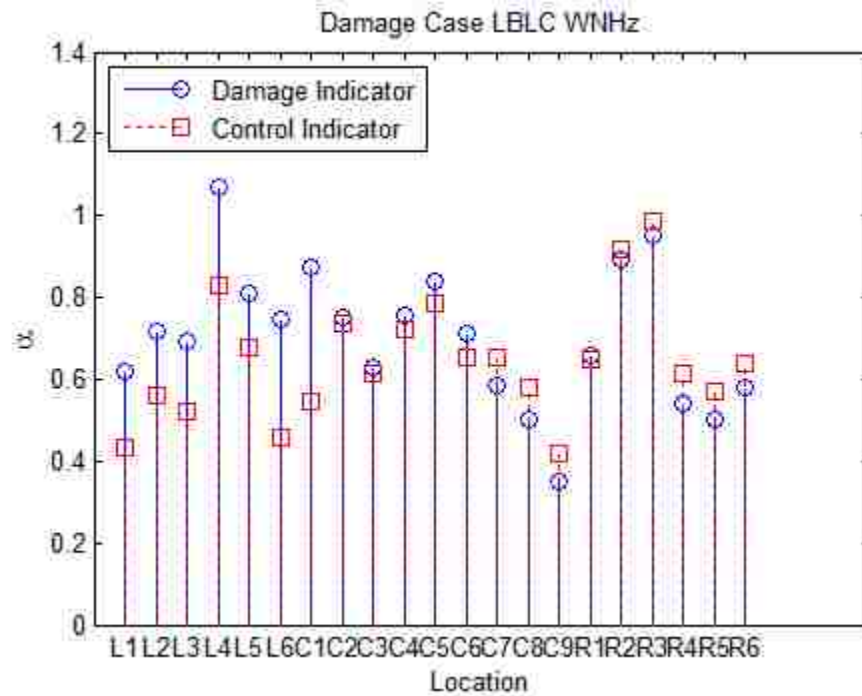**Figure 5.4 Random Input Test Result for Damage Scenario LB Using Full Data**

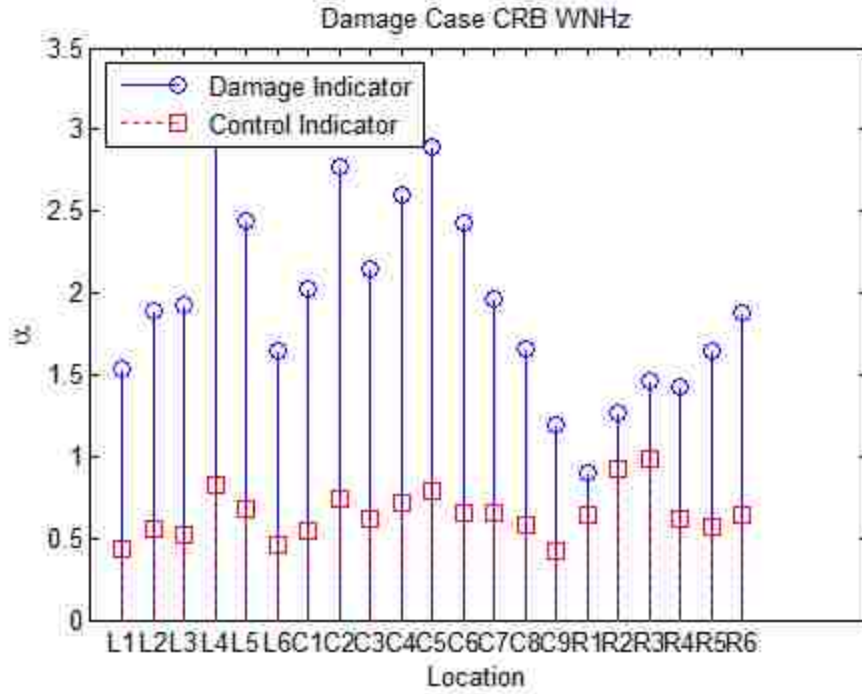**Figure 5.5 Random Input Test Result for Damage Scenario LBLC Using Full Data**

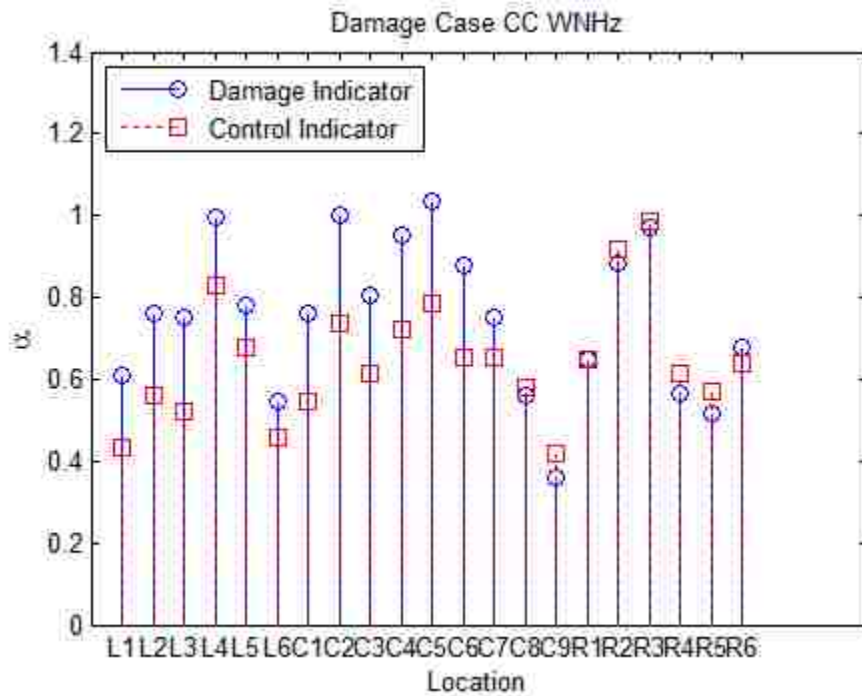**Figure 5.6 Random Input test Result for Damage Scenario CRB Using Full Data**

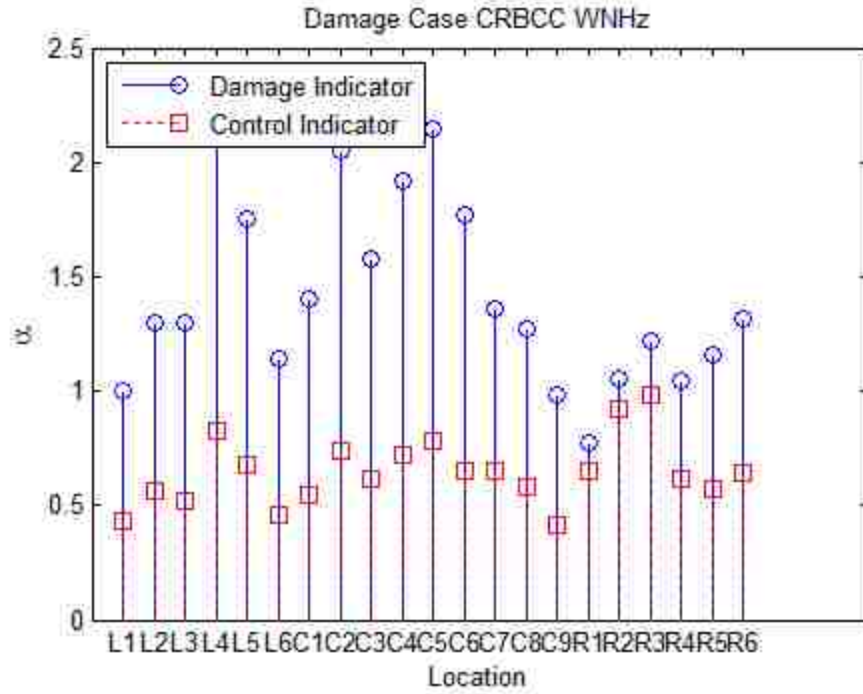**Figure 5.7 Random Input test Result for Damage Scenario CC Using Full Data**

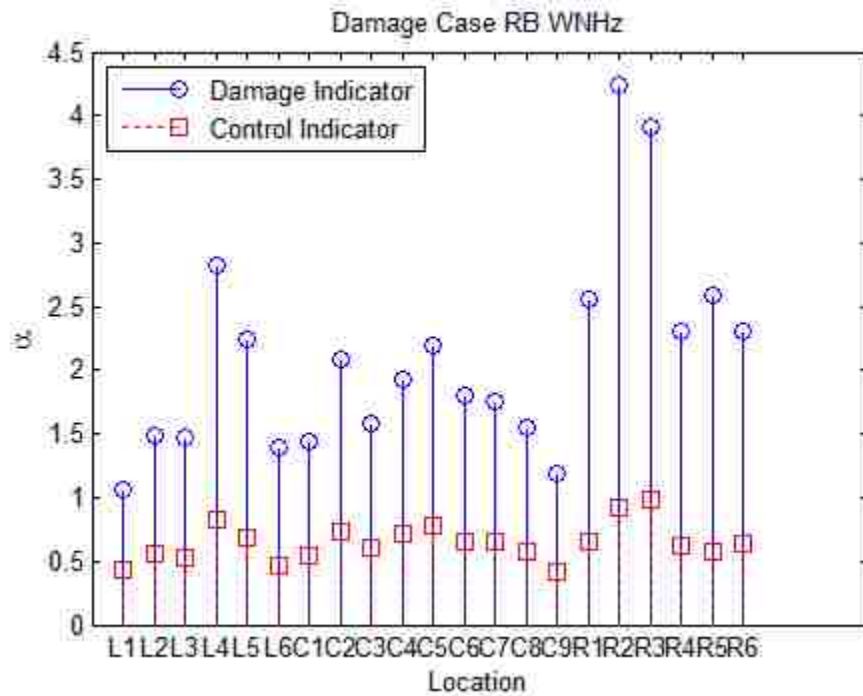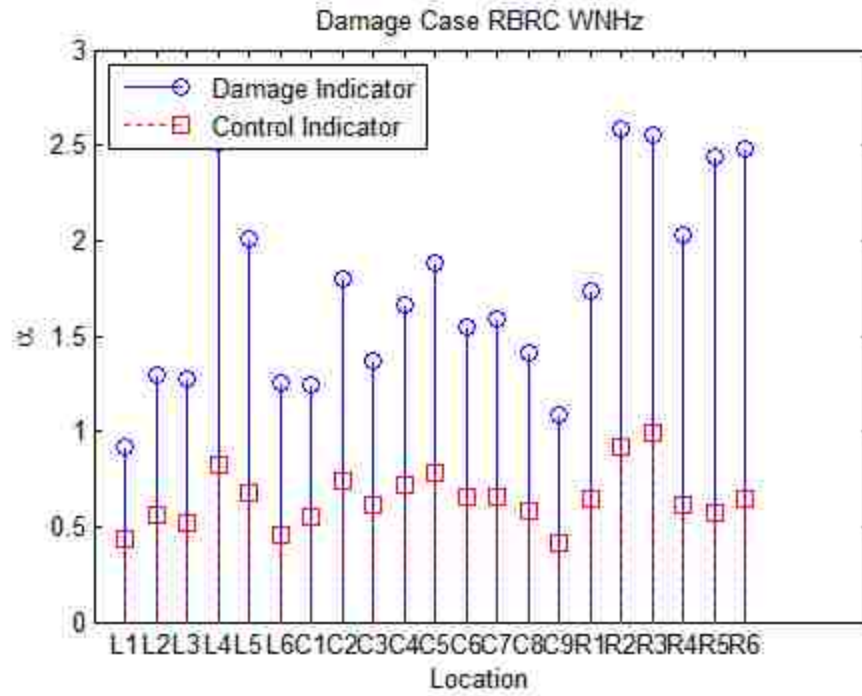**Figure 5.8 Random Input test Result for Damage Scenario CRBCC Using Full Data**
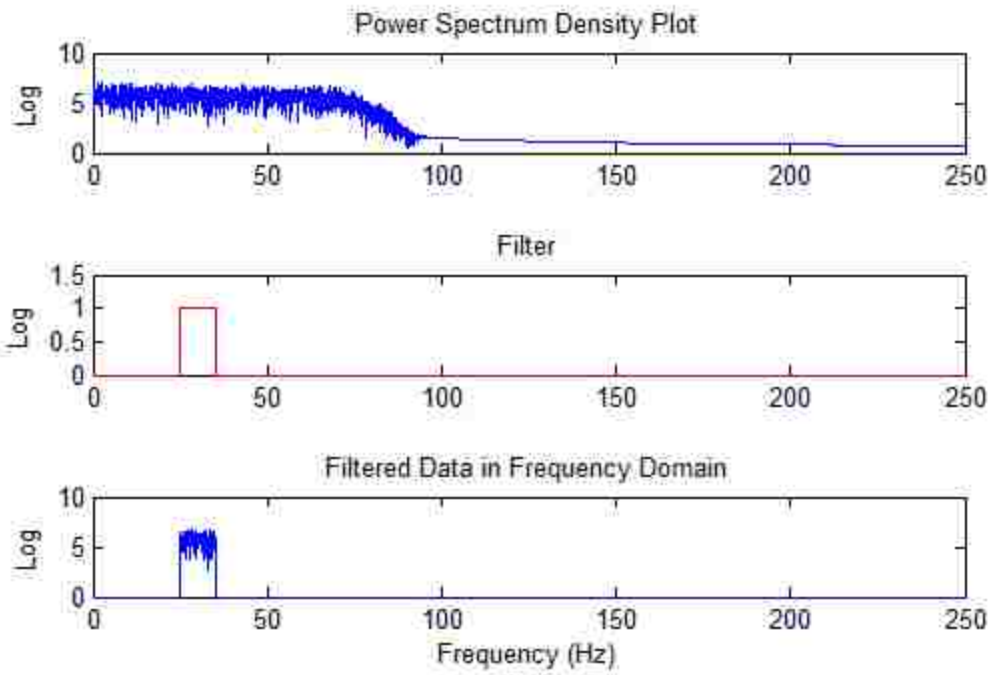

Figure 5.9 Random Input test Result for Damage Scenario RB Using Full Data
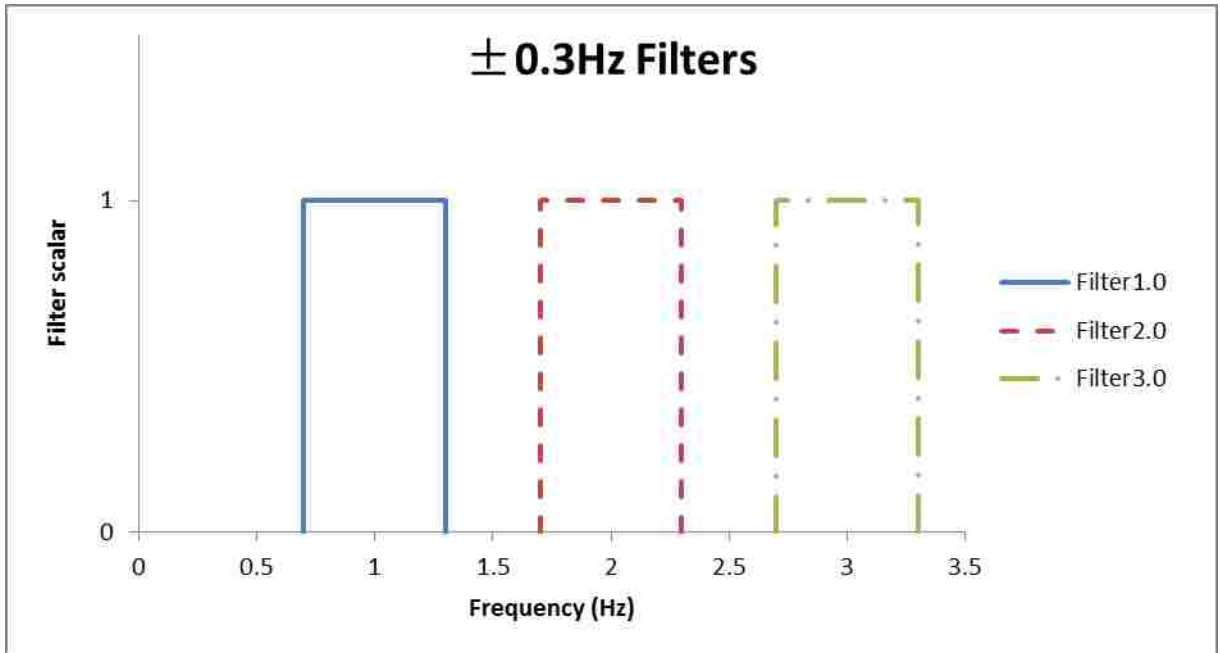
Figure 5.10 Random Input test Result for Damage Scenario RBRC Using Full Data

Figure 5.11 Filtering Data with a Band-pass Filter

Figure 5.12 Filters with Passing Band of ±0.3Hz
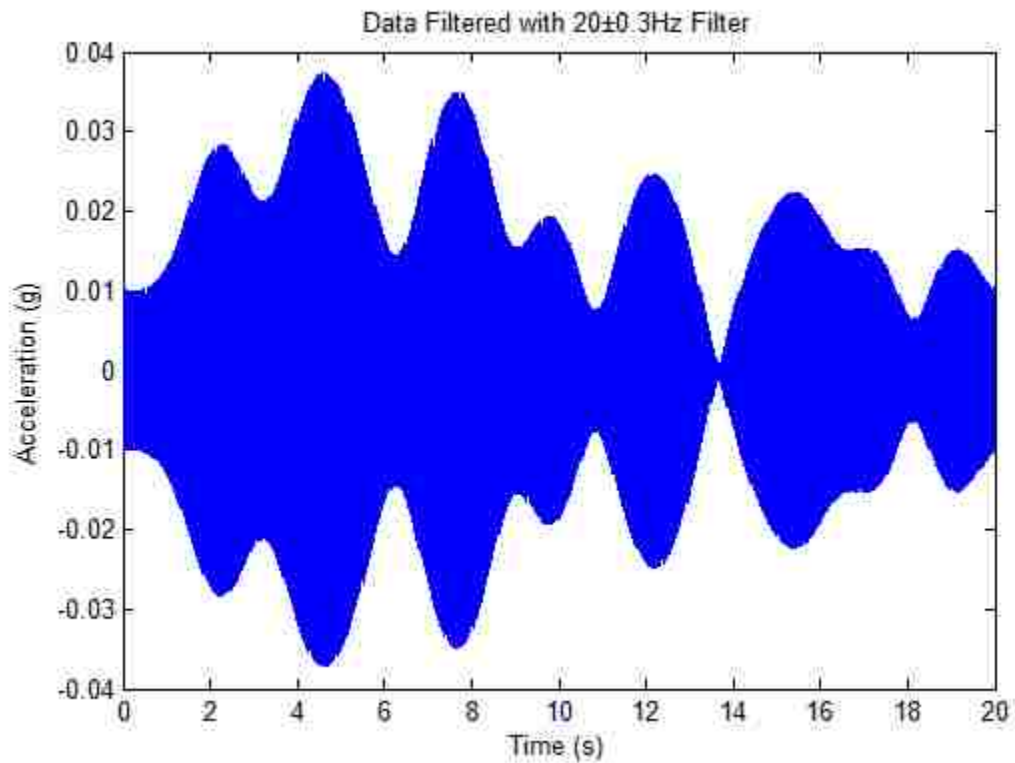
Figure 5.13 Data Filtered with 20±0.3Hz Filter
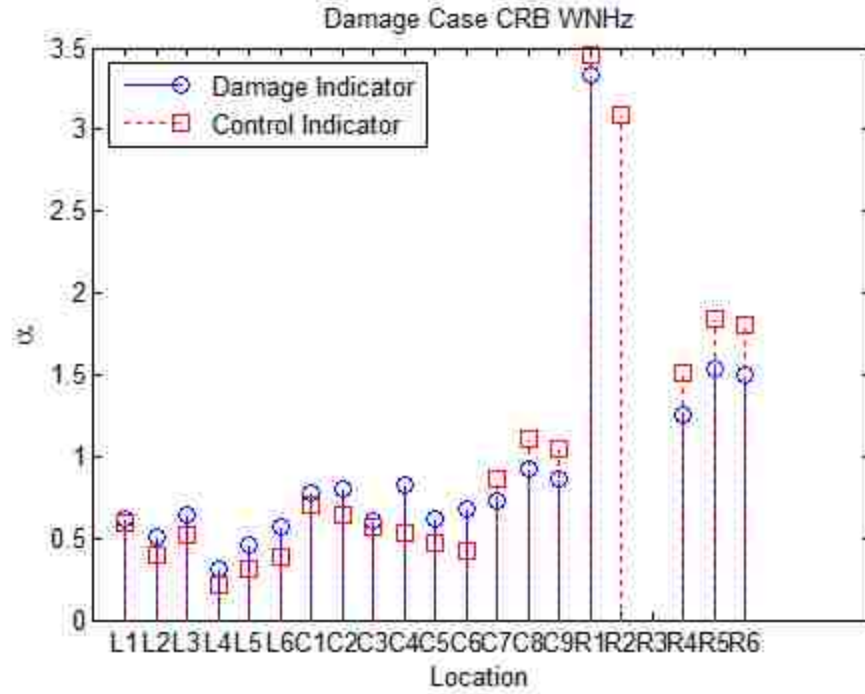
**Figure 5.14 Example of an 'X' Case of High Control Indicator:
Damage Scenario CRB with Random Input through an 18Hz Band-Pass Filter**
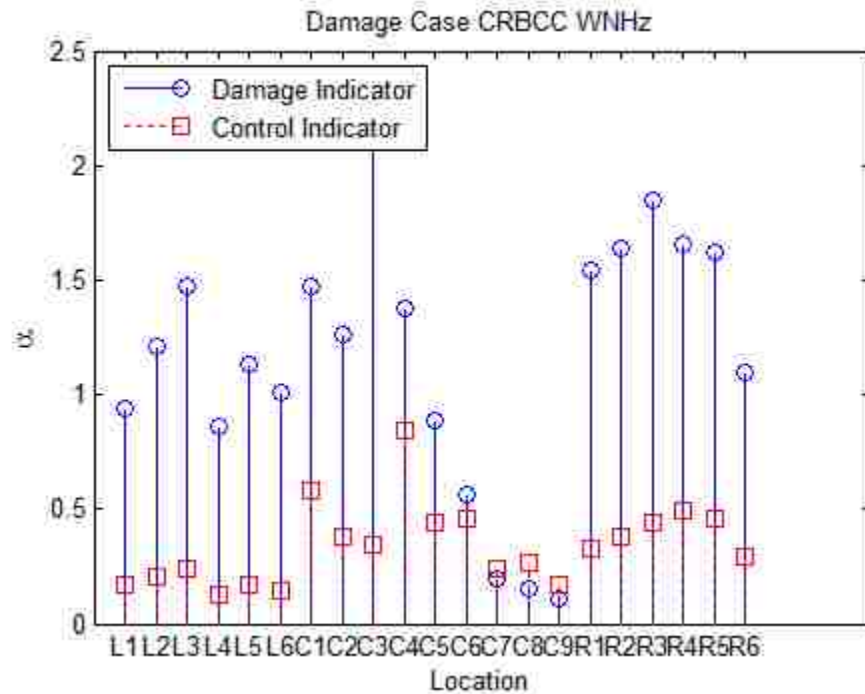
**Figure 5.15 Example of an 'X' Case of No Outstanding Damage Indicators:
Damage Scenario CRBCC with Random Input through a 15Hz Band-Pass Filter**
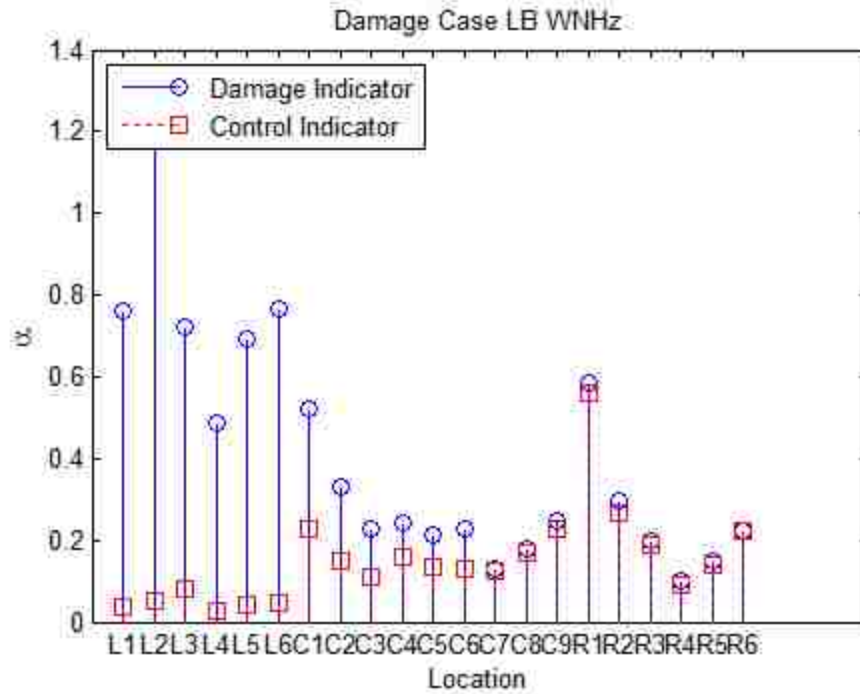
Figure 5.16 Example of an 'L' Case:
Damage Scenario LB with Random Input through a 20Hz Band-Pass Filter
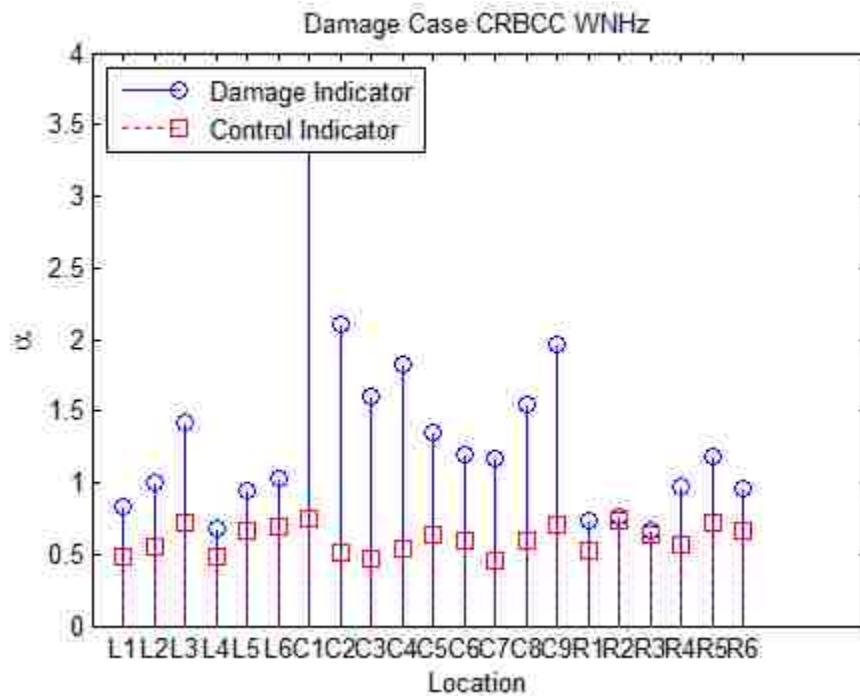
Figure 5.17 Example of a 'C' Case:
Damage Scenario CRBCC with Random Input through a 40Hz Band-Pass Filter
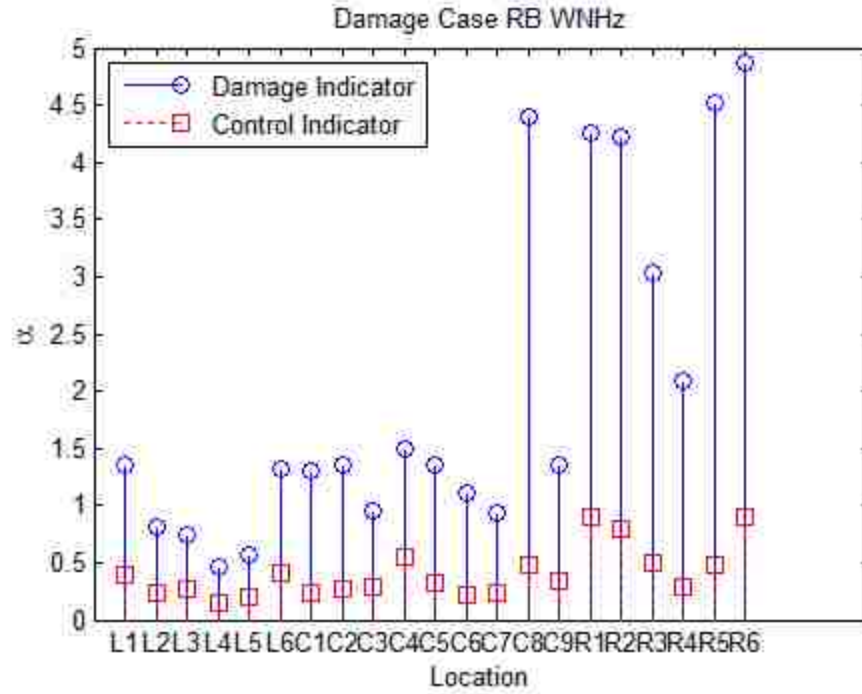
Figure 5.18 Example of an 'R' Case:
Damage Scenario RB with Random Input through a 20Hz Band-Pass Filter
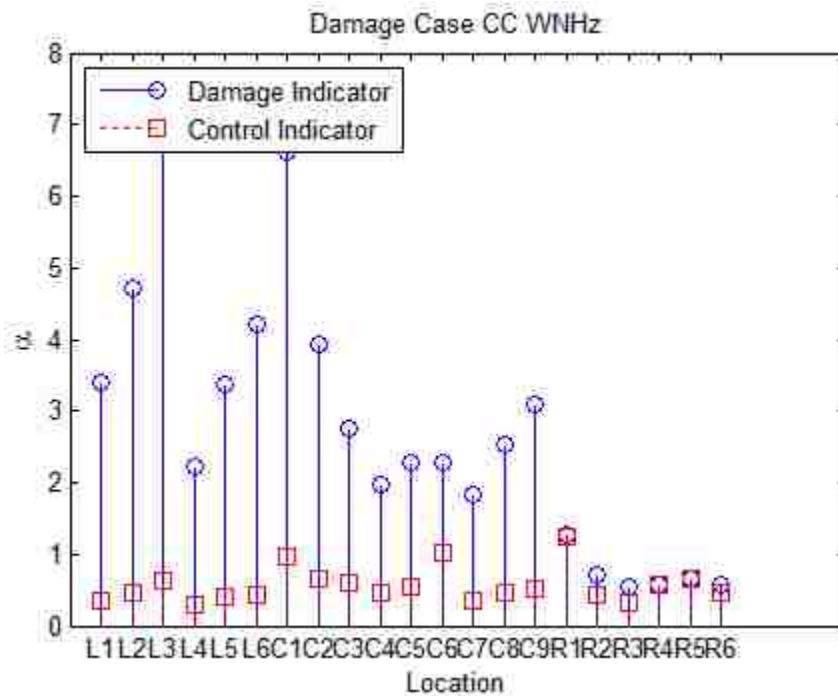
Figure 5.19 Example of an 'L/ C' Case:
Damage Scenario CC with Random Input through a 38Hz Band-Pass Filter
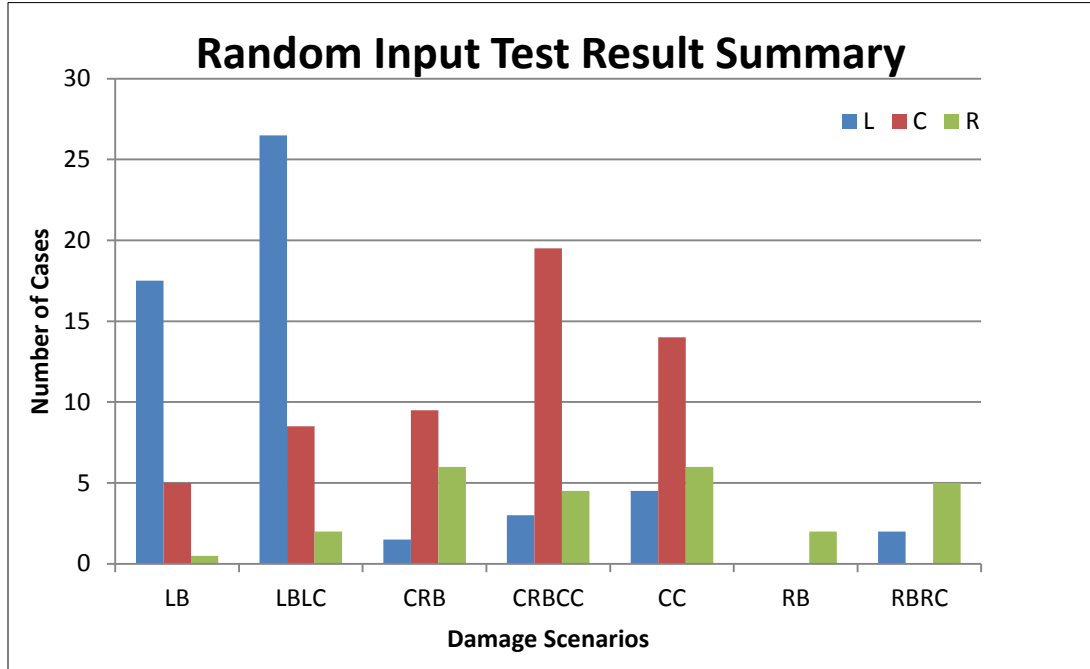
Figure 5.20 Random Input with ±0.3Hz Filters Test Results Summary
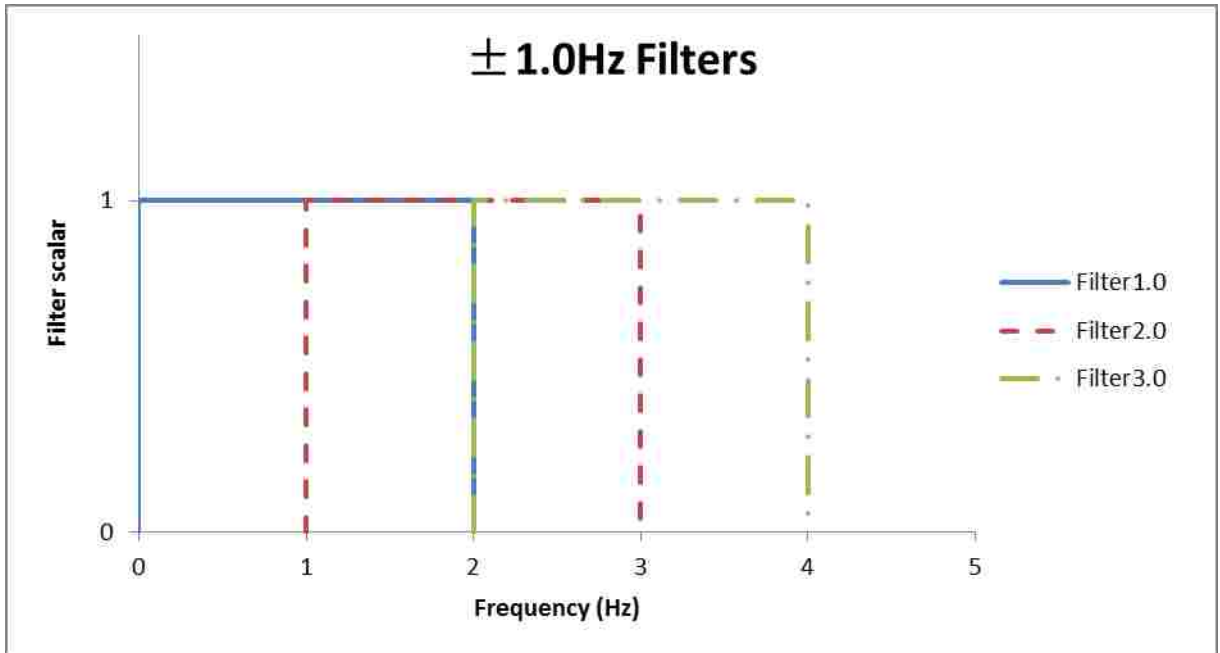
Figure 5.21 Filters with Passing Band of ±1.0Hz
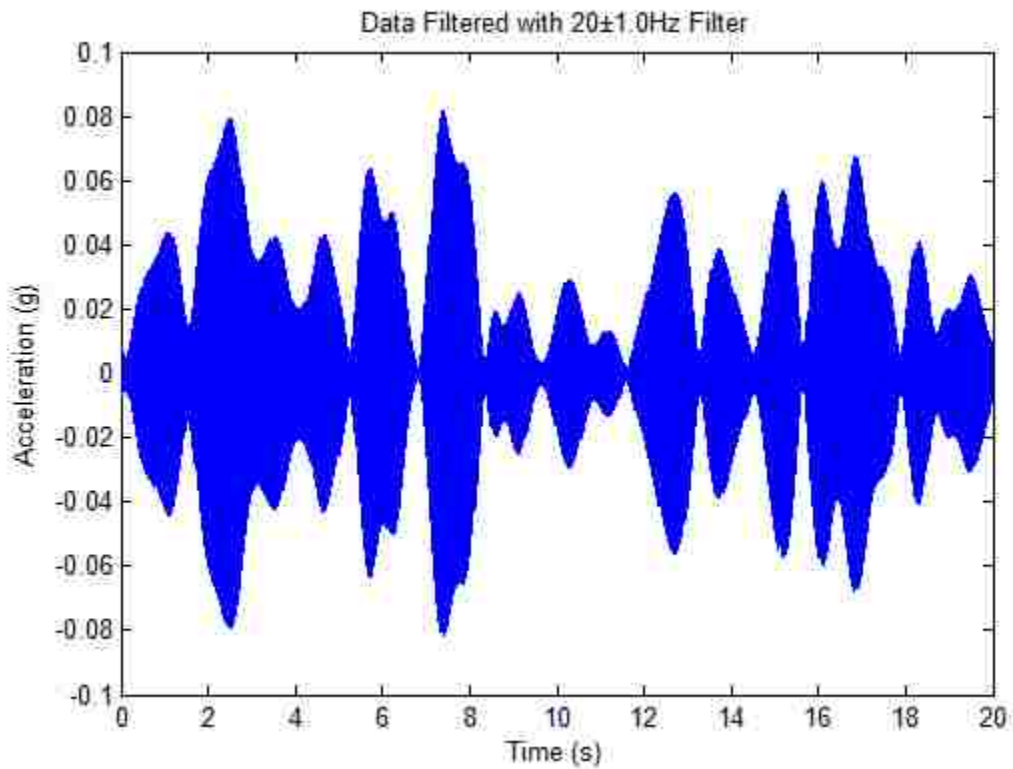
Figure 5.22 Data Filtered with 20±1.0Hz Filter
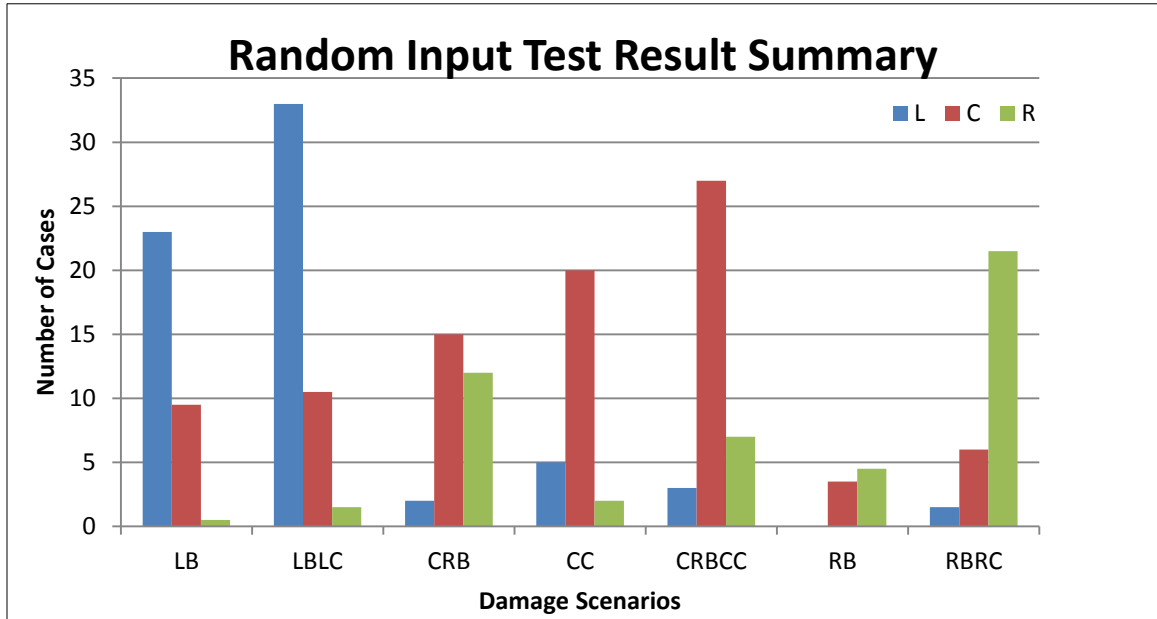
Figure 5.23 Random Input with ±1.0Hz Filters Test Results Summary
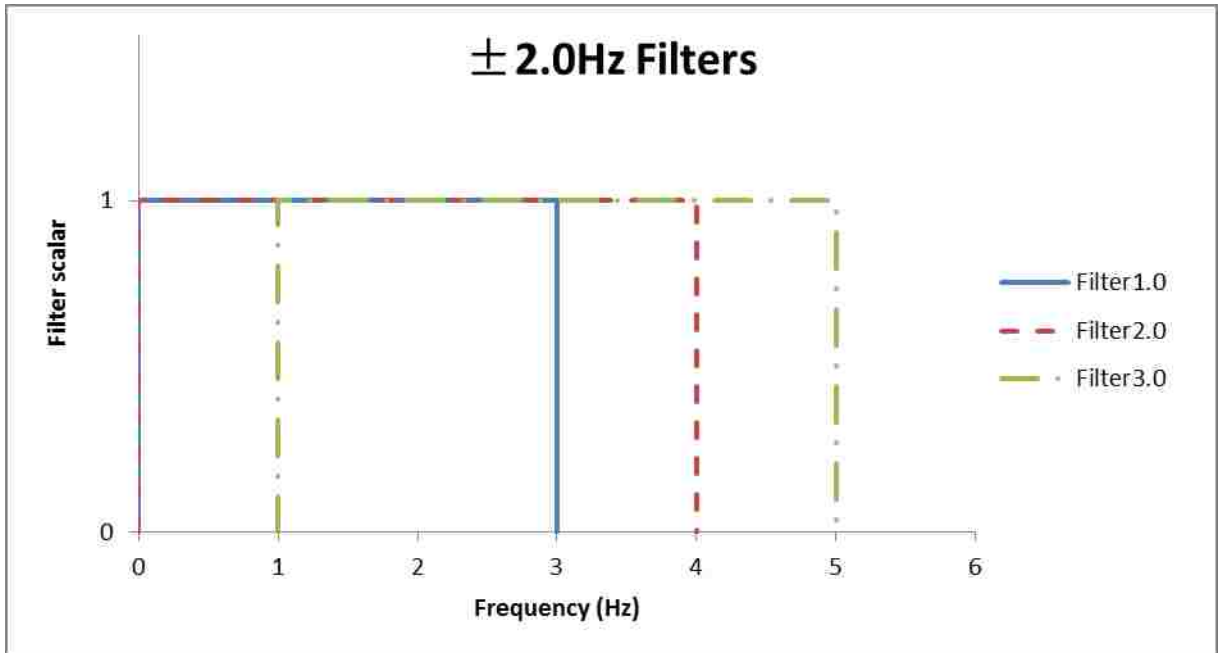
Figure 5.24 Filters with Passing Band of ±2.0Hz
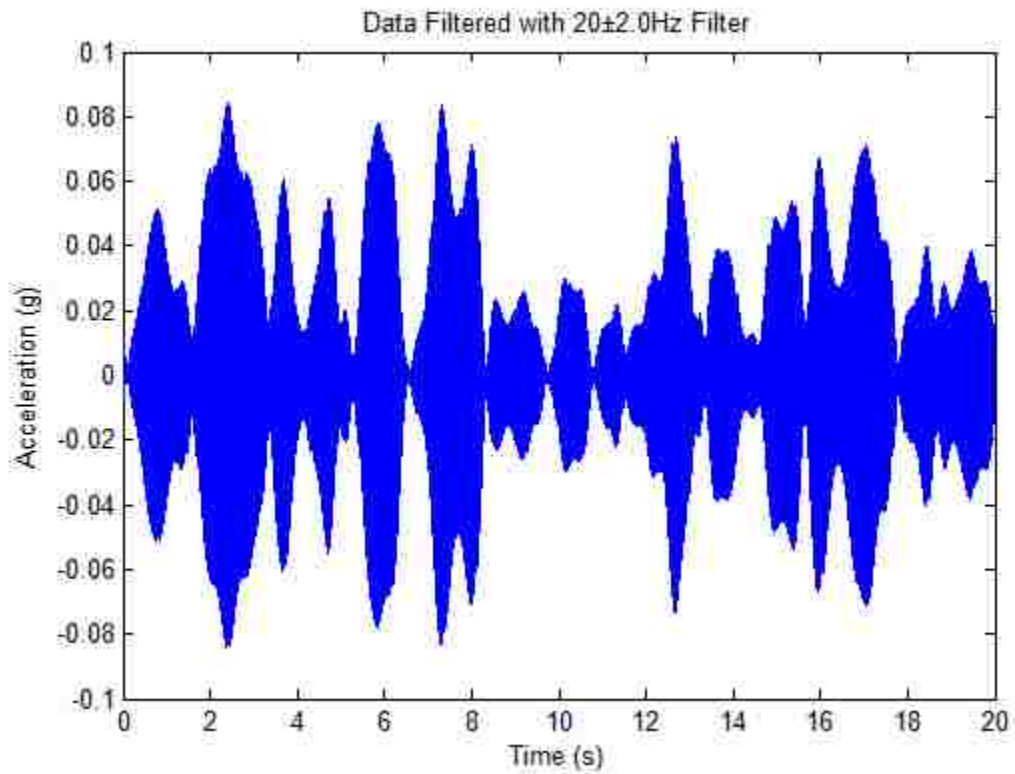
Figure 5.25 Data Filtered with 20±2.0Hz Filter
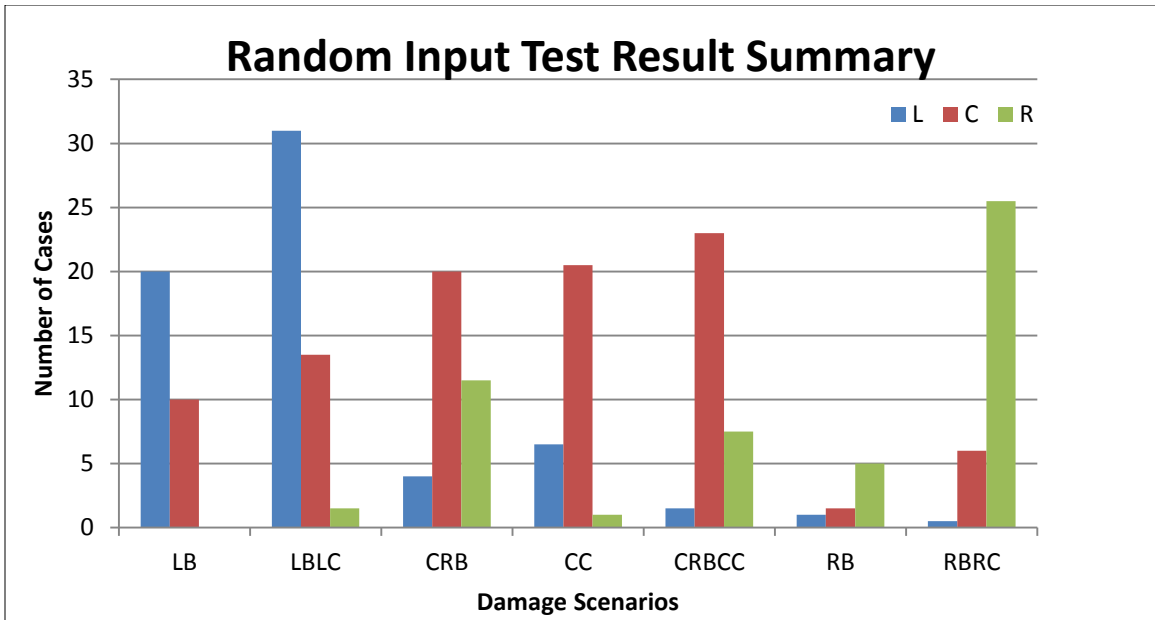
Figure 5.26 Random Input with ±2.0Hz Filters Test Results Summary

Chapter 6   Summary and Future Work

Advanced the linear regression based damage detection algorithms using data collected from a densely clustered sensor network is introduced in this thesis. Coefficients in the linear regression functions before and after damage are compared with each other to get damage indicators, thus indicate damage location. Three different algorithms, single-variable linear regression based algorithm, two-variable linear regression based algorithm and iterative variable linear regression based algorithm, were introduced. Tests were done on a scaled two-bay steel frame and its finite element model. Totally nine interchangeable parts which could be switched between undamaged the damaged status are placed on the frame to simulate various damage situations. In this research, seven damage scenarios are performed. Results were presented and discussed in the previous contents.

The first algorithm discussed is a single-variable linear regression based algorithm. The dynamic response from one node is used to express that from another node. A straight line in the 2-D plane is used to present the linear relationship between the responses and the angle between the 'undamaged' line and the 'damaged' line is the damage indicator. A factor called coefficient of determination is introduced to check the effectiveness of such linear regression by showing to which percent the dependent variable is expressed by the independent variable in the function. Also control indicators, calculated by comparing coefficients from two undamaged cases, are provided to set up a base line to the damage indicators. Those damage indicators which are not clearly larger than their corresponding control indicators are considered less reliable. First, test results from the simulation tests with or without noise and lab tests were listed. Although all the results are showing that this algorithm works in the harmonic input case, still there some

other conclusions can be drawn from these results. By comparing the result from simulation tests with and without noise, it is observed that the control indicators reflect the level of noise in the case and while damage indicator in undamaged areas are covered by the control damage indicators, those in the damaged area are still clearly larger than the control indicators. A phenomenon is also observed that when damage is on one side of the beam, behavior of the node on the other side of the beam, although it is far away from the damage location, will be significantly changed. At last comparison was made between damage detection results from the same damage scenario but different input frequencies. And it appears that different inputs will excite different parts of the frame and some damage will be more easily detected under input with a certain frequency. Basically work done in this algorithm doesn't just prove that the single-variable linear regression based algorithm is useful, it also gives some ideas of how the whole damage detection procedure works and what can be expected in the results.

The second algorithm introduced is based on two-variable linear regression. Instead of having just one independent variable in the linear function, another independent variable contains information from one previous time step will be added. The idea is to cover the information that is carried by the delayed response of the structure. In this algorithm, besides the coefficient of determination and the control indicator that were introduced in the one-variable linear regression algorithm, a new factor, the variable inflation factor, is also applied to check the robustness of the linear regression result. This factor is used to express the overlapping of the two independent variables. When the overlapped part of the two variables is too large, the linear regression will be unstable and so will the damage detection result. Damages are successfully

detected by applying the two-variable linear regression based algorithm. Two new and important conclusions are drawn in this part. The first one is that since one more variable is included in the function, the effect of noise is amplified. It is more clearly seen in the cases when 10% noise is added in the test data, damage prediction level was degraded when compared with the same case using the single-variable linear regression based algorithm. And the second conclusion is that in some of the cases including a second independent variable is unnecessary. Sometimes, the coefficient for the second independent variable is very small and that means the contribution made by the second variable is actually is very small. This conclusion gives a spark for the next damage detection algorithm.

The third algorithm is floating-number-variable linear regression based damage detection method. In this algorithm, the number of independent variables is not determined at first and it will increase until the dependent variable is 80% expressed. Since the workability of both single-variable and two-variable linear regression on data from sinusoidal input tests is checked, there is no need to do that again, the data used for this algorithm comes from random input tests which is more complicated and has more frequency content in it. The first attempt to apply this method to the original test data was successful because of the 5-variable-stop applied in the algorithm to save computing time. Then band-pass filters were applied onto the original data and frequency content in a certain range was selected out. Totally 50 filters were designed and applied to the data one at a time and 50 damage predictions for each damage scenario were collected and analyzed. Statistical results showed that damage location can be revealed by this damage detection algorithm.

Although all three linear regression based damage detection algorithm were proved useful in damage detection, there are still works shall be done in the future. First of all, quantitated criterions are needed for identifying damages from the stem plot. All the damage predictions made in this research are based on observations about the plots, which may contain the subjective opinions of the observer and is not a completely scientific way of making conclusions. Secondly, patterns of how the vibration shape are related to the revealing of damage, i.e. how to vibrate the structure to check if a certain part of it was damage, need to be discovered more and it may be a useful information to apply this output-based damage detection algorithm. At last, to take advantage of this algorithm in the real damage detection cases, a base line, meaning an undamaged status of the structure is needed. However, in most of the case, it is impossible to get such information, because no one would keep recording data from the first day service of a structure. How to solve this problem would be the most important issue for the future research on this damage detection method, or any other structural-feature-based methods.

Reference

Bodeux, J.B. and Golinval, J.C., 2001, "Application of ARMAV Models to the Identification and Damage Detection of Mechanical and Civil Engineering Structures," *Smart Materials and Structures*, Vol. 10, pp. 479–489.

Bonato, P., Ceravolo, R., De Stefano, A. and Molinari, F., 2000, "Use of Cross Time Frequency Estimators for Structural Identification in Non-stationary Condition and Under Unknown Excitation," *Journal of Sound and Vibration*, Vol.273 Issue 5, pp. 775–791.

Burton T.D., Farrar C.R. and Doebling S.W., 1998, "Two methods for model updating using damage Ritz vectors," *16th International Modal Analysis Conference*, 1998, vol. 3243 (1), pp.973-979.

Chopra, A. K., 2007, "Dynamics of Structures: Theory & Applications to Earthquake Engineering 3rd Edition," Englewood Cliffs, NJ: Prentice-Hall.

Fritzen, C.P., Jennewein, D. and Kiefer, T., 1998, "Damage Detection Based on Model Updating Methods," *Mechanical Systems and Signal Processing*, Vol.12, pp. 163–186.

Ichoku, C., Chu, D. A., Mattoo, S., Kaufman, Y. J., Remer, L. A., Tanre´, D., Slutsker, I., and Holben, B. N., 2002, "A Spatio-temporal Approach For Global Validation and Analysis of MODIS Aerosol Products," *Geophysical Research Letters*, 29(12), 8006, doi:10.1029/2001GL013206.

Izenman, A. J., 2008, "Modern Multivariate Statistical Techniques: Regression, Classification, and Manifold Learning," Springer, New York.

Jaishi, B. and Ren, W-X., 2007, "Finite Element Model Updating Based on Eigenvalue and Strain Energy Residuals Using Multiobjective Optimisation Technique," *Mechanical Systems and Signal Processing*, Vol.21, Issue 5, pp. 2295–2317.

Katanoda, K., Matsuda Y., and Sugishita, M., 2002, "A Spatio-temporal Regression Model for the Analysis of Functional MRI Data," *NeuroImage*, Vol.17, Issue 3, pp. 1415–1428.

Kawiecki, G., 2001, "Modal Damping Measurement for Damage Detection," *Smart Materials and Structures*, Vol.10, No.3, pp. 466–471.

Kim, J-T., Ryu, Y-S., Cho, H-M., and Stubbs, N., 2003, "Damage Identification in Beam-type Structures: Frequency-based Method vs. Mode-shape-based Method," *Engineering Structures*, Vol. 25, Issue 1, pp. 57–67.

Labuz, E. L., Pakzad, S. N. and Cheng L., 2011, "Damage Detection and Localization in Structures: A Statistics Based Algorithm Using a Densely Clustered Sensor Network," *Proceedings of the 2011 Structures Congress*, April 14-16, 2011, Las Vegas, Nevada.

Lew, J.S. and Juang, J.N., 2002, "Structural Damage Detection Using Virtual Passive Controllers", NASA/TM-2001-211251.

Mottershead, J.E., Friswell, M.I. and Mares, C., 1999, "A Method for Determining Model-Structure Errors and for Locating Damage in Vibrating Systems," *Meccanica*, Vol.34, No.3, pp.153-166.

Pandey, A.K., Biswas, M., and Samman, M.M., 1991, "Damage Detection from Changes in Curvature Mode Shapes," *Journal of Sound and Vibration*, Vol.145, Issue 2, pp. 321–332.

Pandey, A.K. and Biswas, M., 1994, "Damage Detection in Structures Using Changes in Flexibility," *Journal of Sound and Vibration*, Vol.169, Issue 1, pp. 3–17.

Ruotolo, R. and Surace, C., 1997, "Damage Assessment of Multiple Cracked Beams: Numerical Results and Experimental Validation", Journal of Sound and Vibration, Volume 206, Issue 4, pp. 567–588.

Rytter, A., 1993, "Vibration Based Indpection of Civil Engineering Structure," Ph. D. Thesis, University of Aalborg.

Salawu, O.S., 1997a, "Detection of Structural Damage Through Changes in Frequency: A Review," Engineering Structures, Vol. 19, No. 9, pp. 718-723.

Shi, Z.Y., Law, S.S., and Zhang L.M., 1998, "Structural Damage Localization from Modal Strain Energy Change," *Journal of Sound and Vibration*, Vol.218, Issue 5, pp. 825–844.

Silicon Designs, Inc. (2010). "Model 2210 Analog Accelerometer Module"

Sohn, H., and Farrar, C.R., 2001, "Damage Diagnosis Using Time Series Analysis of Vibration Signals," *Smart Materials and Structures*, Vol.10, pp. 446–451.

Sohn, H., and Law, K. H., 2001, "Damage Diagnosis Using Experimental Ritz Vectors," *Journal of Engineering Mechanics*, Vol.127, No.11, pp. 1184-1193.

Spectral Dynamics, Inc. (2001). "SigLab User Guide S2022D1/A." San Jose, CA..

Staszewski, W.J., Worden, K., and Tomlinson, G.R., 1997 "Time–frequency Analysis in Gearbox Fault Detection Using the Wigner–Ville Distribution and Pattern Recognition" *Mechanical Systems and Signal Processing*, Vol.11, pp. 673–692.

Trendafilova, I., 2003, "State Space Modelling and Representation for Vibration-Based Damaged Assessment," *Key Engineering Materials*, Vol. 245-246, pp. 547-556.

Vita

Yuchen Pan, son of Jianrong Pan and Ruiqiu Yu, was born on March 26th, 1988, in HangZhou, ZheJiang, China. Yuchen received his Bachelor of Science degree in Civil Engineering from Hohai University in NanJing, JiangSu, China. Yuchen began his graduate studies in the Department of Civil and Environmental Engineering at Lehigh University in Bethlehem, PA in August 2010. He will receive his Master of Science in Structural Engineering in January of 2013.